

AN ABSTRACT OF THE THESIS OF

NORKUN SITTHIPHONG for the degree of DOCTOR OF PHILOSOPHY

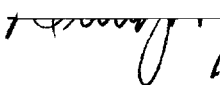
in MECHANICAL ENGINEERING presented on October 31, 1980

Title: EXPERIMENTAL STUDIES OF A PARTIALLY DEFLUIDIZED BED WITH

IMMERSED HEAT EXCHANGE TUBES.

*Redacted for Privacy*

Abstract approved:

 Dwight J. Bushnell

The object of this research study is to investigate and provide some fundamental information about bed slumping in a partially defluidized bed combustor. Due to the difficulty in making measurements and observations at high temperature, a dynamically similar cold phase fluidized bed was used to model the high temperature case.

Experiments were conducted in a 0.305 m by 2.44 m cold fluidized bed which has plexiglass windows along the sides to provide adequate visualization of the fluidizing phenomena. The heat exchange tube array comprising six staggered rows of horizontal tubes 0.0125 m O.D. was placed in the bed. Zirconia sand particles of diameter  $d_p = 305$  microns were used to simulate the mixture of 1200 micron limestone and coal particles. Gas velocities used in the experiment were varied from minimum fluidizing velocity to six times minimum fluidizing velocity.

On defluidizing half of the fluidized bed, bed material from the active portion of the bed began transferring to the slumped side of the bed, this caused a ridge of solids to form and grow on the slumped surface. Correlations were then developed to describe the changing contours of the slumped bed surface.

A major factor in the entrainment of bed material from the fluidized beds is the ejection of particles when bubbles break the bed surface. The initial velocities of ejected particles can be associated with the velocity of rising bubbles from potential flow theory. A simple model was developed to predict the motions and trajectories of ejected particles in the freeboard region. This model predicted the rate of bed material transfer from the active side to the defluidized section of the bed. These predictions were tested by experiment and showed good agreement. A correlation of the experimentally found particle density function for transferred material is presented. This can be used to determine the total amount of bed material transfer at any defluidization time.

The study of the gas flow in the slumped portion of the bed was also conducted by measuring the pressure profiles in both sections of the bed. The amount of gas bypass through the slumped bed was determined by the Ergun equation and these pressure profiles. The results indicate that the percentage of the gas bypass through the slumped section does not depend on the superficial velocity.

Necessary conditions required to completely refluidize the slumped section of the bed after a long period of defluidization were obtained from the pressure-time trace study. It was found that complete refluidization of the slumped section could not be achieved by using superficial refluidizing velocities of less than two times minimum fluidizing velocity.

Study of the lateral mixing of solids in a wide shallow fluidized bed was conducted by using the ferrite tracer technique. A simple unsteady diffusion equation was used successfully to model the dispersion of solids from the refluidized bed to the active bed. The

lateral dispersion coefficient of solids was found to depend on the superficial velocity and so was the rate of the solids mixing.

Finally, the results obtained from the room temperature bed were converted to those in the high temperature case by using similarity analysis. Comparison of the converted results with the available data from the high temperature bed indicated good agreement, and thus, a successful simulation.

Experimental Studies of a Partially Defluidized Bed with  
Immersed Heat Exchange Tubes

by

Norkun Sitthiphong

A THESIS

submitted to

Oregon State University

in partial fulfillment of  
the requirements for the  
degree of

DOCTOR OF PHILOSOPHY

Completed October 1980

Commencement June 1981

APPROVED:

*Redacted for Privacy*

Associate Professor of Mechanical Engineering  
in charge of major

*Redacted for Privacy*

Head of Department of Mechanical Engineering

*Redacted for Privacy*

Dean of Graduate School

Date thesis is presented October 31, 1980

Typed by Mary Syhlman for NORKUN SITTHIPHONG

## ACKNOWLEDGEMENTS

I would like to express my gratitude to my major professor, Dr. Dwight Bushnell for his guidance and assistance with my dissertation research. Also, I wish to thank Dr. Lorin R. Davis who is my former advisor during my master program and also one of my committee for his guidance and understanding.

Particular thanks are extended to my committee: Dr. Octave Levenspiel for introducing me to fluidized bed technology, to Dr. Robert E. Wilson, Dr. Gordon M. Reistad for their advice and guidance in my graduate program and to Dr. Kenneth L. Peddicord for spending his valuable time serving as a graduate representative in the committee.

Also, I wish to acknowledge the following for particular contributions: Babcock and Wilcox Company for their financial support; Steve Crane, project manager for his suggestions and assistance in constructing the fluidized bed; Riley Chan for providing all of the excellent electronics equipments; Rich Fobes for introducing me to the Nova Computer.

Finally, I come to my family. A special note of gratitude goes to my parents, Captain Thongkam and Mrs. Jurai Sitthiphong who sacrifice every thing in their lives for me. I would like to thank Bularat Sitthiphong, my beloved wife, for her compassion, understanding and assistance during our three year stay at Oregon State University. To my daughter, Patiporn, a special thank for her patience and for being a good girl while her parents completed their education.

## TABLE OF CONTENTS

<u>Chapter</u>	<u>Page</u>
I. INTRODUCTION	1
II. SIMILARITY ANALYSIS	4
III. APPARATUS AND INSTRUMENTATION	8
3.1 Fluidized Bed and Bed Media	8
Fluidized Bed	8
The Tube Array	9
Bed Media	9
Air Supply System	13
3.2 Pressure Measurement	14
Pressure Probes	14
Pressure Transducer and Amplifier	15
3.3 Bed Material Transfer Measurement	15
3.4 Solids Mixing Measurement	18
Ferrite Tracer Particles	20
Ferrite Tracer removal System	20
The Inductance Probes	22
The Inductance Bridge Circuit	25
3.5 Data Aquisition System	25
IV. SLUMPED BED SURFACE PROFILES	29
4.1 Background	29
4.2 Procedure	30
4.3 Result	32
4.4 Discussion	38
V. BED MATERIAL TRANSFER, MODEL AND EXPERIMENT	41
5.1 Background	41
Entrainment	41
Effect of Bubbles on the Entrainment	43
5.2 Physical Models	44
Introduction	44
Initial Velocities of Ejected Particles	45
The Diameter of a Bubble at the Surface of a Fluidized Bed	50
The Trajectories of Ejected Particles in the Freeboard Region	60
The Amount of Ejected Particles Per an Eruption	64
Particle Density Function and Bed Material Transfer	67
5.3 Experiment	68
Particle Density Function Measurement	68
Experimental Data	70
Correlation of the Experimental Data	70
5.4 Comparison of the Particle Density Function Bewtween Model Predictions and Experimental Results	76

<u>Chapter</u>	<u>Page</u>
5.5 Bed Material Transfer by Using Particle Density Function	78
The Effect of Slumped Bed Surface Profiles on Bed Material Transfer	78
Results and Discussion	81
VI. PRESSURE DROP AND GAS FLOW IN A PARTIALLY DEFLUIDIZED BED	84
6.1 Introduction	84
6.2 Pressure Loss Profiles	84
6.3 Gas Flow in the Slumped Bed	86
6.4 Discussion	90
VII. REFLUIDIZATION OF A SLUMPED SECTION	92
7.1 Qualitative Studies	92
7.2 Results and Discussion	93
VIII. SOLIDS MIXING STUDIES IN A PARTIALLY DEFLUIDIZED BED	101
8.1 Introduction	101
8.2 Procedure	103
8.3 Experimental Results	104
8.4 Discussion	107
8.5 Model of the Solids Mixing in a Partially Defluidized Bed	112
Mechanism of Solids Mixing	112
Diffusion Equation	144
Lateral Dispersion Coefficient of Solids	117
The Mixing Rate of Solids Between the Refluidized Section and the Fluidized Section	125
8.6 Conclusions	128
IX. THE CONVERSION OF RESULTS FOR FLUIDIZED BED COMBUSTORS	131
X. SUMMARY AND RECOMMENDATION	137
BIBLIOGRAPHY	142
APPENDICES	
Appendix A	148
Appendix B	150



## LIST OF FIGURES

<u>Figure</u>	<u>Page</u>
3.1 Photograph of the slumped fluidized bed (front view).	10
3.2 Schematic diagram of the slumped fluidized bed.	11
3.3 Photograph of the dummy heat exchange tube array.	12
3.4 Photograph of the pressure transducer.	16
3.5 Schematic drawing of the differential pressure transducer amplifier.	17
3.6 Schematic drawing of the location of the receptable array in the fluidized bed.	19
3.7 Photograph of the magnetic drum ferrite removal system.	21
3.8 Arrangement of the tube array in the bed (end view). The six inductor coils are located in a tube marked by an X.	23
3.9 The position of each coil on the tube.	24
3.10 Schematic drawing of an inductance bridge card.	27
4.1 The location of the slumped bed surface profile in the experimental fluidized bed.	31
4.2a The slumped bed surface profiles as a function of time at $u = 0.45$ m/s	33
4.2b The slumped bed surface profiles as a function of time at $u = 0.61$ m/s	34
4.2c The slumped bed surface profiles as a function of time at $u = 0.76$ m/s	35
4.3 Comparison of the slumped bed surface profiles as a function of time between analytical model and the experimental data at $u = 0.61$ m/s	37
4.4 Schematic drawing indicates part of the active bed is defluidized	39
4.5 Comparison of the slumped bed surface profiles between the experimental data and the correlation	40
5.1 The motion of solids in the vicinity of a rising three dimensional bubble as viewed by a stationary observer from potential theory	46

<u>Figure</u>	<u>Page</u>
5.2 Schematic representation of a bubble rising in a fluidized bed.	48
5.3 Comparison of $d_0$ in an open bed between experimental data and the correlations presented by Mori and Wen, Rowe and Darton et al. (bed height 0.28 m).	54
5.4 Comparison of $d_0$ in an open bed between experimental data and the correlation proposed by Darton et al. (bed height 0.127 and 0.28 m).	56
5.5 Comparison of $d_0$ in a fluidized bed with immersed heat exchange tube array between experimental data and the correlation in equation (5.15).	58
5.6 Comparison of $d_0$ in fluidized bed with immersed heat exchange tube array between the experimental data obtained by Nguyen et al. and the correlation in equation (5.15).	59
5.7 The initial velocity of ejected particles as a function of excess gas velocity .	61
5.8 Schematic representation of a bulge formation at the moment that a bubble is half above the bed surface and is about to erupt.	63
5.9 The thickness of the bulge at the moment that the eruption occurs as a function of excess gas velocity.	66
5.10 The frequency of the eruption of bubbles at the bed surface as a function of velocity.	69
5.11a Particle density function as a function of x at y = 0.07 m.	72
5.11b Particle density function as a function of x at y = 0.15 m.	73
5.11c Particle density function as a function of x at y = 0.23 m.	74
5.11d Particle density function as a function of x at y = 0.31 m.	75
5.12 Comparison of particle density function between the correlation from the equation (5.32) and the experimental data at y = 0.15 m.	77
5.13a Comparison of the weight of particles collected in each cup between the model and the experimental data at u = 0.76 m/s.	79

<u>Figure</u>		<u>Page</u>
5.13b	Comparison of the weight of particles collected in each cup between the model and the experimental data at $u = 0.60$ m/s.	80
5.14	Comparison between material transfer, calculated from particle density function and experimental data .	83
6.1	Pressure drop at various location along the bed and at different superficial velocity.	85
6.2	Pressure drop profiles in both slumped and active bed at various superficial velocity.	87
7.1	Pressure-time trace during refluidization at $x = 0.48$ m and $u = 0.22$ m/s.	94
7.2	Pressure-time trace during refluidization at $x = 0.48$ m and $u = 0.46$ m/s.	95
7.3	Time required to refluidize the slumped part of the bed as a function of superficial velocity.	97
7.4	Pressure drop across the slumped bed at the middle of the ridge.	98
8.1	Data of the ferrite concentration readings of all six probes from run number 6.	106
8.2	Reduced data from run number 6 by using the method proposed by Deaton (14).	109
8.3	Reduced data from run number 6 by the method proposed in this study.	111
8.4	Concentration profiles of ferrite from run number 6.	113
8.5	Schematic representation of the coordinate and the location of the tracer initially introduced to the slumped bed.	116
8.6	Plots of the dispersion coefficient of solids obtained from the experiment as a function of superficial velocity.	120
8.7a	Concentration profiles from run number 1 by using equation (8.7) with $D_z = 0.002$ m <sup>2</sup> /s.	121
8.7b	Concentration profiles from run number 5 by using equation (8.7) with $D_z = 0.0012$ m <sup>2</sup> /s.	122
8.7c	Concentration profiles from run number 9 by using equation (8.7) with $D_z = 0.0007$ m <sup>2</sup> /s.	123

<u>Figure</u>		<u>Page</u>
8.8	The relative amount of solids transfer (M) as a function of time after refluidization.	129
9.1	The comparison of $d_{bm}$ in high temperature bed between experimental data and equation (9.6).	136

## LIST OF TABLES

<u>Table</u>	<u>Page</u>
3.1 Scaling values for all six channels.	26
5.1 Summary of the experimental conditions for entrainment studies from other investigators.	42
5.2 Published correlations for estimating bubble size in fluidized beds.	52
5.3 Experimental data showing weight of particles captured in each receptable during the duration of one minute.	71
8.1 Summary of experimental conditions for solids mixing test.	105
8.2 Summary of the experimental conditions and values of $D_z$ obtained from other investigators.	124
8.3 Comparison of $D_z$ values at various superficial velocities between this experiment and other investigators.	126
A1 Zirconia sand sieve analysis.	145

## NOTATION

- a      location in z direction where tracer particles are introduced to the slumped bed (m)
- a'     the distance between the bubble eruption center to the interface region (m)
- $A, A_t$    cross sectional area of the fluidized bed ( $m^2$ )
- $A_0$      the catchment area for the bubble stream at the distributor plate which is usually the area of plate per orifice ( $m^2$ )
- b      location in z direction where tracer particles are introduced to the slumped bed (m)
- c      concentration of ferrite tracer ( $kg/m^3$ )
- $c^*$      concentration of ferrite tracer at equilibrium condition ( $kg/m^3$ )
- $c_i$      initial concentration of ferrite tracer in the slumped bed ( $kg/m^3$ )
- $c(\epsilon)$    constant in equation (2.7)
- $C_D$      drag coefficient
- d      particle diameter ( $\mu$ )
- $d^*$      dimensionless parameter
- $d_b$      mean bubble diameter (m)
- $d_{bm}$    mean bubble diameter at the bed surface (m)
- $d_{bmC}$    mean bubble diameter at the bed surface of the scale bed, eq.(9.5) (m)
- $d_{bmH}$    mean bubble diameter at the bed surface of the high temperature bed, eq.(9.6) (m)
- $d_e$      equivalent spherical diameter of bubble (m)
- $d_{em}$    equivalent spherical diameter of bubble at the bed surface (m)
- $d_i$      initial bubble diameter at the distributor (m)
- dr     thickness of the bulge at the bed surface (m)
- $d_o$      bubble eruption diameter (m)
- $d_o'$     bubble eruption diameter at height  $h_1$  (m)

$d_o''$	growth in bubble sizes as they pass through an array of heat exchange tube (m)
$d_p$	surface mean particle size ( $\mu$ )
$D$	reference particle size ( $\mu$ )
$D_t$	bed diameter (m)
$D_w$	lateral dispersion coefficient of solids in w direction ( $m^2/s$ )
$D_y$	axial dispersion coefficient of solids in y direction ( $m^2/s$ )
$D_z$	lateral dispersion coefficient of solids in z direction ( $m^2/s$ )
$E, E_{ij}$	gas stress tensor ,eq.(2.5)
$E^S, E_{ij}^S$	solid stress tensor, eq. (2.6)
$f$	frequency of the eruption of bubble
$\vec{f}$	force exerted by gas on solid per solid particle
$\vec{g}, g$	acceleration of gravity ( $9.8 m/s^2$ )
$g_c$	conversion factor ( $1kg.m/N.s^2$ )
$h$	height (m)
$h_0$	constant
$h_1$	height of the lowest row of the tube array above the distributor plate (m)
$h_2$	height of the highest row of the tube array above the distributor plate (m)
$h_{max}$	the slumped bed height (m)
$K$	scaling factor
$K_1$	constant in eq.(6.3)
$K_2$	constant in eq.(6.6)
$k_u$	constant in eq.(5.7)
$L$	characteristic length, length of the bed (m)
$L_C$	length of the scale bed (m)
$L_H$	length of the high temperature bed (m)

$\dot{m}_a$	gas flow rate in the active side of the bed; eq. (6.9) (kg/s)
$m_c$	total amount of solids from the refluidized bed that diffused to the active bed (kg)
$m_c$	total amount of bed material transfer in the cold phase scale bed; eq. (9.1) (kg)
$\dot{m}_d$	gas flow rate in the defluidized side of the bed; eq.(6.6) (kg/s)
$m_H$	total amount of bed material transfer in the high temperature bed combustor (kg)
$\dot{m}_{mf}$	gas flow rate at the minimum fluidizing condition; eq. (9.8) (kg/s)
$m^*$	total amount of solids from the refluidized bed that diffused to the active bed at the steady state condition; eq. (8.21) (kg)
$M$	relative amount of diffused solids, $m_c/m^*$
$n$	solid particle number density
$n_d, N_0$	number of orifice openings in the distributor
$p$	pressure (kPa)
$p^*$	dimensionless parameter
$p_0$	reference pressure (kPa)
$p^s$	solid pressure (kPa)
$\Delta p$	pressure drop across the bed (kPa)
$\Delta p_d$	pressure drop across the bed in the defluidized section (kPa)
$\Delta p_{mf}$	pressure drop across the bed at the minimum fluidizing velocity (kPa)
$r$	distance from the center of a bubble (m)
$r_b$	radius of bubble (m)
$r_{bm}$	radius of bubble at the bed surface (m)
$Re_p$	particle Reynolds number
$t$	time, time after defluidization (s)
$t^*$	dimensionless parameter
$T$	reference time (s)



$u, \vec{u}$	gas velocity, gas velocity vector (m/s)
$u^*$	dimensionless parameter
$u_a$	gas velocity in the active bed (m/s)
$u_b$	velocity of a bubble rising through a bed (m/s)
$u_{br}$	velocity of a bubble respect to the emulsion phase (m/s)
$u_i$	initial velocity of ejected particle (m/s)
$u_{mf}$	superficial velocity at the minimum fluidizing conditions (m/s)
$u_r$	solid velocity in r direction at distance r from a rising bubble (m/s)
$u_s$	gas velocity in the defluidized bed (m/s)
$u_t$	terminal velocity of a falling particle (m/s)
$u_\theta$	solid velocity in $\theta$ direction at distance r from a rising bubble (m/s)
$U$	reference gas velocity (m/s)
$v, \vec{v}$	solid velocity, solid velocity vector (m/s)
$v^*$	dimensionless parameter
$v_x$	velocity of ejected particle in x direction (m/s)
$v_y$	velocity of ejected particle in y direction (m/s)
$\Delta v$	concentration readings
$V_C$	volume of transferred bed material in the cold phase bed ( $m^3$ )
$V_H$	volume of transferred bed material in the fluidized bed bombustor ( $m^3$ )
$w$	width of the bed (m)
$W$	weight of the bed material (kg)
$x$	horizontal diatance from the interface region (m)
$x^*$	location where the slope of the ridge change in x direction (m)
$x^{**}$	dimensionless parameter
$x^p$	location of the peak of the ridge in x direction (m)
$y$	vertical distance from the bed surface (m)

$y^P$  location of the peak of the ridge in y direction (m)  
 $z$  horizontal distance from the left end of the bed (m)

### Greek Symbols

$\delta$  fraction of fluidized bed consisting of bubbles  
 $\delta_{ij}$  Kronecker delta  
 $\epsilon$  void fraction  
 $\epsilon_m$  void fraction in the packed bed  
 $\epsilon_{mf}$  void fraction in a bed at the minimum fluidizing velocity  
 $\theta$  angle, degrees  
 $\lambda(\epsilon), \mu(\epsilon)$  viscosity coefficient of gas  
 $\lambda^S(\epsilon), \mu^S(\epsilon)$  viscosity coefficient of solid  
 $\mu_f$  viscosity of gas (kg/m.s)  
 $\rho_f, \rho_g$  gas density (kg/m<sup>3</sup>)  
 $\rho_{fC}, \rho_{fH}$  gas density in scale bed, in fluidized bed combustor (kg/m<sup>3</sup>)  
 $\rho_{sC}, \rho_{sH}$  solid density in scale bed, in fluidized bed combustor (kg/m<sup>3</sup>)  
 $\rho'_{sC}, \rho'_{sH}$  bulk density of solid in scale bed, in fluidized bed combustor (kg/m<sup>3</sup>)  
 $\phi_d$  particle density function (kg/m<sup>2</sup>.min.)  
 $\phi_s$  sphericity of a particle  
 $\psi$  stream function of solid in a vicinity of a rising bubble

# EXPERIMENTAL STUDIES OF A PARTIALLY DEFLUIDIZED BED WITH IMMERSED HEAT EXCHANGE TUBES

## I. INTRODUCTION

Fluidized bed combustion represents a promising method for burning high sulfur content coal in industrial plants. Conventional boilers using bituminous-coal-fired burners no longer meet the standard requirements since the burners can not control sulfur dioxide emissions. Expensive scrubbing systems must be installed to reduce the amount of  $\text{SO}_2$  to the standard regulation. Fluidized bed combustors operate at relatively low combustion temperatures (1050 K) and, therefore, produce less  $\text{NO}_x$  and other undesirable gases while providing optimum conditions for the sulfur retention by limestone or dolomite in the bed.

Operating a fluidized bed combustor at less than full load presents problems which are not present with conventional boilers. Conventional boilers can reduce coal feed rates to accomplish turn downs of up to 90% to follow the electrical load patterns. Fluidized bed combustors, however, must maintain a reasonable air velocity in order to keep solids fluidized. A more difficult constraint comes from the fact that the bed temperature must be kept close to 1050 K or sulfur will no longer be effectively removed from the stack gases.

One method for achieving bed turndown is to locate the heat exchange tubes so that they are entirely immersed at the maximum fluidizing air velocity, as the power generated by the boiler is reduced the air and coal would be reduced in a fixed ratio and hopefully heat exchange surface in the form of steam tubes would be removed from the

bed proportionately so as to keep the bed at a constant temperature. Experience with the fluidized bed combustor at Alexandria, Virginia, operated by Pope Evans and Robins has proved that this is difficult to accomplish, at least with a uniformly spaced bank of tubes. As the fluidizing velocity is reduced the heat exchange area does not decrease rapidly enough. Thus, more heat is removed from the bed than is generated by combustion, and the bed temperature tends to drop precipitously.

A different approach to turndown involves slumping or defluidization of a portion of the fluidized bed, that is, cutting off the flow of air to that region. With the air cut off to half of the distributor, it is expected that the heat output of the bed would drop to approximately one half and that the heat transfer area would be reduced in the same ratio. To bring the bed up to full capacity, the air supply would be returned to that stagnant half of the bed.

However, the slumping process has a complication. Bed material tends to build up in the slumped region of the bed and there is a corresponding depletion of bed solids in the fluidized portion of the bed. This reduces the residence time of gas passing through the bed since the bed is now shallow. The amount of limestone available for scavenging sulfur is also reduced, and there are less solids to enhance heat transfer to the steam tubes. These effects could be countered by adding more bed material to the fluidized region. Another problem facing producers of utility boilers is that after operating a partially slumped bed for a long period of time, it is found that it is difficult

to refluidize that slumped portion of the bed at low velocity.

Refluidization of the slumped part of the bed at high velocity creates another serious problem. The higher velocity of refluidization creates a rapid mixing of the low temperature bed material from the slumped section with the high temperature bed material from the active side, this tends to reduce the temperature of the bed below the limit for the sulfur retention.

The goal of this study is to provide some fundamental data about bed slumping which includes the amount and rate of bed material transfer from the active side to the adjacent slumped section of the bed, the shapes or profiles of the slumped bed surfaces, the necessary condition required for the refluidization of the slumped section and finally the mixing rate of the solids from both sides of the bed after refluidization.

A second objective of this study is to develop models to describe the phenomena of the bed material transfer occurring in the partially defluidized bed and the mixing of solids from both sections after refluidization.

## II. SIMILARITY ANALYSIS

Due to the difficulty in making measurements and observations in the high temperature fluidized bed combustors, a dynamically similar cold phase fluidized bed was used to model the high temperature case. In order to provide a dynamically similar cold phase fluidized bed that would accurately model the high temperature conditions, techniques from dimensional analysis were used in this study.

In order to obtain the similarity parameters required in this study basic flow equations in the fluidized bed were used (29):

$$\text{fluid phase continuity} \quad \frac{\partial \epsilon}{\partial t} + \text{div}(\epsilon \vec{u}) = 0 \quad (2.1)$$

$$\text{solid phase continuity} \quad \frac{\partial}{\partial t}(1-\epsilon) + \text{div}((1-\epsilon)\vec{v}) = 0 \quad (2.2)$$

fluid phase momentum

$$\rho_f \epsilon \left( \frac{\partial \vec{u}}{\partial t} + \vec{u} \cdot \text{grad} \vec{u} \right) = \text{div} \underline{\underline{E}} - n\vec{f} + \epsilon \rho_f \vec{g} \quad (2.3)$$

solid phase momentum

$$\rho_s (1-\epsilon) \left( \frac{\partial \vec{v}}{\partial t} + \vec{v} \cdot \text{grad} \vec{v} \right) = \text{div} \underline{\underline{E}}^S + n\vec{f} + (1-\epsilon) \rho_s \vec{g} \quad (2.4)$$

where stress tensors  $\underline{\underline{E}}$ ,  $\underline{\underline{E}}^S$  and the interaction force  $\vec{f}$  can be expressed in terms of total mean pressure and velocity fields as,

$$E_{ij} = -p \delta_{ij} + \lambda(\epsilon) \frac{\partial u_m}{\partial x_m} \delta_{ij} + \mu(\epsilon) \left( \frac{\partial u_i}{\partial x_j} + \frac{\partial u_j}{\partial x_i} - \frac{2}{3} \delta_{ij} \frac{\partial u_m}{\partial x_m} \right) \quad (2.5)$$

$$E_{ij}^S = -p^S \delta_{ij} + \lambda^S(\epsilon) \frac{\partial v_m}{\partial x_m} \delta_{ij} + \mu^S(\epsilon) \left( \frac{\partial v_i}{\partial x_j} + \frac{\partial v_j}{\partial x_i} - \frac{2}{3} \delta_{ij} \frac{\partial v_m}{\partial x_m} \right) \quad (2.6)$$

and

$$n\vec{f} = n\alpha(\epsilon)(\vec{u}-\vec{v}) + (1-\epsilon)C(\epsilon)\rho_f \frac{d}{dt}(\vec{u}-\vec{v}) + (1-\epsilon) \operatorname{div} \underline{E} \quad (2.7)$$

Equations (2.5) to (2.7) were substituted in equations (2.3) and (2.4). Each of the variables were transformed to the proper reference quantity by introducing dimensionless variables denoted by stars as,

$$\begin{aligned} u &= Uu^* \\ v &= Vv^* \\ x &= Lx^* \\ t &= Tt^* \\ d &= Dd^* \\ \text{and } p &= p_0 p^* \end{aligned} \quad (52).$$

Scharff et al. (53) made substitutions by using the equations above and obtained three dimensionless parameters, i.e.

$$gL/U^2 \quad (2.8)$$

$$L\rho_f/\rho_s D \quad (2.9)$$

$$\rho_f DU/\mu_f \quad (2.10)$$

In addition, the same authors fixed  $L/D$  as the constant in the two different systems. Therefore, four dimensionless groups were obtained as follows,

$$gL/U^2 \quad \text{reciprocal Froude number} \quad (2.11)$$

$$\rho_f/\rho_s \quad \text{density ratio} \quad (2.12)$$

$$\rho_f DU/\mu_f \quad \text{particle Reynolds number} \quad (2.13)$$

and  $L/D$  macroscopic scale to particle scale ratio (2.14)

Dynamic similarity requires these four parameters to be equal in the high temperature fluidized bed combustor and the cold phase bed. Letting the subscript C denote the cold bed system and H denote the high temperature bed gives the density ratios.

$$\rho_{fH}/\rho_{sH} = \rho_{fC}/\rho_{sC} \quad (2.15)$$

The fluid densities in both cases can be calculated assuming ideal gas behavior since the operating temperatures in both cases are known and both of the beds are operated at atmospheric pressure. In the fluidized bed combustor, limestone with bulk solid density between 1440 and 2080 kg/m<sup>3</sup> was used. The density of the material used in the cold bed can be calculated by using the relation from equation (2.15).

In order to determine the scale factor (K) which is the ratio of the macroscopic scale in the high temperature bed ( $L_H$ ) and the macroscopic scale in the cold phase bed ( $L_C$ ), equation (2.11), the square of the equation (2.13) and the square of equation (2.14) were combined to form another dimensionless parameter  $g\rho_f^2 L^3 / \mu_f^2$ .

$$\text{Hence,} \quad K = L_H/L_C = (\mu_{fH}\rho_{fC}/\mu_{fC}\rho_{fH})^{2/3} \quad (2.16)$$

$$\text{or} \quad L_H = KL_C \quad (2.17)$$

$$\text{and} \quad D_H = KD_C \quad (2.18)$$

$$U_H = K^{0.5}U_C \quad (2.19)$$



Accordingly, the value of  $K = 3.76$  was obtained.

$$\text{Hence,} \quad L_H = 3.76 L_C \quad (2.20)$$

$$D_H = 3.76 D_C \quad (2.21)$$

$$U_H = 1.94 U_C \quad (2.22)$$

$$\rho_{SH} = 0.32 \rho_{SC} \quad (2.23)$$

### III. APPARATUS AND INSTRUMENTATION

#### 3.1 Fluidized Bed and Bed Media

##### Fluidized Bed

Experiments were conducted in an 2.44 m long by 0.305 m wide by 3.66 m high fluidized bed which through proper design has been shown to be dynamically similar to a high temperature bed. A distributor plate formed by two pieces of sheet metal with center-aligned holes and a 200 mesh stainless steel screen sandwiched between the plates was used to be the base of the fluidized bed. The upper plate has holes 0.00556 m (7/32 in.) and the diameter of the holes are alligned with a center to center distance between holes of 0.038 m (1.5 in.) on both plates. Plexiglass windows along the sides of the bed provided adequate visualization of the fluidizing phenomenon.

Defluidizing of a portion of the bed was achieved by using an air inlet plenum which was divided into two separate wind boxes with individual butterfly valves to control the amount of air entering the two compartments of the bed. Two venturi orifices, one for each wind box, were inserted in the air inlet ducts and water manometers plumbed to each of them facilitating the equilibrating of air distribution to the plenums and also allowed for the measurement of the air flow rate. The two control valves of the inlets of the plenums were manually controlled such that each section of the open distributor was subjected to an equal flow potential. An air bypass was also installed such that

excess air could be vented to an area above the free board. Figure (3.1) shows the front view of the fluidized bed.

To maintain the fluidized bed height constant while operating in a slumped condition, bed material must be continually added to the active side of the bed. A material feed system was installed on top of the fluidized section of the bed. A hopper with attached scale was used in the feed system such that exact amounts of material could be added to the bed during the experiments. The schematic diagram of the slumped fluidized bed is shown in Figure 3.2.

#### • The Tube Array

The diameter of the heat exchange tubes in the fluidized bed combustor is about 0.05 m (2 in.). By using the scaling factor ( $K = 3.76$ ) the size of the dummy tubes used in the cold bed can be scaled down to 0.013 m in diameter. An array of heat exchange tubes comprising six staggered rows of horizontal tubes with 0.0125 m (0.5 in) O.D. and 0.041 m equilateral triangular pitch were placed in the bed with the lowest row of the tubes 0.127 m above the distributor plate. The tubes were supported by vertical plastic spacers at both ends and horizontal steel bars at the middle to restrict the deflections of the tubes. The tube array is shown in Figure 3.3.

#### Bed Media

A fluidized bed combustor of coal ash and limestone has a bulk density between 1450 and 2050 kg/m<sup>3</sup>. By assuming that the voidage ( $\epsilon$ )

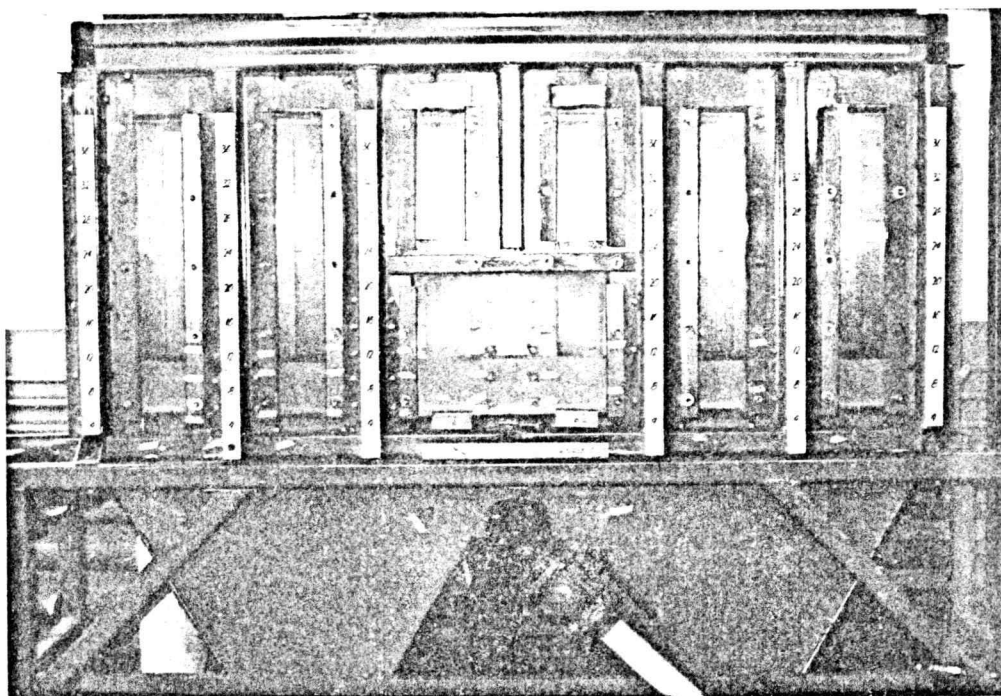


Figure 3.1 Photograph of the slumped fluidized bed (front view)

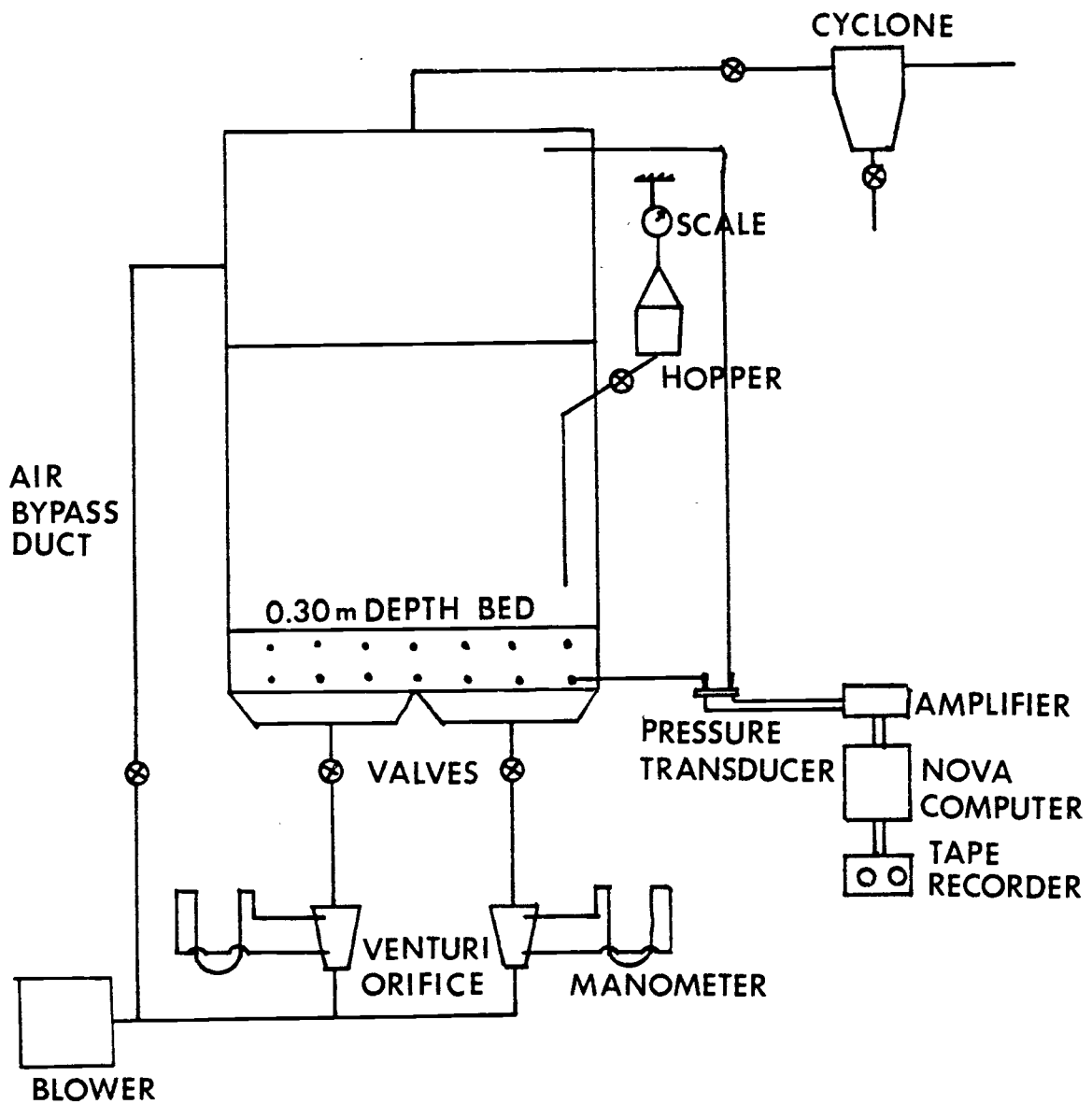


Figure 3.2 Schematic diagram of the slumped fluidized bed.

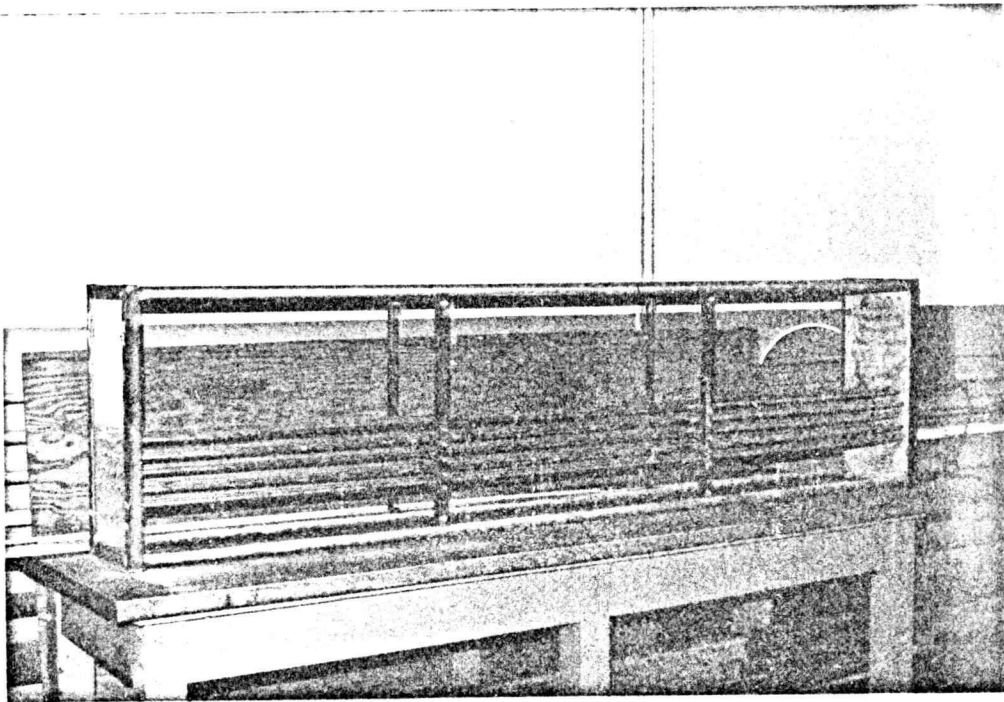


Figure 3.3 Photograph of the dummy heat exchange tube array.

of the bed material is about 0.35, the particle density is then between 2200 and 3150 kg/m<sup>3</sup>. This result was confirmed by McKenzie (40) who reported that a bed of coal and limestone has a density of about 2700 kg/m<sup>3</sup>. In order to determine the density of the particles used in the cold bed, the equation (2.23) was used. It was determined that the density of the bed material required in the experiment bed should have a density of about 6850 kg/m<sup>3</sup>. Zirconia sand (ZrO<sub>2</sub>) which has a density of about 5900 kg/m<sup>3</sup> was used. This type of sand has a surface mean particle ( $d_p$ ) of 305 microns and, a bulk density of about 3000 kg/m<sup>3</sup>.

The mean surface particle diameter ( $d_p$ ) was determined by using the sieve size analysis as described by Kunii and Levenspiel (33). An analysis of the mean surface particle ( $d_p$ ) can be found in Appendix A.

The minimum fluidizing velocity ( $u_{mf}$ ) at room temperature for the zirconia sand particles was obtained by using the semi-theoretical equation given by Wen and Yu (59). According to the calculation, the minimum fluidizing velocity at room temperature was found to be 0.16 m/s. However, when comparing the calculated  $u_{mf}$  with the experimental data, it was found that the value of  $u_{mf}$  obtained from the experiment was higher than 0.16 m/s. The difference between these two values may come from the effect of the tube array in the bed.

### Air Supply System

The air which was used for fluidization was supplied to the fluidized bed by a Roots positive displacement blower model 1228. The maximum flow rate of the blower is 3.78 m<sup>3</sup>/s at 0.51 atm. The blower is driven

by a 242 kW diesel engine (Caterpillar model 3406T) located in a sound-proof room. The temperature of the air after the bed has been warmed-up is about 325 K. Inlet air flow rates to each compartment was measured by using calibrated venturi orifices.

Fine particles which elutriated from the bed were collected in four cyclone separators operating in parallel. The particle-free gas then flows through another calibrated venturi meter to check the superficial air velocity through the system. All experiments were conducted at atmospheric pressure.

### 3.2 Pressure Measurement

#### Pressure Probes

It was required to measure the pressure drop across the bed and to determine the pressure profile throughout the bed. Pressure probes were installed along the bed at 0.025 m, 0.33 m, 0.46 m, 0.74 m, 0.86 m, 1.17 m, 1.58 m, and 1.98 m from the left end of the bed and at heights of 0.025 m, 0.15 m, 0.23 m, and 0.30 m above the distributor plate. The probes themselves consist of 0.0064 m (0.25 in.) pipes which are welded to the side of the bed. They terminate in 0.0064 m (0.25 in.) tubing which connects them to the pressure transducers.

The holes of the pressure probes are covered with a 200 mesh stainless steel screen to prevent bed material from entering them. The screen is sufficiently coarse so that there is a negligible pressure drop across it.



### Pressure Transducers and Amplifier

The pressure transducers shown in Figure 3.4 are manufactured by National Semiconductor (model LX1601 D) and are integrated circuit type transducers. The output voltage is linearly related to the differential pressure across the transducer with an output of 7.5 volts corresponding to zero differential pressure. The transducers can be operated with either a positive or negative differential pressure with a maximum range of  $\pm 34.47$  kPa (5 psi).

The output signal from each of the transducers is the pressure difference between the pressure at that particular point in the bed and the reference pressure which is the atmospheric pressure. The output signal is scaled and zeroed using two operational amplifiers with a zeroing potentiometer and a gain potentiometer. The amplifier circuit is shown in Figure 3.5. The amplifier model consists of 16 circuits hence 16 sets of data can be measured at the same time.

The output electrical signals which are already scaled by using amplifiers were transformed to the main control module by means of a 25 pin Amphenol connector. The signals are finally transferred to the analog-to-digital converter.

### 3.3 Bed Material Transfer Measurement

In order to determine the rate of bed material transfer, the particle density function which is defined as the amount of transferred material accumulated in a unit area of the slumped section, per unit time, must be measured. This can be accomplished by installing an array



Figure 3.4 Photograph of the pressure transducer.

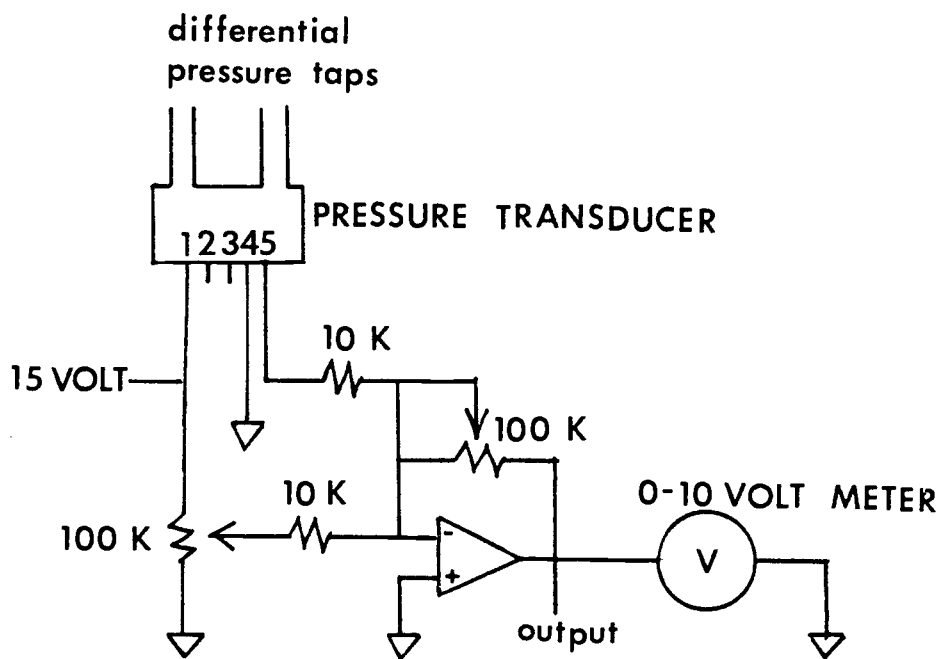


Figure 3.5 Schematic drawing of the differential pressure transducer amplifier.

of receptables in the slumped section of the bed. The weight of the bed material collected in each receptable per unit time is the rate of material transferred at that particular point.

The array of receptables consists of eight 0.0762 m (3 in.) diameter plastic cups. Each cup is inserted in a 0.0762 m (3 in.) diameter hole drilled in a piece of plywood. The centers of the holes are aligned with a center to center distance between holes of 0.0762 m. The plywood is 0.10 m wide and 0.62 m long and is attached to a cast iron frame. The frame was then placed over the slumped section so that the rim of the first receptable was at the interface region. The height of the frame over the distributor plate could be chosen between 0.38 m, 0.45 m, 0.53 m, and 0.61 m (15, 18, 21, 24 in. above the distributor plate). The location of the receptable array is shown in Figure 3.6.

### 3.4 Solids Mixing Measurement

In order to turn down a fluidized bed combustor, a section of the fluidized bed needs to be defluidized by cutting off the air supply and the flow of coal to that region. The temperature of the slumped part of the bed will then supposedly decrease since the combustion of coal no longer exists in that section of the bed. To bring the bed up to full capacity, the air supply would be returned to that stagnant part of the bed. It is required to measure the rate of mixing between material in the slumped part (low temperature) and the fluidizing media in the active part (high temperature). The technique of the inductance

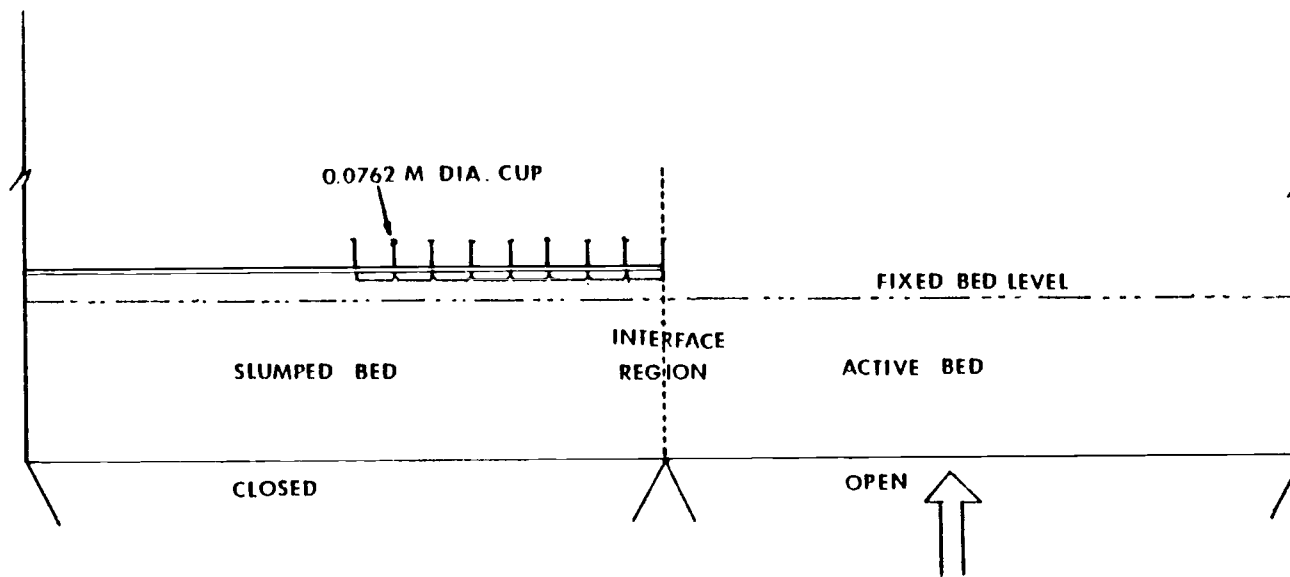


Figure 3.6 Schematic drawing of the location of the receptable array in the fluidized bed.

probe method which was conceived and developed by Dr. Thomas J. Fitzgerald was used in this study (17).

### Ferrite Tracer Particles

The ferrite particles that were first available were found to be too large for the test since their corresponding  $u_{mf}$  was higher than the operating velocity in the cold bed. Thus, the ferrite particles were required to be crushed until their sizes were small enough that their corresponding  $u_{mf}$  were in the range of operating velocities. The ferrite used in the experiment had a surface mean diameter ( $d_p$ ) of 1000 microns and the corresponding  $u_{mf}$  was 0.98 m/s.

### Ferrite Tracer Removal System

Ferrite tracer particles were introduced to the slumped section of the fluidized bed by first opening a small portion of the wall above the slumped bed level and then spreading them evenly over the slumped bed surface. After a run was made, the ferrite material was separated from the bed media by refluidizing the whole bed and draining the sand-ferrite mixture onto a conveyor belt which passed over a magnetic drum. The non-ferrite material (sand) fell off the edge of the drum into a container, the ferrite material stuck to the belt until the belt separated from the magnetic drum and dropped into a second container. The magnetic drum ferrite removal system with a vibrating tray to control the flow rate of the mixture onto the belt is shown in Figure 3.7.

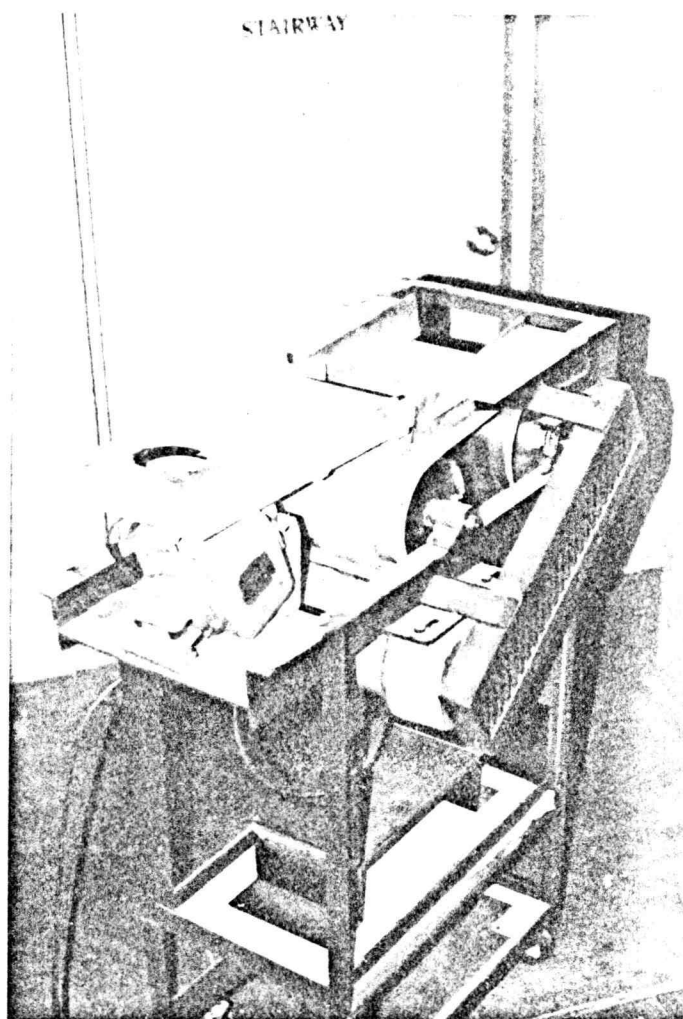


Figure 3.7 Photograph of the magnetic drum ferrite removal system.

### The Inductance Probes

Six inductance probes were used to measure the concentration of ferrite tracer particles as they spread through out the bed after the refluidization. The arrangement of the dummy tubes and the location of the rod containing inductance probes within the array is shown in Figure 3.8. Each inductor coil is 0.095 m (3.75 in.) long and the center of each coil is 0.43 m (1.5 in.) apart. The position of each coil on the rod is shown in Figure 3.9. The coils consist of approximately 7100 turns of fine copper wire (# 34 gage) wound on a 0.013 m (0.5 in.) O.D. fiberglass rod. Each coil has an inductance of 0.1 Henry and can monitor the concentration of ferrite in a volume with a radius of about 0.05 m (2 in.) from the center of the coil. A balanced active bridge circuit for monitoring ferrite concentration was built. When the tracer is near a coil, the inductance of the coil is increased and the bridge goes out of inductive balance. The signal output from the coil is plotted against the ferrite concentration and found to be linear with respect to the ferrite concentration.

The signal output for a particular ferrite concentration is slightly different from others. It is required to adjust the output from each probe so that the final output will be in the same magnitude. To accomplish this, the probes were calibrated to give a uniform response to a 0.00635 m (0.25 in.) diameter and 0.05 m (2 in.) long ferrite rod. The signal output measured in volts were recorded for each probe when the ferrite rod was held adjacent to each individual probe. The scaling value for each probe was obtained by dividing the average



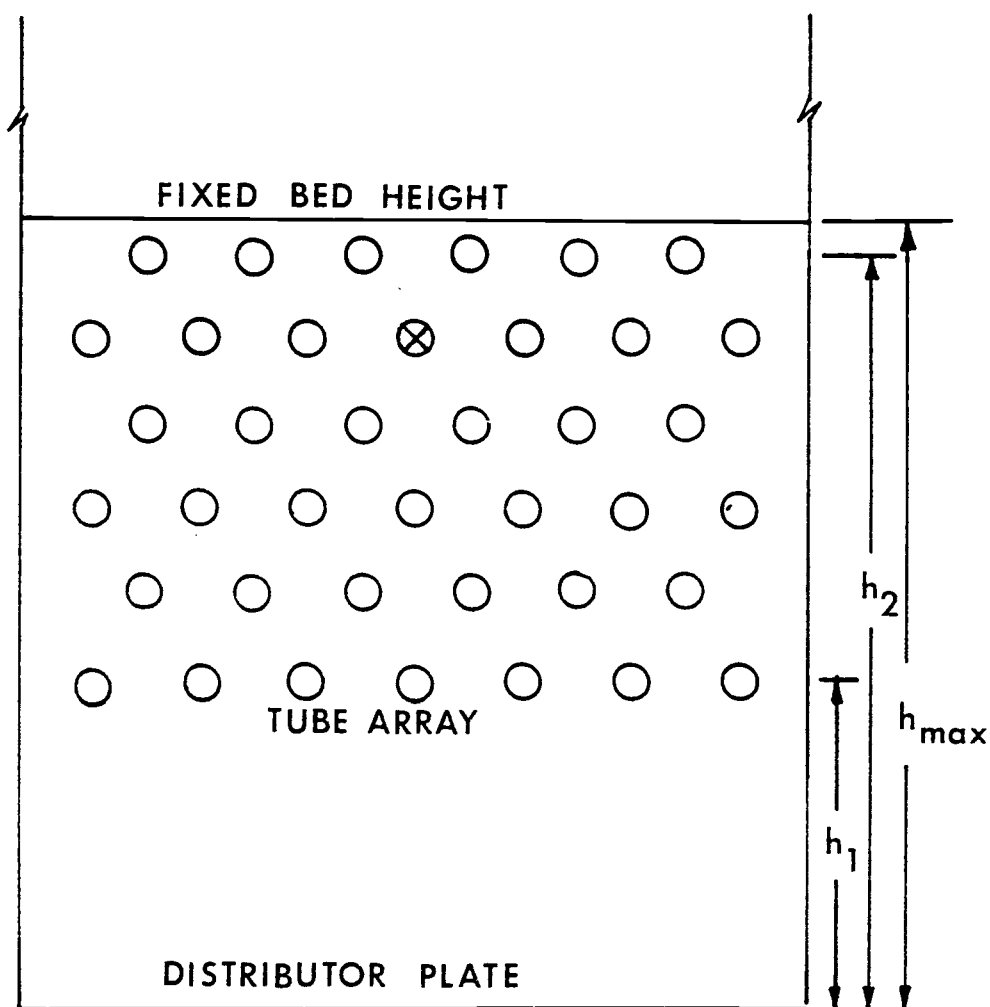


Figure 3.8 Arrangement of the tube array in the bed (end view).

The six inductor coils are located in a tube marked by an X.

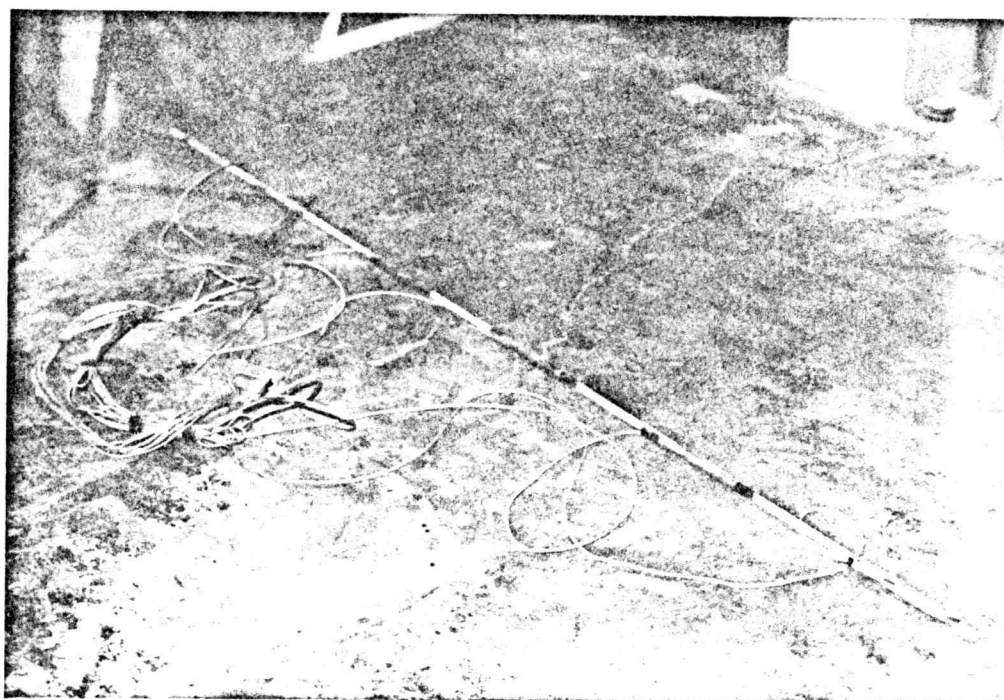


Figure 3.9 The position of each coil on the tube.

signal output by the signal output of a particular probe. The scaling values for each of the six channels are shown in Table 3.1. Thus, the adjustable outputs from all probes were comparable on the same basis.

### The Inductance Bridge Circuit

The inductance bridge circuit for measuring ferrite is shown in Figure 3.10. The 0.1 Henry inductor coil which is one leg of the bridge is balanced with the second leg, the 0.1 Henry terroid located on the printed circuit card. When the ferrite tracer is in the vicinity of an inductance probe, the inductance of the coil will be increased and the bridge goes out of inductive balance. The signal output is gained by the multiplier then passed through a two time- constant filter to eliminate the carrier frequency and the harmonics from the signal output.

### 3.5 Data Acquisition System

To record the pressure profile during the refluidization, sixteen pressure transducers were used to sample data 20 times per second or once every 50 milliseconds for 8 seconds. The first few data points (first 0.5 second) were used as the reference or zero pressures.

To record the mixing rate after refluidization, six inductance probes were used. Data were taken 20 times per second for 300 seconds. Data were collected for about 10 seconds before starting refluidization in order to determine the background or zero level for the inductance probes.

Table 3.1    Scaling Values for all 6 Channels:

Channel	$\Delta V$ (Voltage Difference)	Scaling Value
1	384	0.958
2	439	0.838
3	304	1.211
4	305	1.197
5	384	0.958
6	391	0.941

$$\Sigma = 2207$$

$$\overline{\Delta V} = 367.83$$

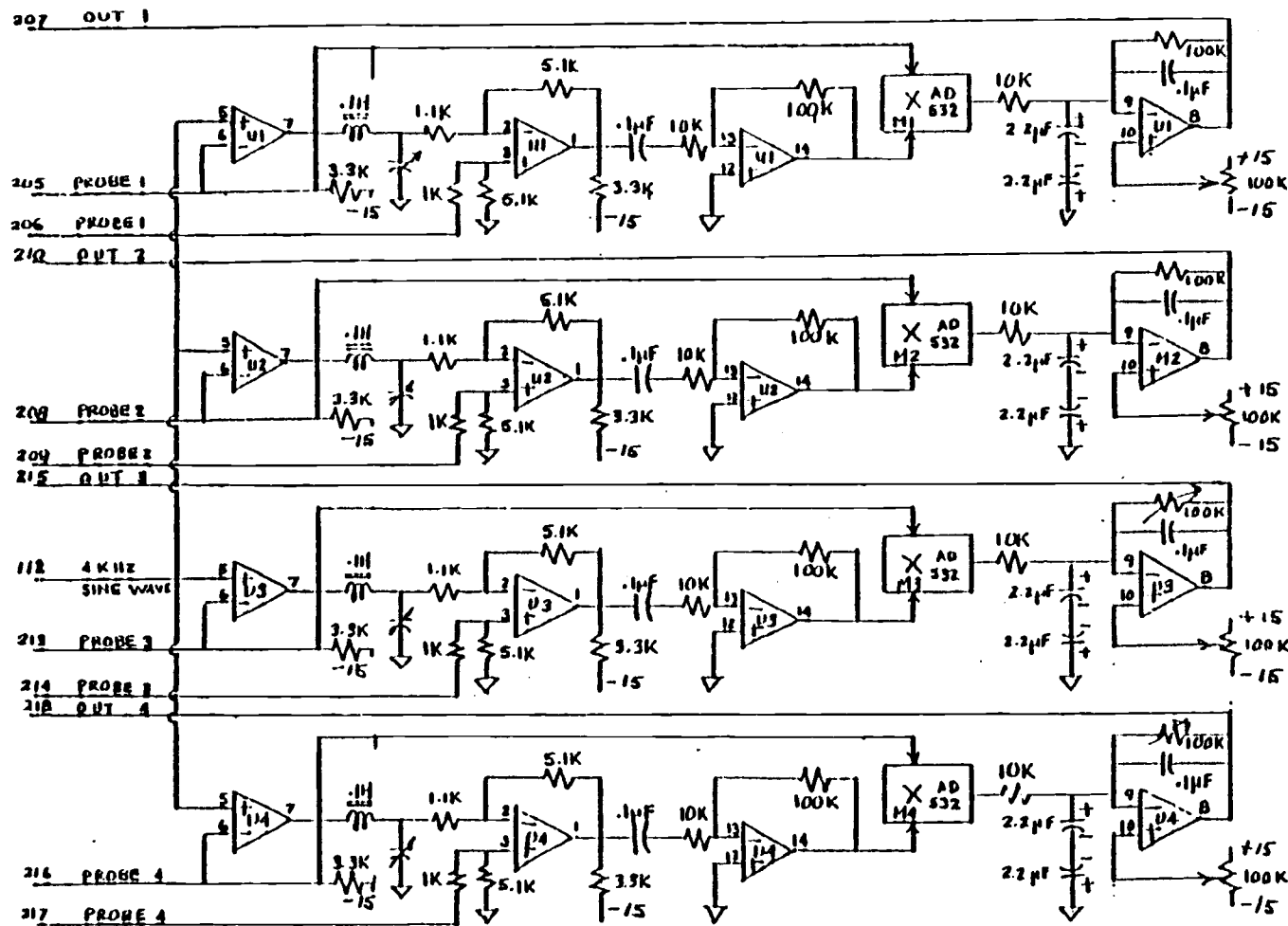


Figure 3.10 Schematic drawing of an inductance bridge card.

There are four inductance bridge amplifiers on a card.

All of the signals were sent to a 128- channel analog to digital converter which forms the real-time interface with the Data General Nova 840 Minicomputer where all of the data were collected and processed. The CDC 3000 computer was used for more complicated calculations.

#### IV. SLUMPED BED SURFACE PROFILES

##### 4.1 Background

The first study concerning slumping behavior conducted in the partially defluidized bed was the investigation of the slumped bed surface profiles or the shape of the ridges as they appeared in the slumped section during the time of partial fluidization.

Bauver et al. (3) presented a report about the evaluation of slumped bed testing. Active and slumped bed surface profiles in a 1.72 m by 0.86 m cold fluidized bed were recorded. The authors concluded that equilibrium bed levels can be expected in approximately one hour or less. In their experiments, the fluidized height of the active bed was decreased due to the transferring or entrainment of the bed material to the adjacent slumped section and no compensating bed material was added to the active side of the bed.

Chao (8) investigated the slumping behavior in a cold phase fluidized bed. He primarily observed the slumped bed surface profiles at different slumping ratio and also developed a model to predict a pressure loss parameter in the active and the slumped bed sections of the fluidized bed.

Lackey and Withers (34) also conducted a slumping test in a 1.20 m by 1.20 m cold phase fluidized bed. Effects of gas flow to the slumped section on the surface profiles during the refluidization were observed. They found that a slip plane zone existed and the contours or profiles of the slumped bed changes as a function of the air supplied to the slumped section of the bed.

However, none of these studies above were concerned about the depletion of the bed material in the active side due to particle entrainment. In reality, the residence time of gas passing through the bed was reduced since the bed was now shallow. The amount of limestone available for scavenging sulfur was also reduced, and there were less solids to enhance heat transfer to the steam tubes. In this experiment, the effect of active bed material depletion was included. Material was continuously added to the active part to keep the active height constant.

#### 4.2 Procedure

To obtain slumped bed surface profiles, half of the bed was defluidized or slumped by simultaneously closing the butterfly valve to the windbox under half of the bed and opening the air bypass valve, hence leaving the velocity in the fluidized or active section unchanged. A ridge of material was immediately observed in the slumped section and continued to grow with time. Figure 4.1 shows the location of the slumped bed surface profiles in the bed. Profiles of the slumped bed were traced and recorded at every 5 minutes. After the first profile was observed, a polar planimeter was used to determine the area of the profile. The measured cross sectional area obtained by the polar planimeter times the width of the bed represents the volume of the bed material transferred. The weight of the material transferred was obtained since the bulk density of the bed media was known. The amount of the material corresponding to the calculation above was added to the active



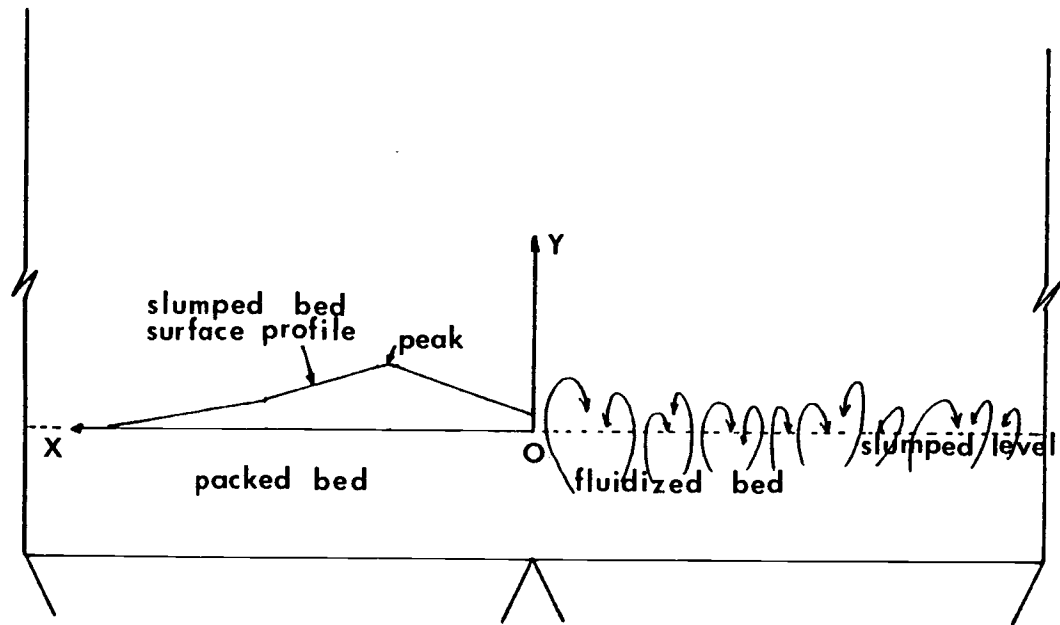


Figure 4.1 The location of the slumped bed surface profile in the experimental fluidized bed.

part of the bed. It was found that the active bed level after adding the material remained the same as before defluidization. Another profile was then obtained and the whole process was repeated at 5 minutes intervals for 45 minutes after defluidization. Sets of slumped bed surface profiles were obtained at different superficial velocities, i.e., 0.38 m/s, 0.45 m/s, 0.53 m/s, 0.61 m/s, 0.69 m/s and 0.76 m/s (1.25, 1.50, 1.75, 2.0, 2.25 and 2.5 ft/s respectively). Samples of the recorded profiles are shown in Figures 42 a, b, and c.

#### 4.3 Result

From the sample bed profiles recorded as shown in Figures 4.2a to 4.2c, it can be seen that the profiles can be divided into three separate regions,

1. The side of the ridge that slopes into the interface region.
2. The side of the ridge that slopes away from the interface region to the point  $x^*$  where the slope changes.
3. From the point  $x^*$  to the bottom of the ridge.

By setting a coordinate  $(x,y)$  at the interface region of the surface level (Figure 4.1), a set of equations to describe the profiles can be made in terms of the abscissa  $(x)$ , and the ordinate  $(y)$ , location of the peak of the ridge in the  $x$  direction  $(x^p)$ , location of the peak of the ridge in the  $y$  direction  $(y^p)$ , the location where the slope of the ridge change in the  $x$  direction  $(x^*)$ , excess velocity  $(u-u_{mf})$  and the time after defluidization  $(t)$ .

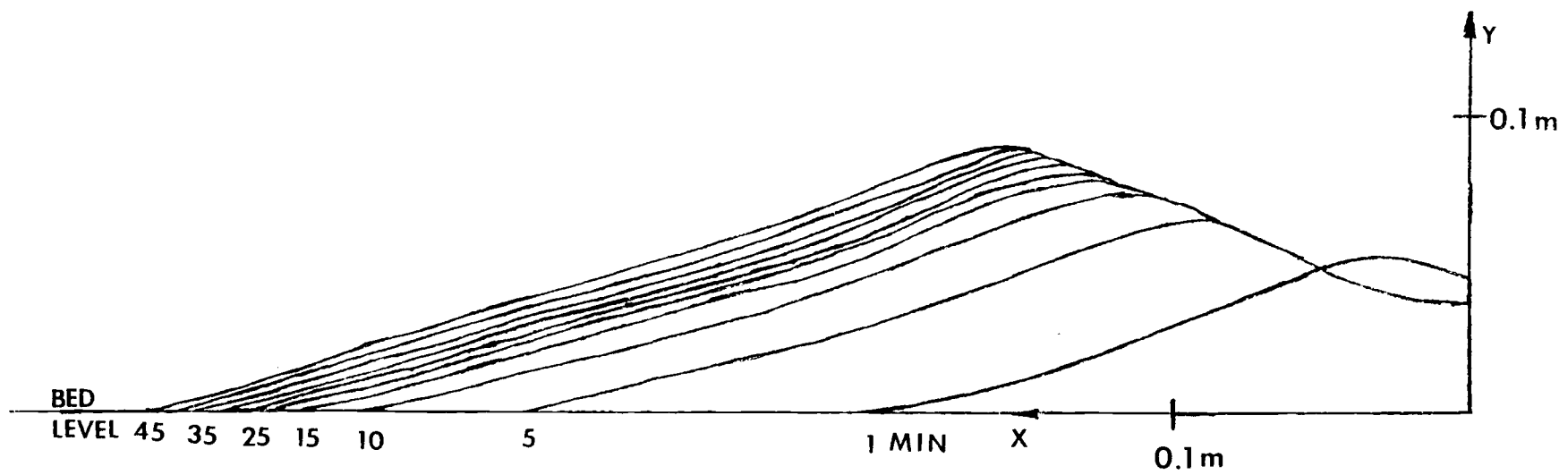


Figure 4.2a The slumped bed surface profiles as a function of time at  $u = 0.45$  m/s.

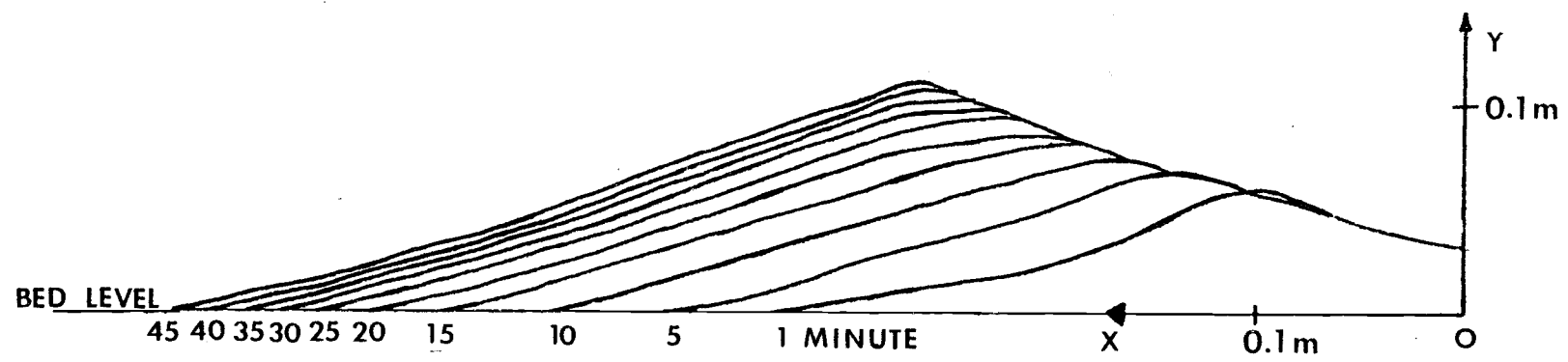


Figure 4.2b The slumped bed surface profiles as a function of time at  $u=0.61$  m/s.

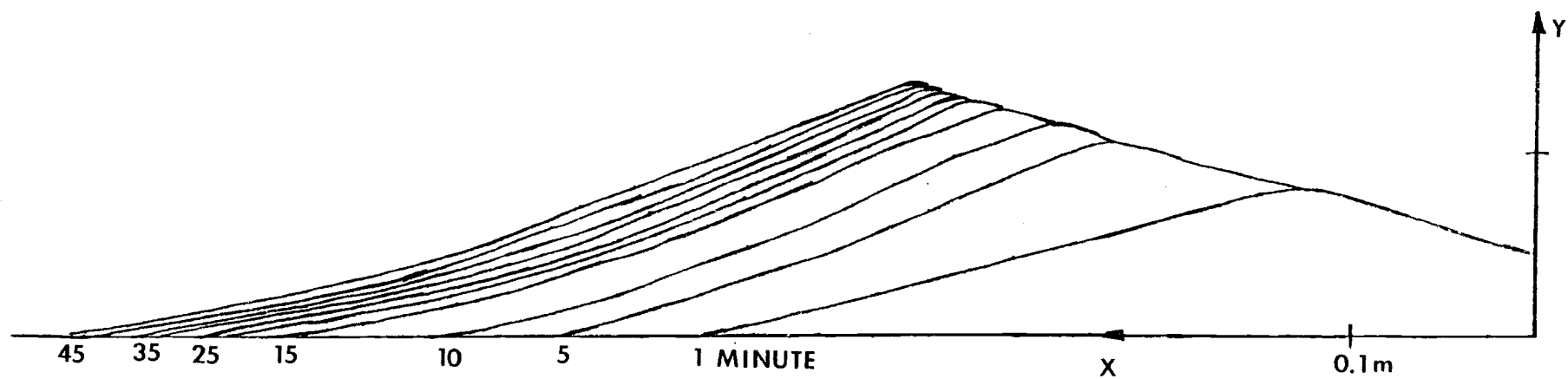


Figure 4.2c The slumped bed surface profiles as a function of time at  $u=0.76$  m/s.

First, the location of the peak of the ridge can be related to the time ( $t$ ) and the excess gas velocity ( $u-u_{mf}$ ) by

$$x^p = 0.3464 t^{0.1257} (u-u_{mf}) \quad (4.1)$$

$$y^p = 0.03 + 0.1086 t^{0.1333} (u-u_{mf}) \quad (4.2)$$

The profiles of the three separate regions can be described by

$$y = 0.03 + 0.28 (u-u_{mf})^{0.21} x^{0.79} \quad \text{for } x < x^p \quad (4.3)$$

$$y = y^p \left( 1.0 - \left( \frac{(x-x^p) t^{(0.066(u-u_{mf})-0.066)}}{0.01 \exp(2.83+0.633(u-u_{mf}))} \right) \right) \quad \text{for } x^p < x < x^* \quad (4.4)$$

$$y = y_x^* \left( 1.0 - \left( \frac{(x-x^*) t^{(1.17(u-u_{mf})-1.13)}}{0.01 \exp(-2.56+6.33(u-u_{mf}))} \right) \right) \quad \text{for } x^* < x \quad (4.5)$$

where  $y_x^*$  is the value of  $y$  evaluated at  $x^*$  from equation (4.4) and  $x^*$  is obtained from

$$x^* = x^p + 0.01 \exp \left( (3.1245 - 1.64(u-u_{mf}) + 0.2222(u-u_{mf})^2) + (3.145 \times 10^{-3} - 3.653 \times 10^{-2}(u-u_{mf}) + 2.667 \times 10^{-2}(u-u_{mf})^2) t \right) \quad (4.6)$$

The plot by using the correlations above is demonstrated in Figure 4.3 where they are compared to an actual profile as measured in the experimental study.

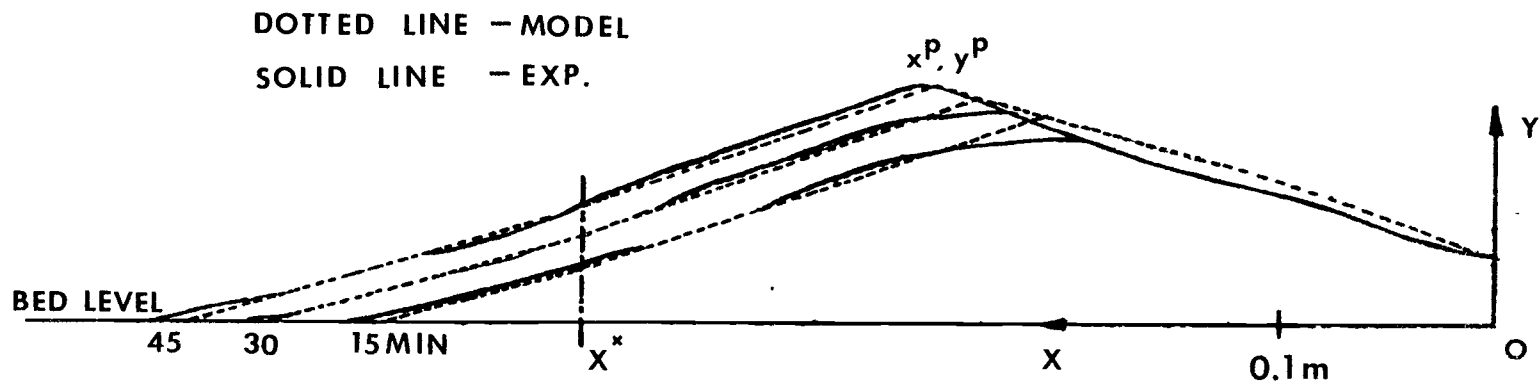


Figure 4.3 Comparison of the slumped bed surface profiles as a function of time between analytical model and the experimental data at  $u = 0.61$  m/s.

#### 4.4 Discussion

As half of the fluidized bed is slumped, the ridge formed by the transferred material was observed instantly. The location of the peak of the ridge changed in both x and y directions as time increased. It was observed that the rate of change of location of the peak ( $x^p, y^p$ ) depended on both excess gas velocity and time after defluidization. It was also observed that the angle of the ridge that slopes into the interface region is approximately 17 degrees which is the same as the angle of repose of the material used in the experiment.

Further observations about the interface region were made. It was found that part of the active bed that was adjacent to the slumped section was also defluidized even though fluidizing air was supplied to the entire active bed (Figure 4.4). This confirms the results obtained by both Bauver et al. (3) and Lackey (34). This partially active bed defluidization may occur because of the hydrostatic pressure differential between both sides of the bed or the effect of air bypassing from the active bed through this section to the adjacent slumped bed. The effect of air bypassing will be discussed more in the next chapter.

The area under each profile times the width of the bed represents the volume of the bed material transferred during the defluidization period. A numerical method (Simpson's rule) listed in Appendix B was used to obtain the area under the profiles. Results obtained from the model are compared to the experimental data obtained by using polar planimeter to measure the area of the recorded slumped bed profiles. The comparison shown in Figure 4.5 indicated that there are good agreements between the data and the correlations are within  $\pm 10\%$ .



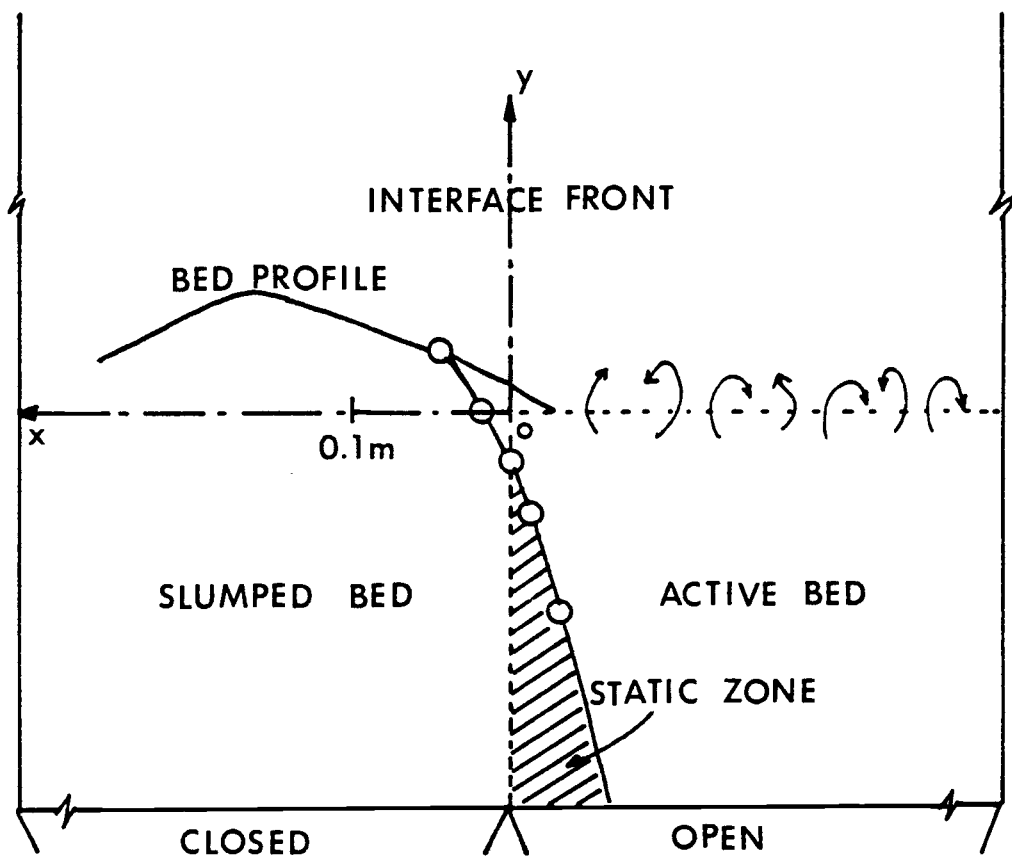


Figure 4.4 Schematic drawing indicates part of the active bed is defluidized.

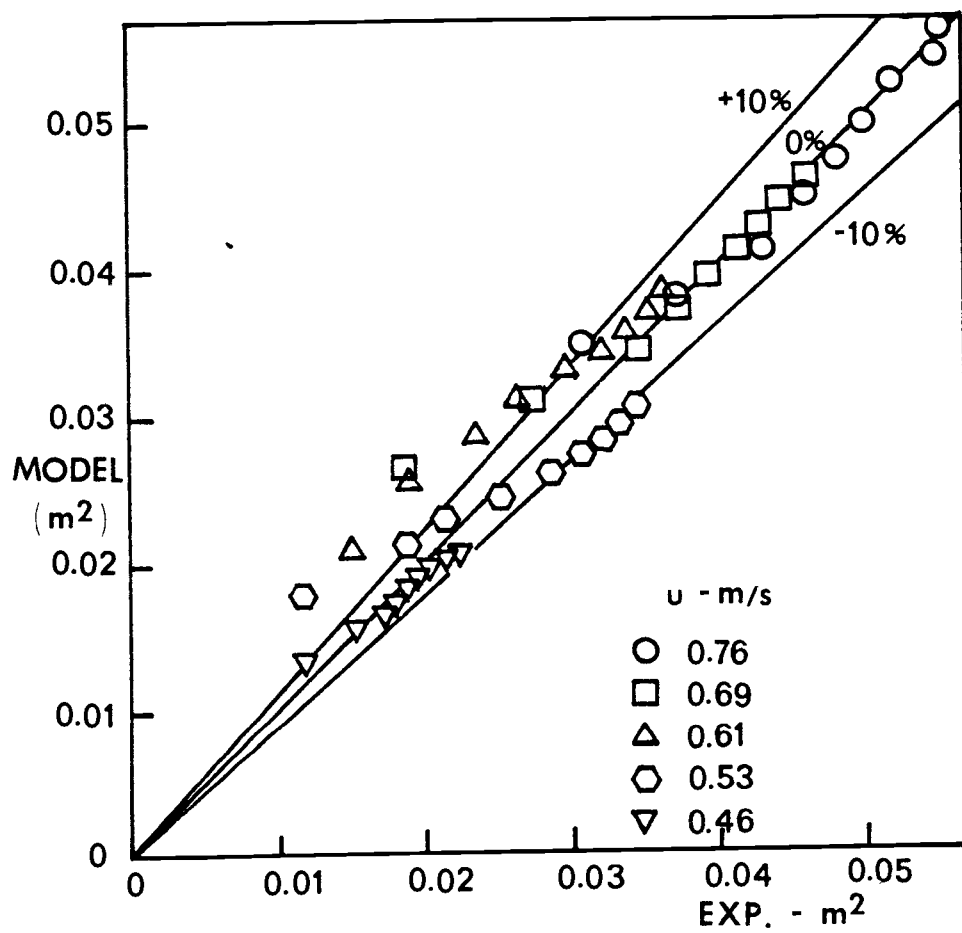


Figure 4.5 Comparison of the slumped bed surface profiles between the experimental data and the correlation.

## V. BED MATERIAL TRANSFER, MODEL AND EXPERIMENT

### 5.1 Background

#### Entrainment

As half of the bed is defluidized, bed material from the active side of the bed was transferred to the adjacent slumped section. This phenomena occurred because of the entrainment of bed particles from the active bed surface. The word "entrainment" was described by Kunii and Levenspiel (32, 33) as "the removal of solids from the bed by fluidizing gas". Solids which entrain from the surface of the active bed will fall back to both sections of the bed. Solid particles that fall back to the slumped section and deposit themselves over the static bed are defined to be transferred bed material.

Several investigations were conducted in various aspects of entrainment. These are summarized and shown in Table 5.1.

Zenz and Weil (63) were the first to develop a model to describe the entrainment mechanism. They used the theoretical approach through forces acting on the particles to find the rate of entrainment of solids from a commercial-size fluidized bed. The same authors also found that the intermittent bursting action of bubbles causes a higher irregular velocity fluctuation above the surface of the dense bed. These fluctuations dissipated with the height above the surface of the dense bed.

Lewis et al. (35) indicated that entrainment of closely sized particles is not significant at low velocity ( $u < u_t$ ), but it will

Table 5.1 Summary of the conditions for entrainment of particles studies from other investigators.

Investigator	Vessel Diameter, $d_t$ Bed height, $L_m$ Freeboard, $H_m$ (cm)	Gas	Particles	Size ( $\mu$ )	Superficial velocity (cm/sec)
Zenz and Weil (63)	2-D bed, 5.1 by 61, $d_t=5.1, 10.2$	air	FCC catalyst with size distribution	200- 1500	30-72
Lewis, Gilliland and Lang (35)	$d_t=1.9-14.6$ $L_m=10.2-71$ $H_m=92-316$	air	glass, iron polystyrene, cracking ca- talyt	510- 3610	28-476
Andrews (1)	$d_t=3-10$	air $N_2$	Fluid coke, FCC catalyst	50- 100	30-762
Do et al. (15)	2-D bed, 56 by 1	air	glass beads	117- 250	

increase strongly, roughly by a factor of 100 for a doubling of gas velocity when  $u > u_t$ .

Andrews (1) indicated that as bubbles rise through the dense phase and erupt at the surface of the bed, solid particles will be ejected into the freeboard. By assuming that the energy of particles at the surface of the dense phase follows the Maxwell-Boltzmann distribution, he was able to show an exponential decay of the entrainment rate with respect to the freeboard height.

Do et al. (15) also developed a model to predict the motion of particles in the freeboard by using the theoretical approach through forces acting on the ejected particles. They obtained the velocities of ejection when bubbles broke the surface by using photography of a 2-D column and found that initial velocities of ejected particles are somewhat higher than the rise velocity of the corresponding bubble. They also concluded that the velocities of ejection are much higher when bubbles coalesce right at the surface of the bed.

#### Effect of bubbles on the entrainment

Several investigations were conducted to study how bubbles affect the entrainment of solids from the surface of the bed. Lewis et al. (35) pointed out that gas bubbles rising through the fluidized bed may entrain solids or bed particles in two different ways,

1. Individual particles falling or raining through the top of the bubble and then carried away by the gas at the moment they leave the dense bed.

2. The bursting of gas bubbles at the surface of the dense bed removes particles from the dense bed and projects them upward. The same authors also pointed out that the first possibility did not dominate the solid entrainment and can be neglected.

Chen and Saxena (9) included another possibility that may cause entrainment. Particles in the bubble wake are thrown up into the free-board after bubble eruptions. However, Rowe and Partridge (50) indicated that as a bubble rises in a bed it carries a wake of circulating particles behind it, after the bubble and wake break the surface the wake is left on the surface as the bubble bursts. Therefore, it can be concluded that there is only one possibility that causes solid entrainment, solids are ejected at the surface of the bed as the bubble erupts.

## 5.2 Physical Model

### Introduction

In order to develop a model to describe the entrainment of particles from an active bed and the accumulation of entrained particles in the adjacent slumped bed, the initial velocities of ejected particles, the amount of ejected particles and their trajectories after an eruption must be determined. To study the rate of entrainment, the frequency of bubble eruption must also be measured. The amount of entrained particles that accumulates in the slumped section can be determined finally by knowing the particles trajectories.

### Initial velocities of ejected particles

As bubbles rise to the surface of a fluidized bed, bulges are formed at the surface of the bed. The bulges grow larger as bubbles approach the surface of the bed. The bulges will finally burst as the bubbles immerse from the dense phase. It is presumed that the velocities of particles released from the domes of bubbles during eruption are the same as the velocities of the moving bulges formed at the surface of the fluidized bed. Further assumptions have to be made, i.e.,

1. the dense phase of the fluidized bed is assumed to be an incompressible inviscid fluid,
2. the rising bubbles are assumed to be solid-free and circular in shape.

As the fluid is inviscid, the potential flow theory can be applied to the dense phase of the bed. Davidson and Harrison (13) successfully developed a model for a bubble rising velocity. Furthermore, the stream function of the solids in a vicinity of the rising bubble is also developed and can be expressed as,

$$\psi = - \frac{u_b r_b^3 \sin^2 \theta}{2r} \quad (5.1)$$

The stream function described in equation (5.1) is shown in Figure 5.1. If  $u_r$  is defined as the velocity of solids at any distance  $r$  away from the center of the rising bubble in  $r$  direction, then

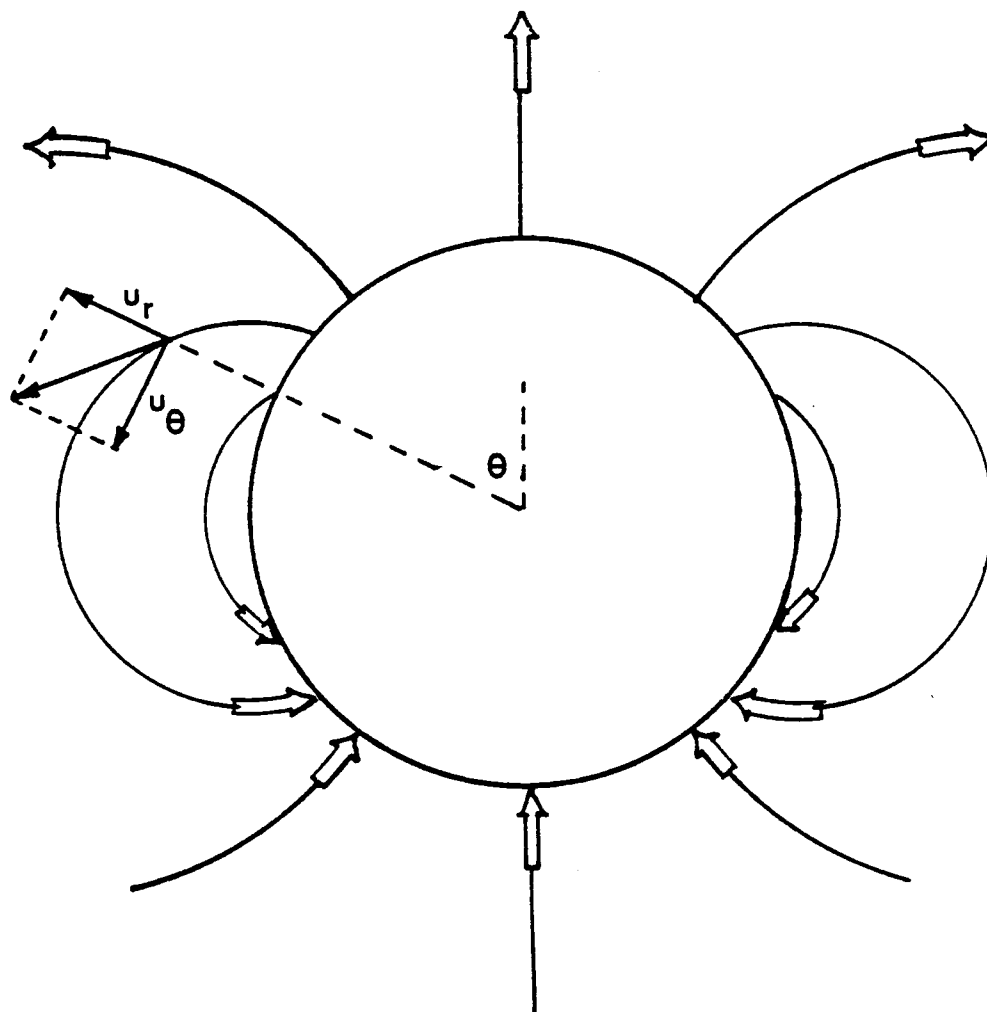


Figure 5.1 The motion of solids in the vicinity of a rising three dimensional bubble as viewed by a stationary observer from potential theory.



$$\begin{aligned}
 u_r &= - \frac{1}{r^2 \sin \theta} \frac{\partial \psi}{\partial \theta} \\
 &= - \frac{1}{r^2 \sin \theta} (-u_b r_b^3 \sin \theta \cos \theta / r) \\
 &= u_b \left( \frac{r_b}{r} \right)^3 \cos \theta
 \end{aligned} \tag{5.2}$$

For a single rising bubble, the velocity of the rising bubble is equal to the velocity of the bubble relative to the surrounding emulsion phase,  $u_{br}$ , which was proposed by Davidson and Harrison (13) as,

$$\begin{aligned}
 u_{br} &= 0.711 (gd_b)^{0.5} \\
 &= 22.26 d_b^{0.5}
 \end{aligned} \tag{5.3}$$

However, single bubbles are not often found in any commercial fluidized bed. The swarms of bubbles move continuously through the bed. The velocity of rising bubbles in a swarm was expressed by the same authors as,

$$\begin{aligned}
 u_b &= u - u_{mf} + u_{br} \\
 &= u - u_{mf} + 22.26 d_b^{0.5}
 \end{aligned} \tag{5.4}$$

Thus, the velocity of any particle in the bed at a distance  $r$  from the center of the rising bubble can be expressed as,

$$u_r = (u - u_{mf} + 22.26 d_b^{0.5}) \left( \frac{r_b}{r} \right)^3 \cos \theta \tag{5.5}$$

The schematic representation is shown in Figure 5.2.

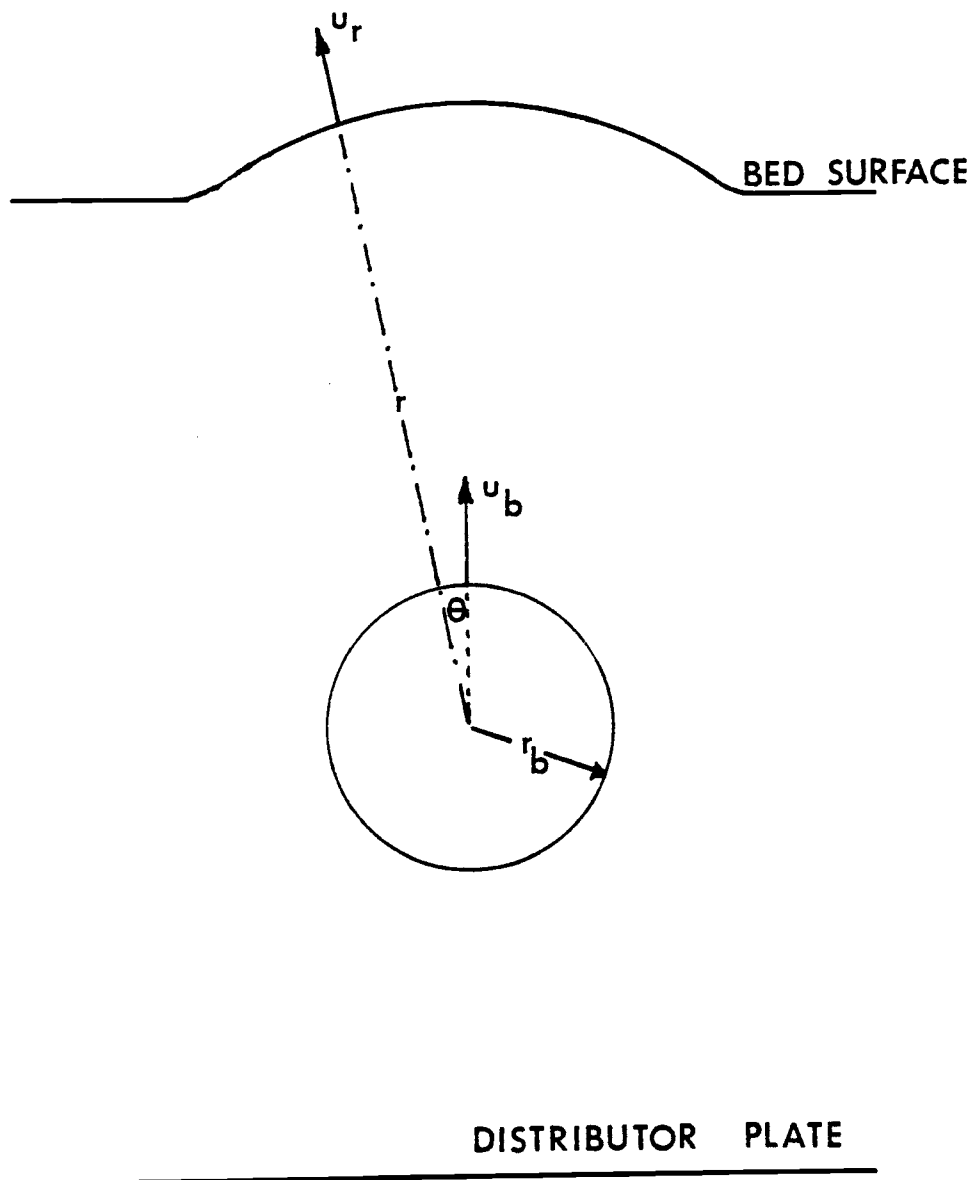


Figure 5.2 Schematic representation of a bubble rising in a fluidized bed.

To find the initial velocities of ejected solid particles ( $u_i$ ), the value of  $u_r$  in equation (5.5) must be calculated at the moment the eruption occurs. It is hypothesized that the eruption happens when half of the bubble merges from the dense bed or the center of the bubble is at the surface of the bed. It is further assumed that the ejected solid particles are the particles that are attached to the bursting bubble. Therefore, the distance  $r$  can be approximately equal to  $0.5 d_{bm}$ , where  $d_{bm}$  is the diameter of the bubble at the surface of the fluidized bed. Thus,

$$u_i = (u - u_{mf} + 22.26 d_{bm}^{0.5}) \cos \theta \quad (5.6)$$

However, Do et al. (15) who measured the initial velocities of ejected particles in a two dimensional bed indicated that the initial velocity of the ejected particles exceeded the steady bubble rise velocity by 15%. The causes of this effect may come from either the expansion of bubbles as they reach the surface or the gas through flow inside the bubbles in fluidized beds (10).

During most of the experiments, it was observed that two bubbles coalesced at the surface of the bed and particles were ejected from the bursting bubbles with initial velocities exceeding the initial velocities obtained from equation (5.6), typically by 100%. The cause of this phenomenon is due to the projection of particles from a trailing bubble to a leading bubble when two bubbles coalesce (10). Therefore, the initial velocities of ejected particles when two bubbles coalesce at the surface of the bed can be modified as,

$$u_{i, \text{ measured }} = k_u u_{i, \text{ theory }} \quad (5.7)$$

where  $k_u$  is the constant that was obtained from the experiments to relate the measured initial velocity ( $u_{i, \text{ measured }}$ ) with the theoretical initial velocity ( $u_{i, \text{ theory }}$ ) which is calculated from equation (5.6). From the experiment, when the superficial velocity varies from 0.46 m/s to 0.76 m/s, it was found that the value of  $k_u$  was equal to 2.0 ( $\pm 20\%$ ). George and Grace (24) who conducted experiments about the entrainment of particles from aggregative fluidized beds indicated that the ratio of the initial velocity to the rising velocity of a bubble varied from 1.5 to 6.5 and 50% of the ejected particles have a velocity of 2.1 times the bubble rising velocity. The average value of the ratio  $u_i/u_b$  from their experiment was found to be 2.45. It can be seen that the value of  $k_u = 2.0$  obtained from this experiment is in the good agreement with their experimental data. Thus,

$$u_i = 2.0 (u - u_{mf} + 22.26 d_{bm}^{0.5}) \cos \theta \quad (5.8)$$

From equation (5.8), the initial velocities of ejected particles can be determined if the diameter of bubbles at the surface of the bed ( $d_{bm}$ ) are known.

#### The diameter of a bubble at the surface of a fluidized bed

It was found that coalescence of bubbles lead to an increase of bubble size with bed height. The coalescence of bubbles involves lateral movement of bubbles, and bubbles tend to rise in preferred paths (62). It was also observed that the number of paths decrease with height above

the distributor plate (20). Many researchers have developed the model to determine the size of bubbles in a fluidized bed. Mori and Yen (43), Rowe (46), Kato and Wen (31), Geldart (21) and Darton et al. (12) all found that the diameter of the bubble in a fluidized bed is mainly a function of excess gas velocity ( $u - u_{mf}$ ), height above distributor plate ( $h$ ) and the initial size of bubble at the distributor plate ( $d_i$ ) which in turn depends on the type of the distributor plate (Table 5.2). The models and equations proposed by the workers above apply only in an open fluidized bed (no internal heat exchange tubes). However, a fluidized bed to be used as a fluidized bed combustor would require a bundle of heat exchange tubes to be placed in the bed which will affect the size of bubbles in the bed. Nguyen et al. (44) indicated that the eruption diameters of bubbles at the surface of a bed with immersed horizontal tubes were smaller than the bubble eruption diameters in an open bed at the same height and velocity. Thus, it is required to develop a model to determine a bubble size in a fluidized bed with immersed heat exchange tubes.

The size of bubbles used in the experiments are measured in terms of eruption diameter at the surface of the bed ( $d_o$ ). Botterill et al. (4) indicated that when a bubble breaks the surface the diameter of the eruption bubble was nearly 50% larger than of the bubble causing it. Geldart (23) also confirmed this result, he points out that the diameter of a bubble was estimated as  $2/3$  of the eruption diameter. George and Grace (24) found this ratio to be 1.41 for silica sand with  $d_p$  of  $358 \mu\text{m}$  compared with the value of 1.55 found by Harrison and Leung (27).

Table 5.2 Published correlations for estimating bubble size in fluidized beds.

Author	Correlation
Mori and Wen (43)	$d_e = d_{em} - (d_{em} - d_i) \exp(-0.3h/D_t)^{0.4}$ <p>where <math>d_{em} = 1.63(A_t(u - u_{mf}))^{0.4}</math>  <math>d_i = 0.87(A_t(u - u_{mf})/n_d)^{0.4}</math>  for perforated plate  <math>d_i = 0.376(u - u_{mf})^2</math>  for porous plate</p>
Rowe (46)	$d_e = (u - u_{mf})^{0.5} (h + h_o)^{0.75} / g^{0.25}$
Kato and Wen (31)	$d_e = 1.4 \rho_s d_p (1 + (u - u_{mf})/u_{mf}) h + d_i'$ <p>where <math>d_i' = (6G/\pi)^{0.4} / g^{0.2}</math></p>
Galdart (21)	$d_b = 1.43((u - u_{mf})\pi D^2/4N_o)^{0.4} / g^{0.2} + 2.05(u - u_{mf})^{0.94} h$
Darton et al. (12)	$d_b = 0.68(u - u_{mf})^{0.4} (h + 4\sqrt{A_o})^{0.8} / g^{0.2}$

In this experiment, a value of about 1.4 was found and used to relate the eruption diameter and mean bubble diameter, i.e.,

$$d_o = 1.4 d_b \quad (5.9)$$

From Table 5.2, most of the correlations were developed in terms of an equivalent spherical diameter of bubble ( $d_e$ ). It is required to relate the equivalent spherical diameter ( $d_e$ ) which is defined as the diameter of the sphere having the same volume as the bubble, and the eruption diameter ( $d_o$ ) measured in this study. Rowe (47) suggested that the shape of bubbles are essentially spherical with radius,  $r_b$  and wake fraction,  $f_w$ . The wake fraction, which is defined as the fraction of bubble sphere occupied by wake particles, is found to be mainly a function of particle diameter. According to the size of particles used in the experiment, a value of  $f_w = 0.25$  was chosen. This leaves the volume of the bubble to be about 75% of the sphere. Hence, the mean bubble diameter ( $d_b$ ) was found to be about 110% of the equivalent diameter ( $d_e$ ). Thus,

$$d_o = 1.54 d_e \quad (5.10)$$

Comparison between the correlations proposed by Mori and Wen (43), Rowe (46) and Darton et al. (12) from Table 5.1 and equation (5.10) and the data obtained from the experiment of an open bed at bed height = 0.28 m is shown in Figure 5.3. It can be seen that the correlation proposed by Darton et al.

$$d_e = 0.54 (u - u_{mf})^{0.4} (h + 4 \sqrt{A_0})^{0.8} / g^{0.2} \quad (5.11)$$

gives the best fit to the experimental data. To obtain an expression for eruption diameter ( $d_o$ ), equation (5.11) is substituted into equation (5.10) which gives,

$$d_o = 0.83 (u - u_{mf})^{0.4} (h + 4 \sqrt{A_0})^{0.8} / g^{0.2} \quad (5.12)$$

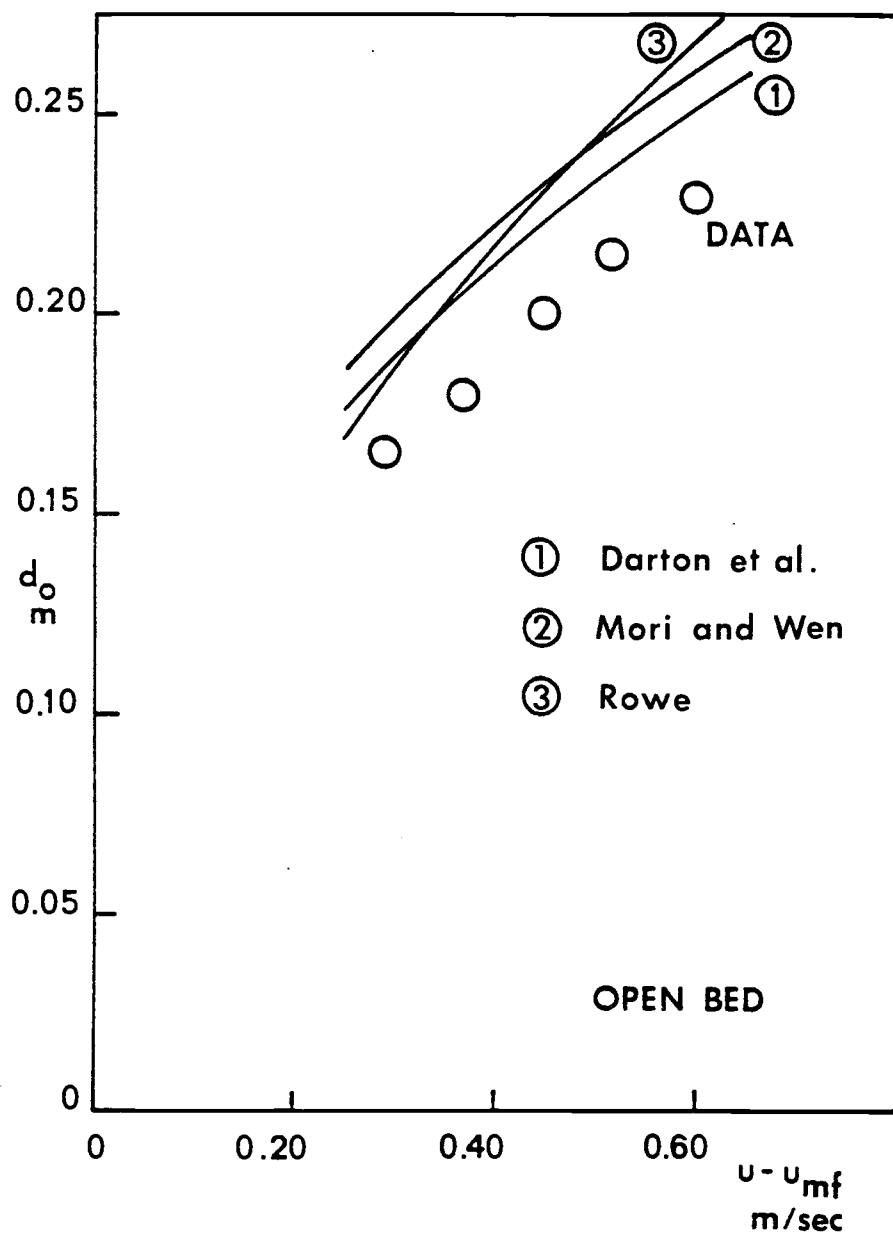


Figure 5.3 Comparison of  $d_o$  in an open bed between experimental data and the correlations presented by Mori and Wen, Rowe and Darton et al. (bed height 0.28 m).



This expression was plotted and compared to the experimental data obtained from an open bed at height 0.127 m and 0.28 m (Figure 5.4). It was observed that this correlation gave a good agreement in an open bed at two different bed heights.

In the experiment, an array of heat exchange tubes was placed in the bed with the lowest row of tubes 0.12 m above the distributor plate (Figure 3.8). It was found that as bubbles rise from the distributor plate, they will coalesce and increase in size. The rising bubbles will split as they hit the lowest row of the tube array with the resulting size of bubble being smaller and the number of bubbles increased. Botterill et al. (4) found that bubbles colliding with an obstruction (a 0.017 m diameter horizontal bar mounted 0.20 m above the distributor plate) tended to split apart and the resulting bubble frequency increased by approximately 50%. This phenomenon was confirmed by the studies conducted by Lockwood (37) and Lowe et al. (38). With different kinds of tube arrays inserted in fluidized beds, both found that air bubbles passed through the array between the individual elements and a bubble broke up into two bubbles as a result of a direct collision with a cylindrical tube.

However, as the split bubbles pass through the lowest row of the tube array, they again tend to coalesce with adjacent bubbles. The effect of bubbles splitting and coalescence as they pass through a tube array is observed to be mainly a function of excess gas velocity ( $u - u_{mf}$ ) and height of the tube array ( $h_2 - h_1$ ). Thus, an equation for bubble eruption diameter was proposed to be a function of bubble diameter at height  $h_1$ , excess gas velocity and height of the bed above the lowest

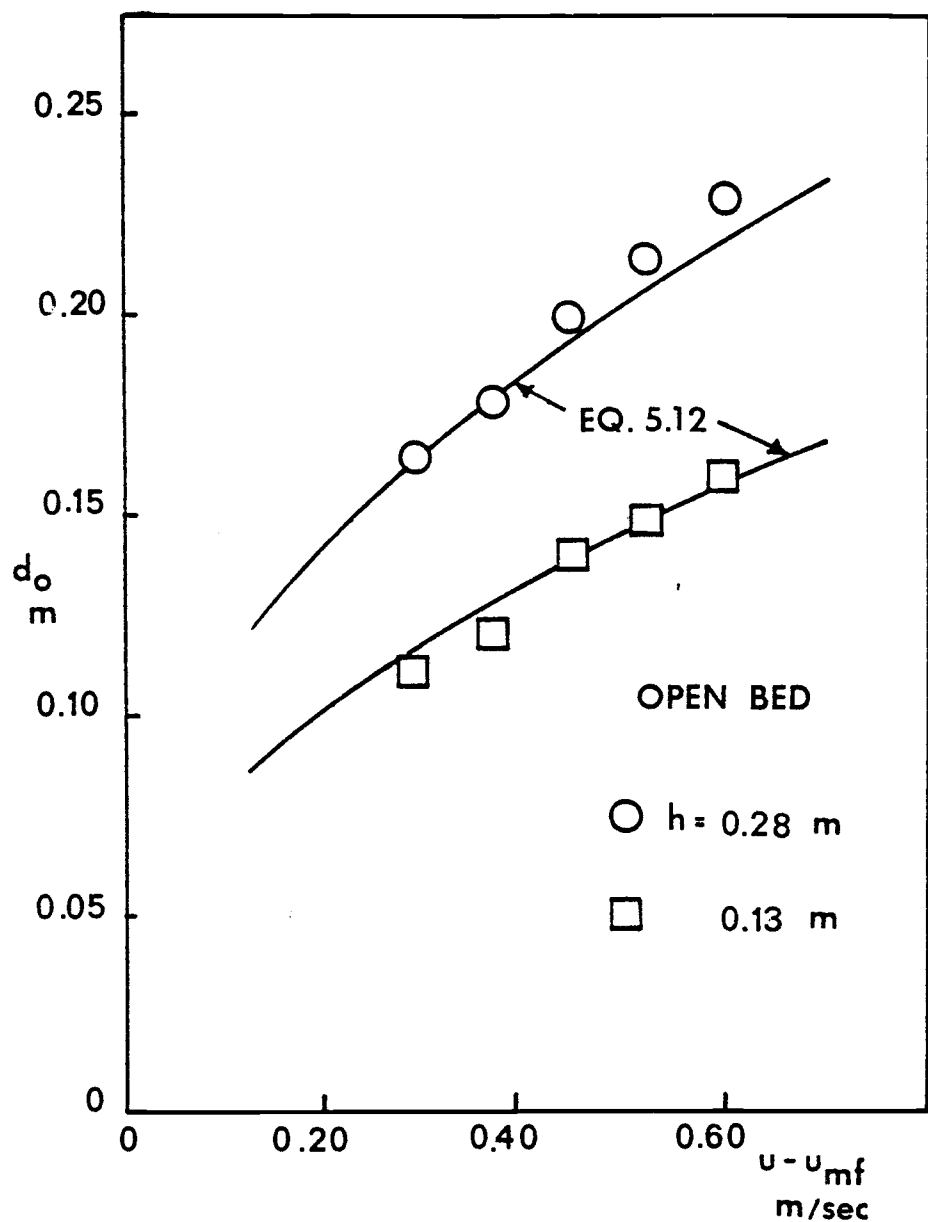


Figure 5.4 Comparison of  $d_o$  in an open bed between experimental data and the correlation proposed by Darton et al. (bed height 0.127 and 0.28 m).

row of the tube array ( $h_{\max} - h_1$ ) as,

$$d_o = d_o' + d_o'' f(u - u_{mf}, h_{\max} - h_1) \quad (5.13)$$

where  $d_o'$  is the eruption diameter at height  $h_1$  which can be obtained from equation (5.12) by replacing  $h$  by  $h_1$ , and  $d_o''$  is the growth of bubble sizes as they pass through an array of heat exchange tubes.

By using the least square method to fit experimental data, the correlation of  $d_o''$  can be expressed as,

$$d_o'' = (-0.05 + 0.0058(u - u_{mf}))(h_{\max} - h_1) \quad (5.14)$$

Thus, the bubble eruption diameter in a fluidized bed with immersed heat exchange tubes can be expressed as,

$$d_o = 0.83(u - u_{mf})^{0.4} (h_1 + 4\sqrt{A_0})^{0.8} / g^{0.2} + (-0.05 + 0.0058(u - u_{mf}))(h_{\max} - h_1) \quad (5.15)$$

The comparison between the proposed correlation in equation (5.15) and the experimental data obtained by measuring  $d_o$  at the height 0.28 m is shown in Figure 5.5. Furthermore, both equation (5.12) and (5.15) are plotted and compared to  $d_o$  measured in a 1.22 m square bed by Nguyen et al. (44) as shown in Figure 5.6. It can be seen that there is good agreement between experimental data and the proposed equations in both an open bed and the bed with an internal tube array.

The diameter ( $d_{bm}$ ) of the bubble at the surface of the bed with heat exchange tubes can be related to the eruption diameter by using the equation (5.9) and can be expressed as,

$$d_{bm} = 0.594(u - u_{mf})^{0.4} (h_1 + 4\sqrt{A_0})^{0.8} / g^{0.2} + (-0.036 + 0.0041(u - u_{mf}))(h_{\max} - h_1) \quad (5.16)$$

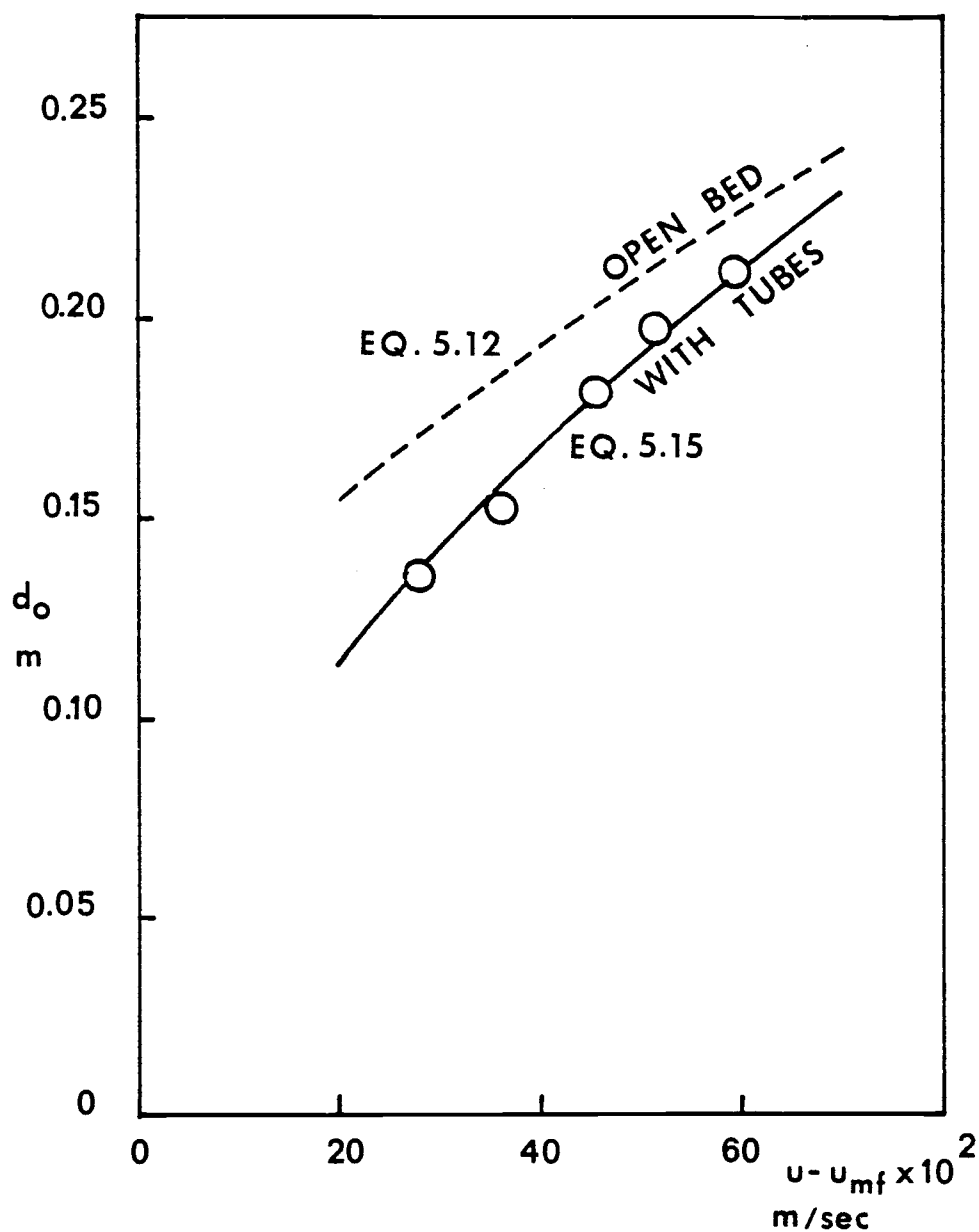


Figure 5.5 Comparison of  $d_o$  in a fluidized bed with immersed heat exchange tube array between experimental data and the correlation in equation (5.15).

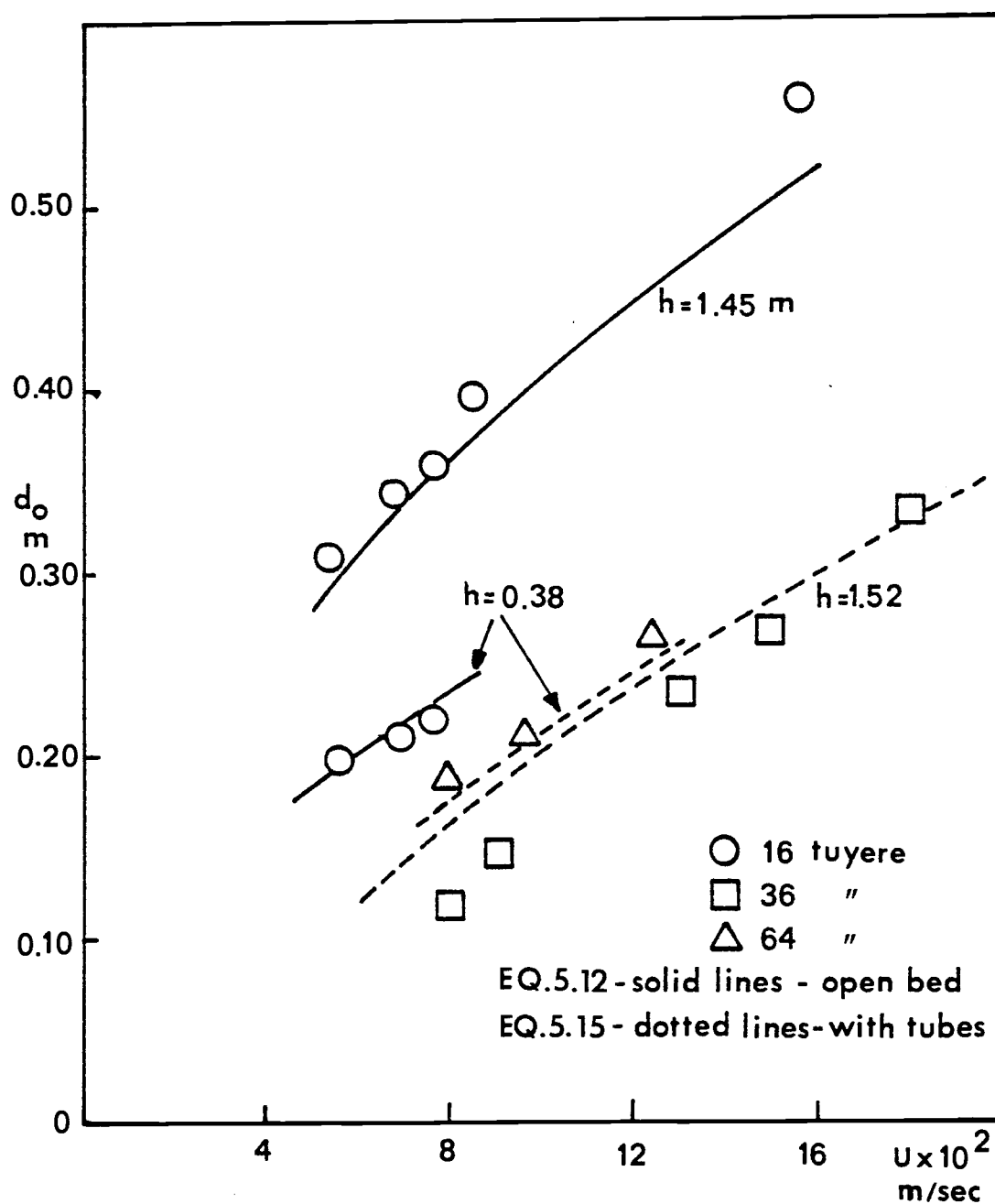


Figure 5.6 Comparison of  $d_o$  in fluidized bed with immersed heat exchange tube array between the experimental data obtained by Nguyen et al. and the correlation in equation (5.15).

This equation is substituted into equation (5.8) to determine  $u_i$ . The resulting  $u_i$  is obtained and shown as a function of excess gas velocity in Figure 5.7.

#### The trajectories of ejected particles in the freeboard region

As a bubble bursts at the surface of a fluidized bed, particles or bed material are ejected from the bursting bubble into the freeboard. If the operating superficial velocity ( $u$ ) is less than the terminal velocity ( $u_t$ ) and the height of the freeboard is longer than the transport disengaging height (TDH), the particles after entering the freeboard will fall back to the surface of the bed. Part of the down coming particles fall back into the active side of the bed and are again projected into the freeboard. However, some portion of the falling particles drop into the adjacent slumped part of the bed and accumulate in that section of the bed.

In order to determine the conditions acting on the entrained particles from the active bed, the behavior of the ejected particles in the freeboard region which includes the motion and trajectories of the particles must be considered. To develop a simple model for the motion of particles, it is required that some assumptions be made:

1. Particles are assumed to be hydrodynamically spherical.
2. Any influence of turbulence is neglected since the particle Reynolds number ( $Re_p$ ) is small.
3. The gas velocity ( $u$ ) in the freeboard is uniform.
4. The added mass is neglected since the gas density is very much less than the particles density.

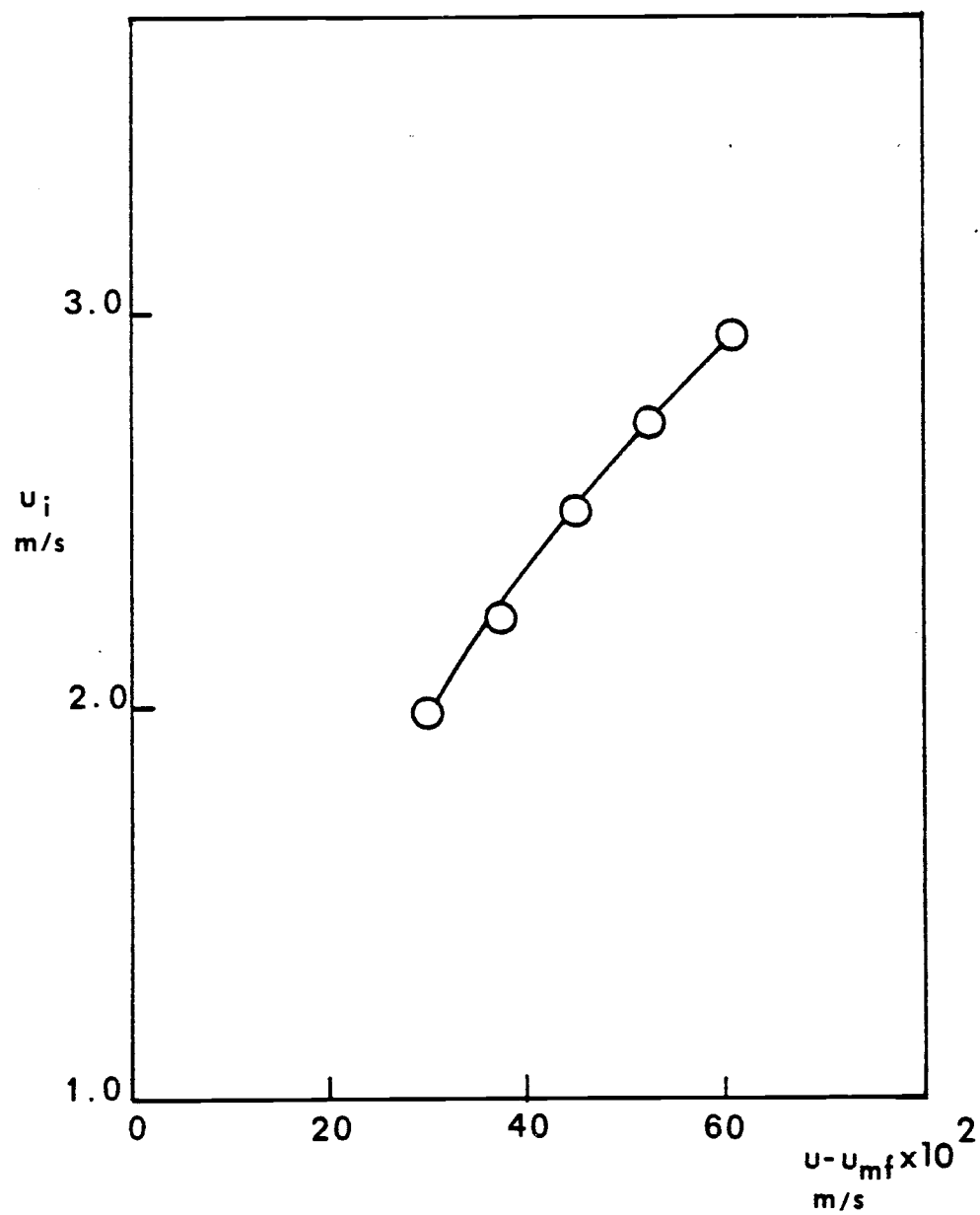


Figure 5.7 The initial velocity of ejected particles as a function of excess gas velocity.

5. Any inter-particle forces may be neglected.

The motion of the ejected particles can be described by the equation,

$$\text{inertia force} + \text{gravitational force} + \text{drag force} = 0 \quad (5.17)$$

or in mathematical terms, considering upward vectors to be positive

(Figure 5.8):

$$\text{x-direction} \quad \frac{dv_x}{dt} = \frac{3}{4} \frac{C_D \rho v_x^2}{\rho_p d_p} \quad (5.18)$$

$$\text{y-direction} \quad \frac{dv_y}{dt} = \frac{3}{4} \frac{C_D \rho (v_y - u) |v_y - u|}{\rho_p d_p} - \frac{(\rho_p - \rho)g}{\rho_p} \quad (5.19)$$

The drag coefficient ( $C_D$ ) can be expressed in terms of particles Reynolds number ( $Re_p$ ) (52). Zenz and Weil (63) used a modified Stokes Law expression for a drag coefficient, i.e.,

$$C_D = 37.5/Re_p \quad (5.20)$$

Do et al. (15) also developed an empirical equation for the drag coefficient in term of particle Reynolds number as,

$$C_D = \frac{24}{Re_p} (1.0 + 0.15 Re_p^{0.687}) + \frac{0.42}{1.0 + 4.24 \times 10^4 Re_p^{-1.16}} \quad (5.21)$$

This equation is valid for  $Re_p$  less than  $10^5$ . The drag coefficient from equation (5.21) is used in both equations (5.18) and (5.19).



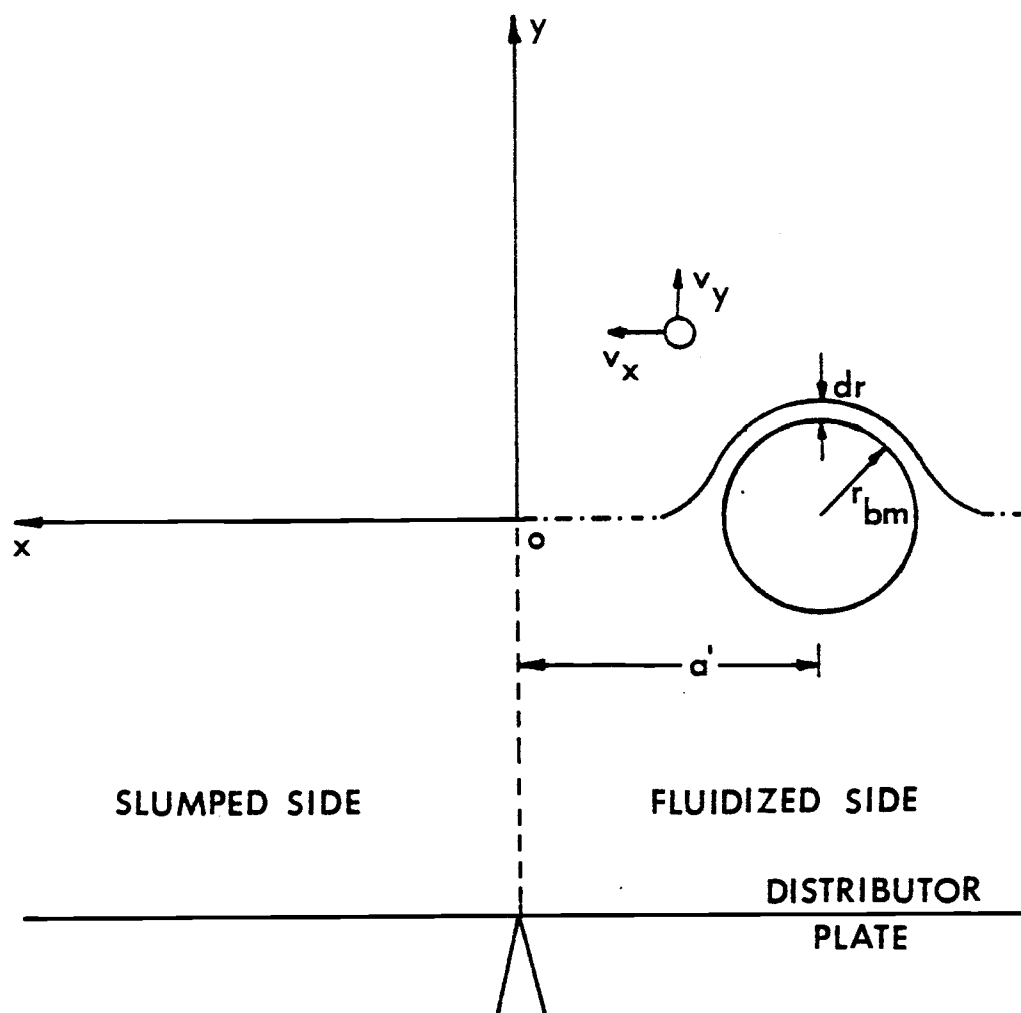


Figure 5.8 Schematic representation of a bulge formation at the moment that a bubble is half above the bed surface and is about to erupt.

Equation (5.18) and (5.19) can be solved for  $v_x$  and  $v_y$  by numerical method, using the fourth order Runge-Kutta integration with initial conditions,

$$\text{at } t=0, \quad v_x = \frac{dx}{dt} = u_i \sin \theta \quad (5.22)$$

$$v_y = \frac{dy}{dt} = u_i \cos \theta \quad (5.23)$$

From equation (5.22) and (5.23),  $x$  and  $y$  can be solved by using the same method as above with initial conditions,

$$\text{at } t=0, \quad x = (0.5 d_b \sin \theta) - a' \quad (5.24)$$

$$\text{and } y = 0.5 d_b \cos \theta \quad (5.25)$$

This model is different from the ones proposed by both Do et al. (15) and Zenz and Weil (63). Both of them assumed that the motion of particles in the freeboard to be in  $y$  direction only and the particles are ejected from the surface of the bed with the uniform initial velocity ( $u_i$ ).

#### The amount of ejected particles per an eruption

In order to determine the amount of solid particles that are ejected from one bursting bubble, it is required to know the thickness ( $dr$ ) of the bulge at the moment that the eruption occurs. Chen and Saxena (9) developed a model to describe solids projection from a fluidized bed during a bubble eruption which included an approach to find the bulge thickness ( $dr$ ). They assumed that the bulge thickness

was uniform around the bubble and was equal to the difference between the radius of bubble at the surface of the bed and the distance from the center of the bubble to the apex of the bulge, i.e.,

$$dr = r_{h=h_{\max}} - r_{bm} \quad (5.26)$$

The schematic diagram is shown in Figure 5.8. They evaluated  $r_{bm}$  by using the correlation developed by Mori and Wen (Table 5.2). They also found that the distance between the bubble center and the apex of the bulge ( $r$ ) depends mainly on the bubble size and  $h$ , and  $r$  can be solved numerically from the following differential equation,

$$\frac{dr}{dh} = \left(\frac{r_b}{r}\right)^3 - 1 \quad (5.27)$$

with the boundary condition,  $h=0$ ,  $r=h_{\max}$ . According to the calculation, it was found that the bulge thickness varied from 0.008 m at 0.45 m/s to 0.013 m at 0.76 m/s. The plots of  $dr$  as a function of superficial velocity is shown in Figure 5.9.

However, the initial velocities of ejected particles are found to depend on the positions of particles around the bubble (equation (5.6)). Thus, the trajectory of each ejected particle is different. To find the trajectory of each particle, the bulge formed at the bed surface is divided into small section with the area,  $da$ , and the thickness  $dr$ . It is further assumed that particles in each small section are formed as agglomerate. This assumption is confirmed by Kunii and Levenspiel (33) who indicated that bursting bubbles of gas projected agglomerates of particles into the space above the bed. The amount of agglomerate in each small section is approximately  $da.dr (1-\epsilon) \rho_s$ , where

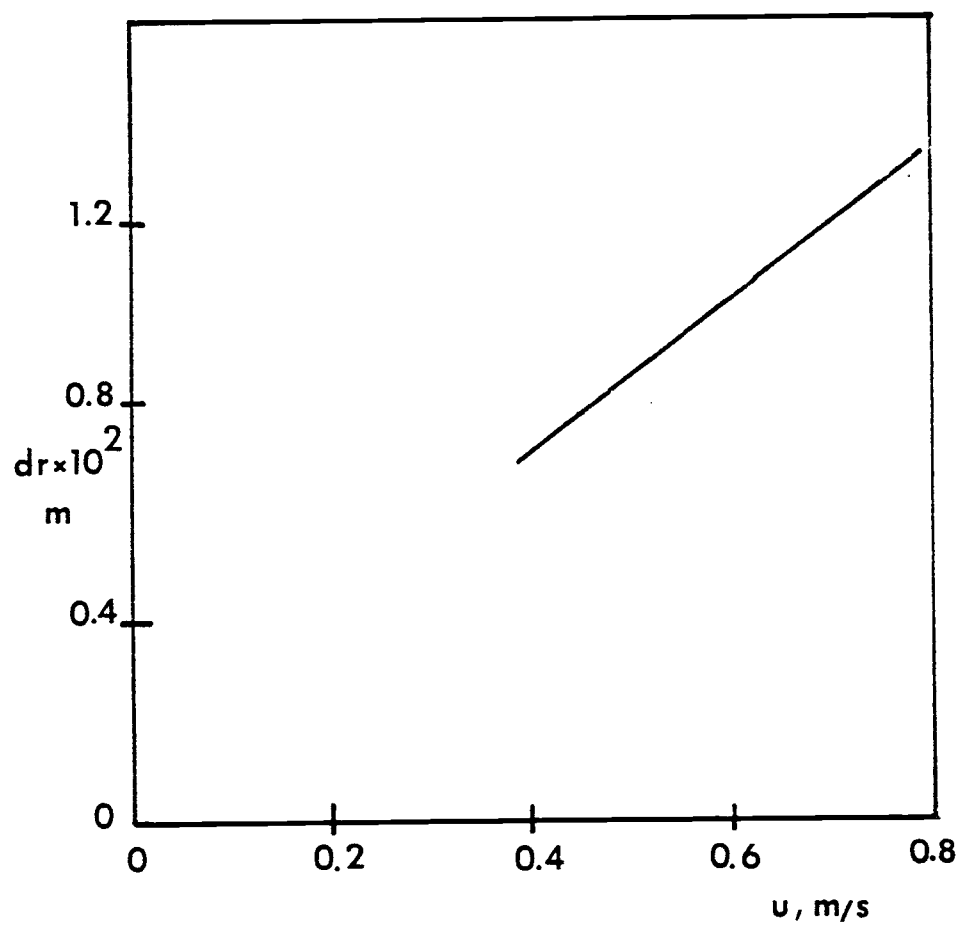


Figure 5.9 The thickness of the bulge at the moment that the eruption occurs as a function of superficial gas velocity.

da can be approximated as  $(2r_{bm}^2 \pi / \text{number of small sections})$ . The total amount of ejected agglomerates during an eruption is determined to be approximately  $2\pi r_{bm}^2 \cdot dr \cdot (1-\epsilon) \rho_s$ .

#### Particle density function and bed material transfer

To determine the rate of bed material or agglomerates that transferred from an active bed to a slumped bed due to the bubble eruption, the particle density function ( $\phi_d$ ) must also be developed. The particle density function is defined as the amount of transferred bed material accumulated in a unit area of the slumped section, per unit time at a particular height and distance from the interface region (5).

It can be seen from Figure 5.8 that particles that accumulate in the slumped part are ejected particles that have their trajectories across the interface front, or the distant that the particles move in the x direction much greater than zero ( $x > 0$ ). The ejected particles that did not cross the interface region ( $x < 0$ ) will fall back in the active side of the bed and will be finally ejected in to the freeboard again.

Computer programs were developed to find the destination of each ejected agglomerate by solving equations (5.18) and (5.19), using the initial conditions in equations (5.22) to (5.25). The values of x and y of each trajectory are obtained. However, the distance between the bubble eruption center to the interface front ( $a'$ ) must be determined first.

To determine the distant ( $a'$ ), the frequency of the bubble eruption ( $f$ ) must be studied. The frequency of bubble eruption at the bed surface was observed over a 0.3 m by 0.61 m section of the bed, and was found to be a function of excess gas velocity when the bed depth is held constant (Figure 5.10). The locations of the bubbles erupting at the bed surface are measured in terms of the distance from the center of the bubble to the interface region ( $a'$ ). The distant ( $a'$ ) can be related to the bubble eruption frequency ( $f$ ) by consuming that there will be  $n$  bubbles erupt in a period of one second, where  $n$  is the integer of the real number  $f$ . It is further assumed that, within a period of one second, the first bubble erupts at the interface region ( $a'=r_{bm}$ ), the successive bubble at  $a'=r_{bm}+\frac{L}{4} \times \frac{1}{n}$ ,  $a'=r_{bm}+\frac{L}{4} \times \frac{2}{n}$ , ..... , and the last bubble at  $a' = r_{bm}+\frac{L}{4}$  ( $\frac{L}{4} = 0.61$  m).

Since the frequency of the bubble eruption, the location of each eruption, trajectories of all agglomerates from every eruption and the amount of particles in each agglomerate are known, the particle density function ( $\phi_d$ ) can be determined.

### 5.3 Experiment

#### Particle density function measurement

The array of receptables as described in section 3.3 was used to measure the particle density function. The array of receptables was placed over the bed surface in the section required to be defluidized (left hand side of the bed). The air supply to that part of the bed was cut off, and the other section of the bed was fluidized for a period

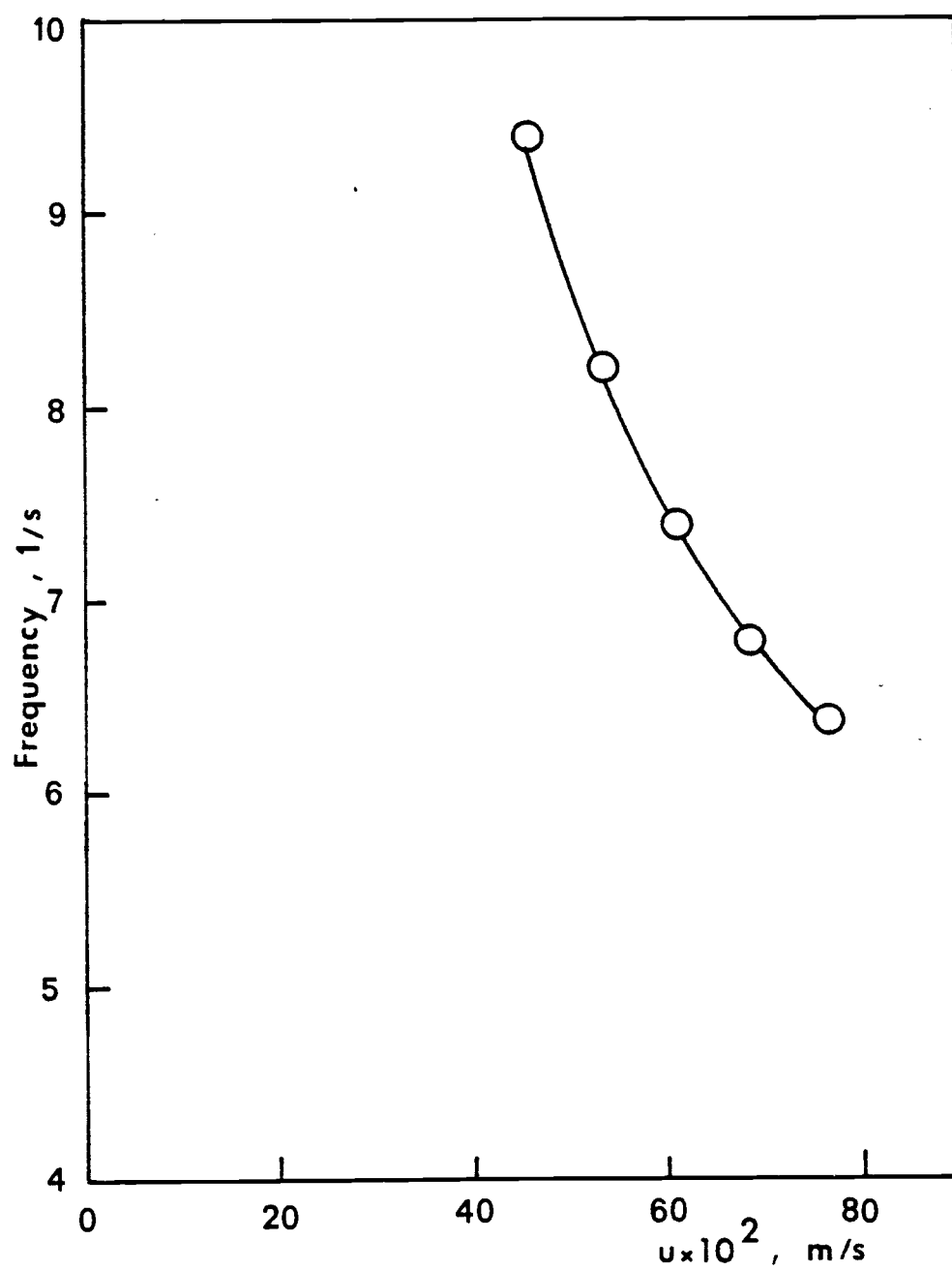


Figure 5.10 The frequency of the eruption of bubbles at the surface of the bed as a function of velocity.

of 60 seconds, then the air supply to both sections was cut off. Bed material that transferred from the active bed and accumulated in each receptable was measured. The experiments were conducted at 6 different superficial velocities over the active bed i.e., 0.38, 0.45, 0.53, 0.60, 0.68, and 0.76 m/s and at 4 different heights over the slumped bed surface i.e.,  $y = 0.076, 0.152, 0.228, \text{ and } 0.305 \text{ m}$ . The height of the static bed was 0.305 m.

### Experiment data

The weight of the bed material measured in each receptable at various superficial velocities ( $u$ ) and the height over the fixed bed ( $y$ ) is shown in Table 5.3. It can be seen that the unit of the data is  $\text{kg}/(\text{area of each receptable})(\text{min})$ . In order to determine the particle density function which has the unit of  $\text{kg}/(\text{m}^2)(\text{min})$ , some conversions had to be made. The area of each receptable is found to be  $4.56 \times 10^{-3} \text{ m}^2$  ( $7.068 \text{ in.}^2$ ). After the conversion is made, the resulting particle density function ( $\phi_d$ ) is plotted as the function of excess gas velocity ( $u - u_{mf}$ ) and the height over the fixed bed ( $y$ ) as shown in Figures 5.11a to 5.11d.

### Correlation of the experimental data

From the plots from Figures 5.11a to 5.11d, it can be seen that the particle density function can be related to the excess gas velocity



Table 5.3 Experimental data showing weight of particles captured in each receptable during the duration of one minute.

y(m)	u(m/s)	Wt.(kg/min)							
		cup#1	cup#2	cup#3	cup#4	cup#5	cup#6	cup#7	cup#8
0.076	0.38	0.0005	0.0009	0.0018	0.0036	0.0095	0.025	0.102	0.53
	0.46	0.0009	0.0018	0.0036	0.0082	0.019	0.045	0.182	0.82
	0.53	0.0018	0.0036	0.011	0.016	0.052	0.052	0.205	0.965
	0.61	0.0036	0.009	0.015	0.027	0.030	0.185	0.865	
	0.69	0.0073	0.041	0.06	0.076	0.205	0.540	1.118	
	0.76	0.0109	0.023	0.045	0.093	0.298	0.793	2.127	
0.15	0.38	0.0005	0.0005	0.0015	0.0025	0.005	0.011	0.032	0.073
	0.46	0.0015	0.0018	0.002	0.004	0.005	0.027	0.046	0.119
	0.53	0.0015	0.0022	0.003	0.007	0.023	0.048	0.097	0.265
	0.61	0.0032	0.0045	0.007	0.016	0.038	0.078	0.195	0.448
	0.69	0.0073	0.012	0.019	0.016	0.070	0.163	0.419	0.99
	0.76	0.0109	0.015	0.027	0.045	0.097	0.261	0.580	1.13
0.22	0.38	0	0	0	0.0005	0.0009	0.0018	0.007	0.011
	0.46	0	0	0.0018	0.002	0.003	0.006	0.009	0.023
	0.53	0.0004	0.0009	0.003	0.003	0.005	0.01	0.02	0.023
	0.61	0.0004	0.001	0.003	0.006	0.012	0.027	0.062	0.156
	0.69	0.0009	0.005	0.006	0.011	0.021	0.045	0.088	0.204
	0.76	0.004	0.008	0.012	0.019	0.036	0.067	0.135	0.296
0.30	0.38	0	0	0	0	0	0	0.0009	0.005
	0.46	0	0	0	0.0004	0.0009	0.0012	0.0027	0.045
	0.53	0	0.0004	0.0013	0.0018	0.002	0.0036	0.010	0.014
	0.61	0	0.0009	0.0016	0.002	0.003	0.010	0.016	0.032
	0.69	0.0013	0.002	0.003	0.005	0.007	0.013	0.024	0.044
	0.76	0.0018	0.003	0.004	0.006	0.01	0.018	0.038	0.071

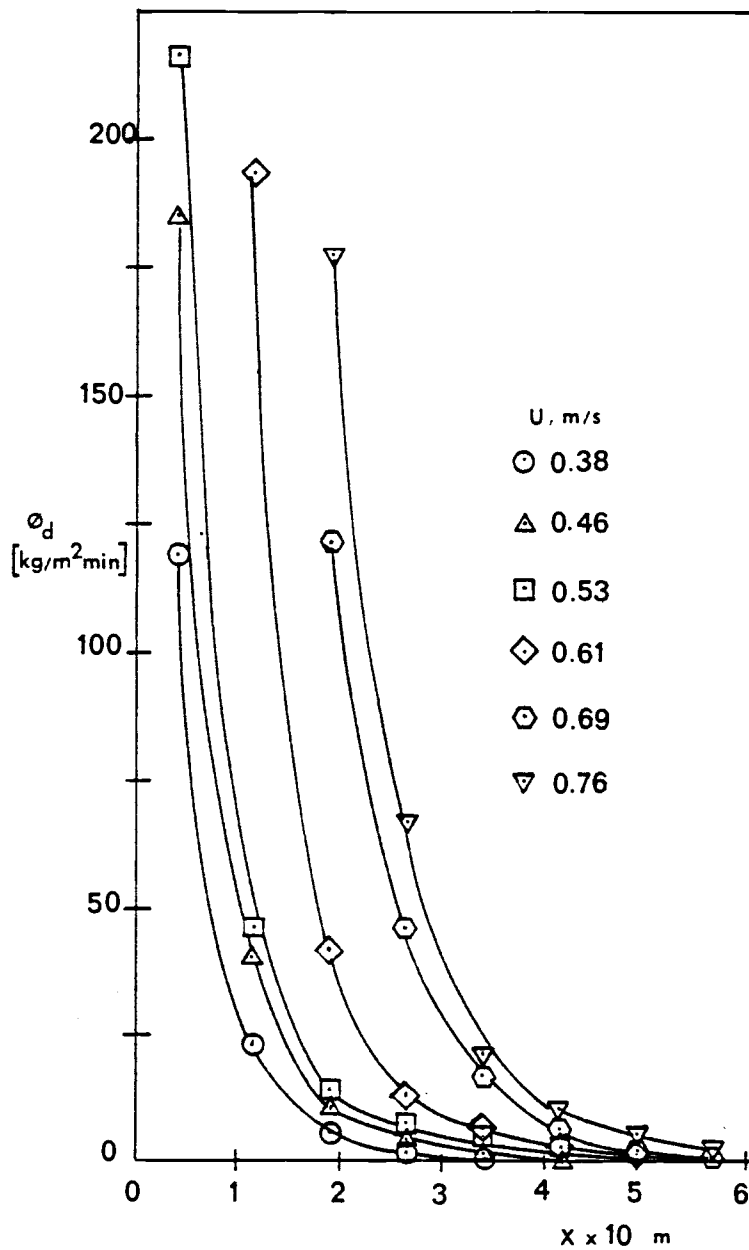


Figure 5.11a Particle density function as a function of  $x$  at  $y = 0.07 \text{ m}$ .

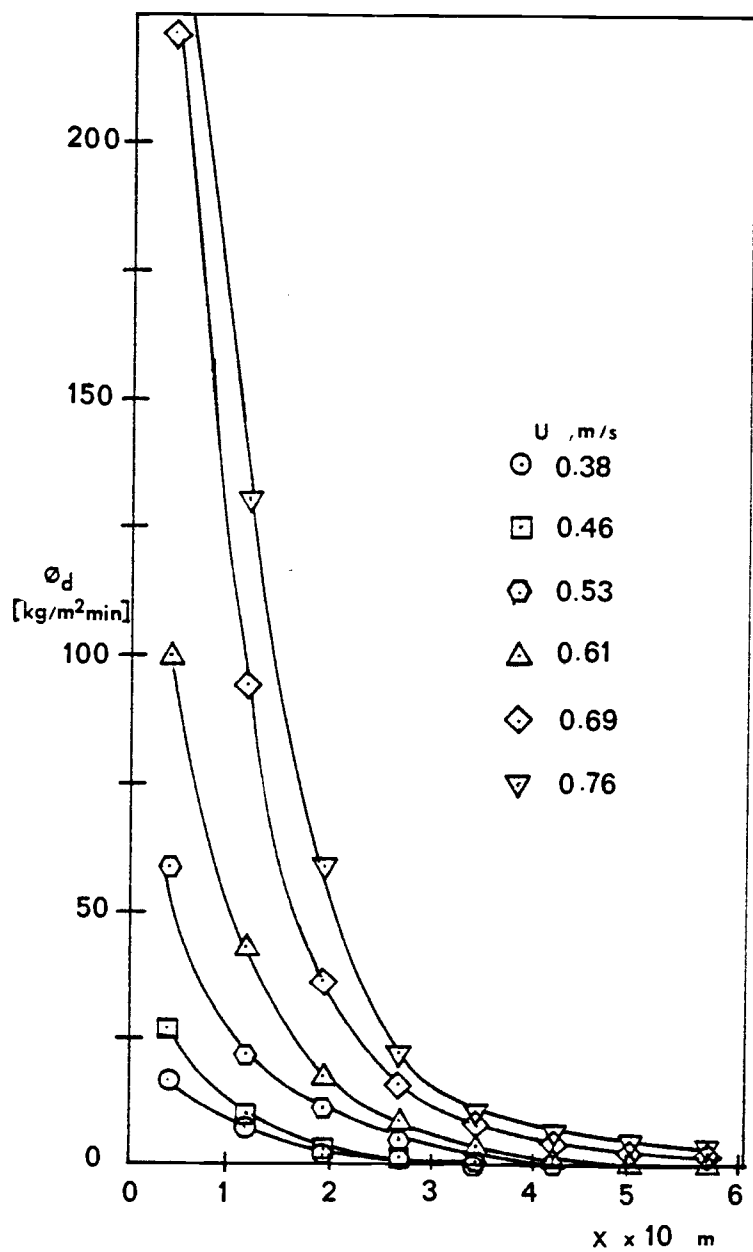


Figure 5.11b Particle density function as a function of  $x$  at  $y = 0.15 \text{ m}$ .

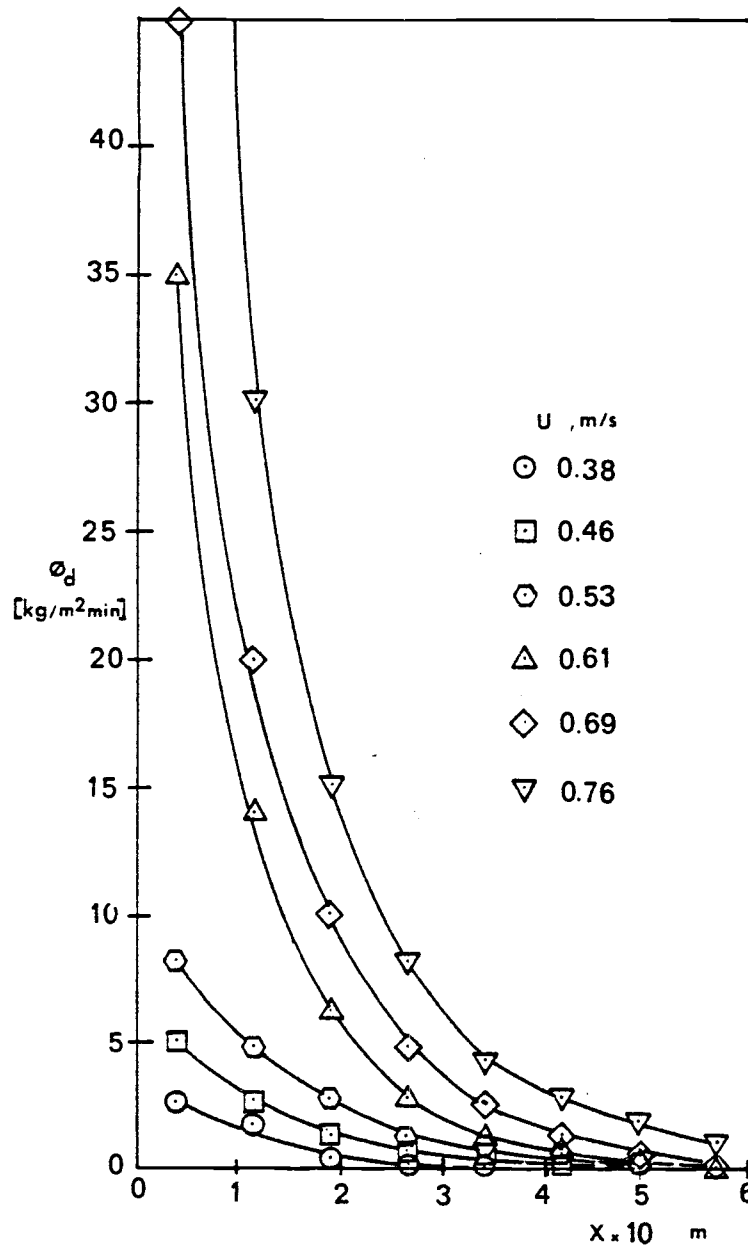


Figure 5.11c Particle density function as a function of  $x$  at  $y = 0.23$  m.

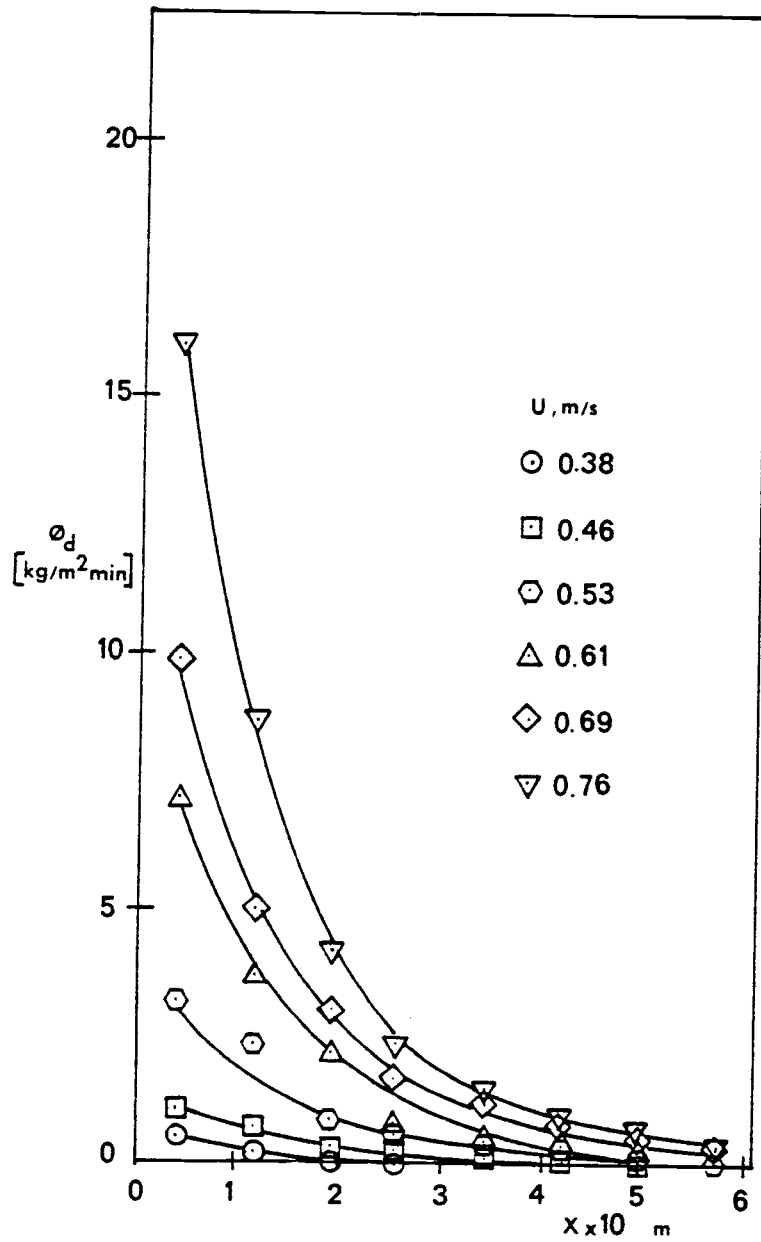


Figure 5.11d Particle density function as a function of  $x$  at  $y = 0.31$  m.

and the distance from the interface region ( $x$ ) by the following correlations,

$$\text{at } y = 0.076 \text{ m, } \phi_d = \exp((1.75-10.50x)+8.85(u-u_{mf})) \quad (5.28)$$

$$y = 0.154 \text{ m, } \phi_d = \exp((0.90-9.70x)+8.20(u-u_{mf})) \quad (5.29)$$

$$y = 0.228 \text{ m, } \phi_d = \exp((0.05-8.90x)+7.55(u-u_{mf})) \quad (5.30)$$

$$y = 0.305 \text{ m, } \phi_d = \exp((-0.80-8.10x)+6.90(u-u_{mf})) \quad (5.31)$$

and finally  $\phi_d$  can be related to the distance  $y$  by,

$$\phi_d = \exp((2.60-11.15y)-(11.30-10.50y)x+(9.50-8.53y)(u-u_{mf})) \quad (5.32)$$

A sample of the comparison between the correlation in equation (5.32) and the experimental data is shown in Figure 5.12.

#### 5.4 Comparison of Particle Density Function Between Model Predicting and Experimental Result

To obtain the particle density function by the proposed model, the computer program listed in Appendix B is used. Since the trajectories of every ejected agglomerates are known, the number of agglomerates collected in a receptable located at  $(x=x_1, y=y_1)$  is the number of trajectories that intercept the line  $y=y_1$  between  $x=x_1+0.0381$  to  $x=x_1-0.0381$  (radius of each receptable is 0.0381 m). The amount of particles collected in that particular receptable is equal to the product of the number of agglomerates collected and the weight of each agglomerate which is approximately  $da.dr. (1-\epsilon) \rho_s$ . Then, the particle

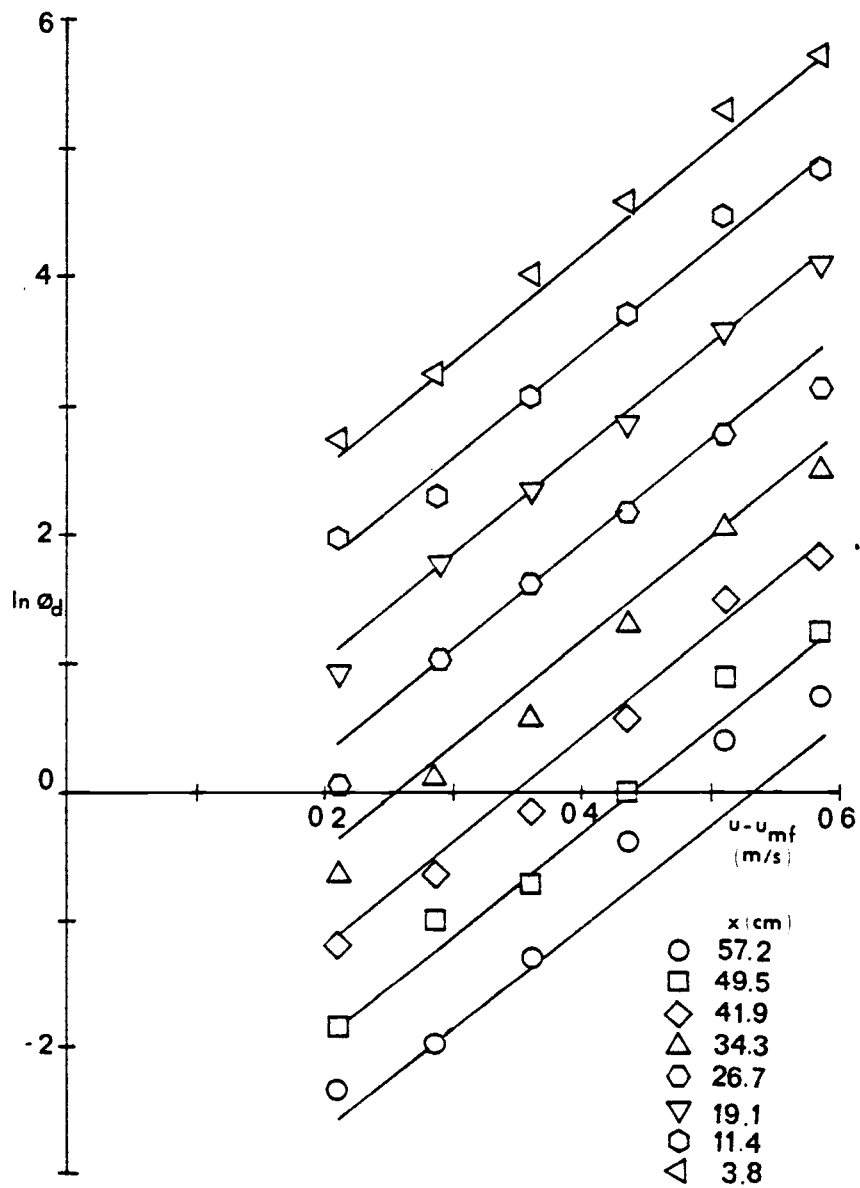


Figure 5.12 Comparison of particle density function between the correlation from the equation (5.32) and the experimental data at  $y = 0.15$  m.

density function is obtained by dividing the amount of particles collected in each receptable with the receptable area.

The plots of the particle density function obtained by this proposed model compared to the experimental data are shown in Figures 5.13a and 5.13b. According to plots, it can be seen that there are good agreement between the proposed model and the experimental data.

### 5.5 Bed Material Transfer by Using Particle Density Function

Since the particle density function represents the amount of bed material transferred from the active bed and accumulated in a unit area of the slumped bed per unit time, the total material transferred during bed turn down can be obtained by integrating the particle density function over the entire slumped section and over the total time during the defluidization period. However, some adjustment about the effect of the slumped bed profile on the limits of integration has to be performed.

#### The effect of slumped bed surface profiles on bed material transfer

During the study of slumping behavior, it was observed that bed material from bubbles erupting in the active section would fall onto the slumped section but would not always accumulate in the slumped section. Part of the material would slide along the interface region back to the active bed. Bed material would accumulate in the slumped section if it travels across the peak of the ridge ( $x > x^p$ ,  $y > y^p$ ) but particles that did not travel past the peak would fall onto the part of



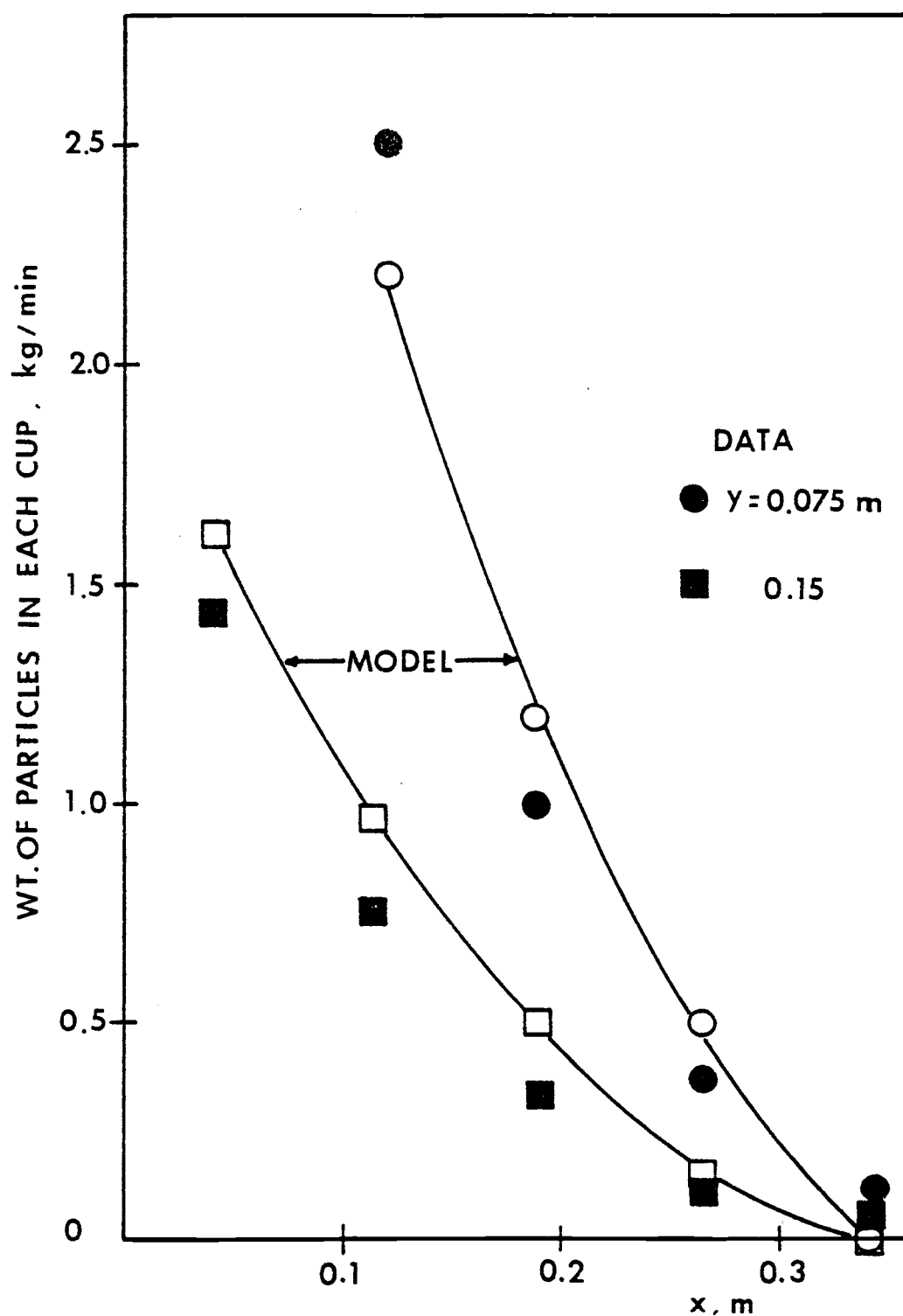


Figure 5.13a Comparison of the weight of particles collected in each cup between the model and the experimental data at  $u = 0.76$  m/s.

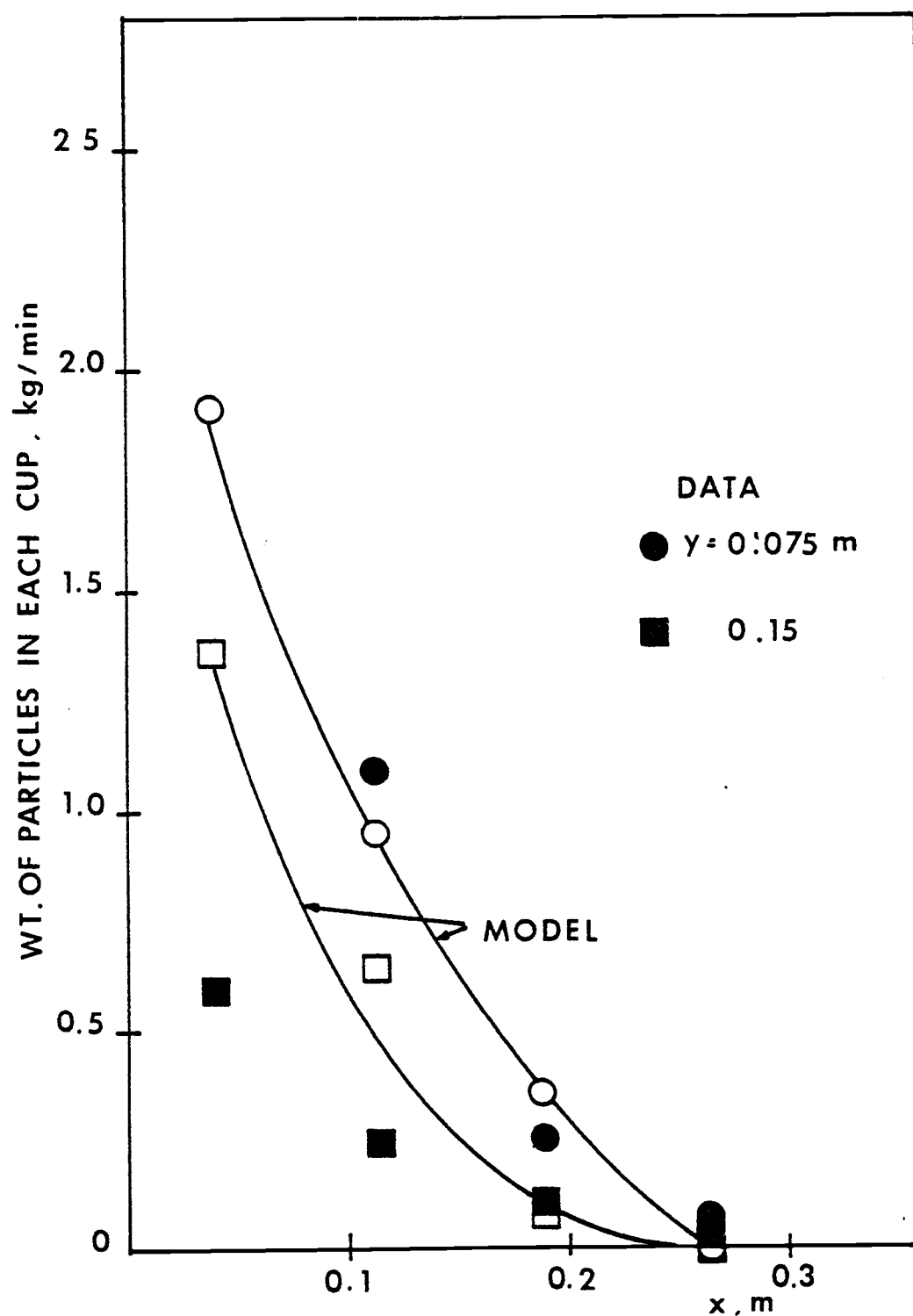


Figure 5.13b Comparison of the weight of particles collected in each cup between the model and the experimental data at  $u = 0.60$  m/s.

the ridge that slopes into the interface front and those particles would slide back to the active side due to the effect of gravity if the angle of the ridge was greater than the angle of repose.

### Results and Discussion

To determine the rate of the slumped bed buildup and the total amount of material that is accumulated in the slumped portion equation (5.32), equation (4.1) and (4.2), which generate the location of the peak of the ridge as a function of time after defluidization ( $t$ ) and excess gas velocity ( $u-u_{mf}$ ), are used as follows:

If the superficial velocity is kept constant during the bed turn down period, then

$$x^p = x^p(t) \quad (5.33)$$

$$y^p = y^p(t) \quad (5.34)$$

in equation (5.32),  $y$  is replaced by  $y^p$  since the bed material will accumulate when  $y, y^p$ , then

$$\phi_d = \exp((2.60-11.15y^p)-(11.30-10.50y^p)x+(9.50-8.53y^p)(u-u_{mf})) \quad (5.35)$$

$$\text{It is observed that} \quad \phi_d = \phi_d(x, t) \quad (5.36)$$

at any instant of time. The rate of bed material accumulated ( $\dot{m}$ ) can be expressed as,

$$\dot{m} = \int_0^{\infty} \phi_d(x, t) dx \quad (5.37)$$

since the bed material will accumulate only when  $x > x^p$ , the lower limit of integration can be changed to  $x^p$ .

Furthermore, the slumped bed length is finite ( $x=L/2$ ), the upper limit of integration can also be changed to  $L/2$ . Equation (5.37) now becomes

$$\dot{m} = \dot{m}(t) = \int_{x^p}^{L/2} \phi_d(x,t) dx \quad (5.38)$$

Equation (5.38) is now used to determine the rate of bed material accumulated over the slumped portion at any instant of time.

To determine the total material transferred from the moment that half of the bed is turn down until any time  $t$ , equation (5.38) is integrated over the total time  $t$ , then

$$\begin{aligned} m &= \int_0^t \dot{m}(t) dt \\ &= \int_0^t \int_{x^p}^{L/2} \phi_d(x,t) dx dt \end{aligned} \quad (5.39)$$

Equation (5.39) was solved numerically at various superficial velocities, and the results compared to the experimental data obtained by finding the total mass from the actual bed profiles. The results shown in Figure 5.14 indicates good agreement with experimental data. It is expected that the material transferred by using the particle density function will also give good agreement for a long period of time during bed turn down.

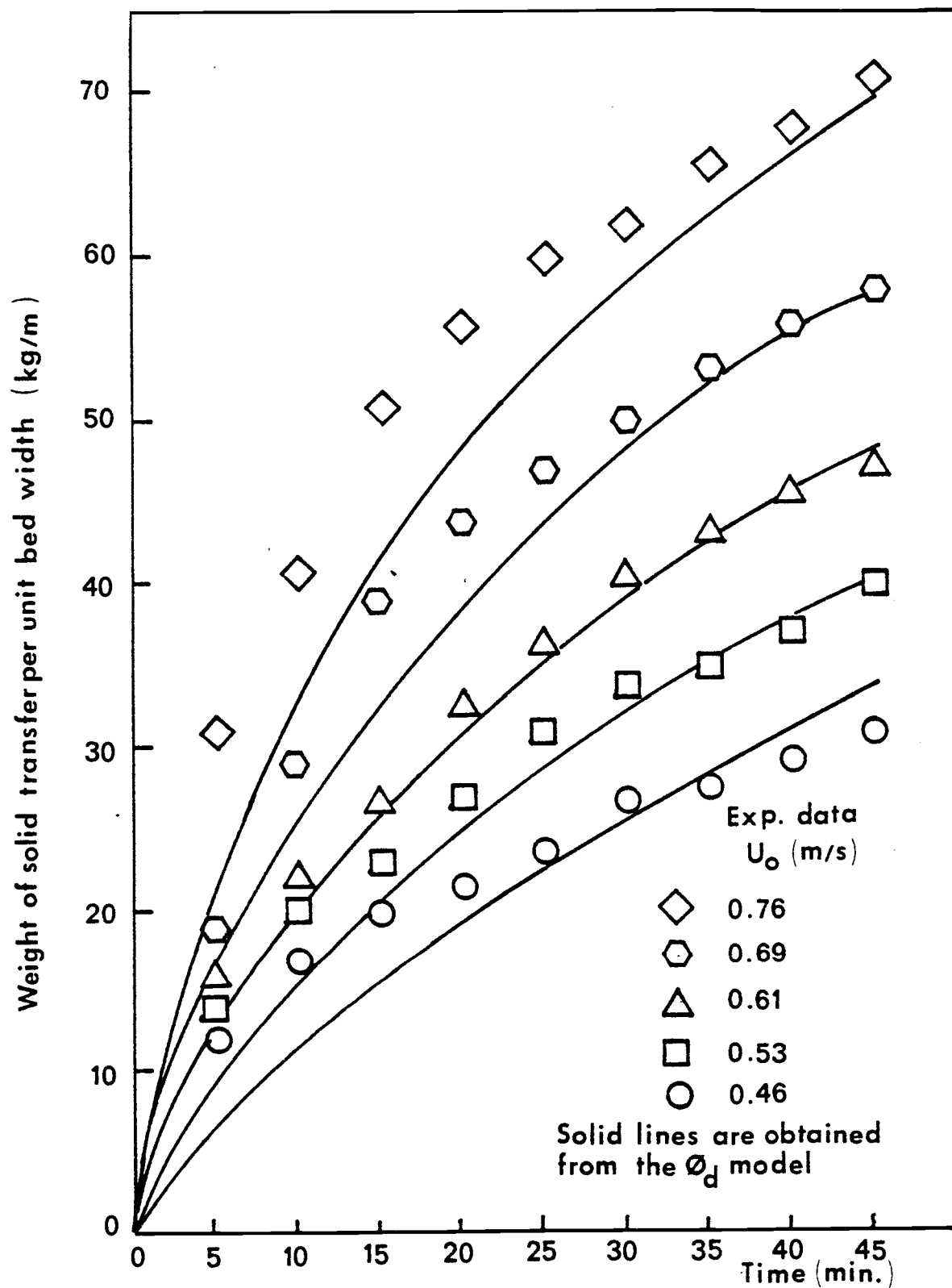


Figure 5.14 Comparison between material transfer, calculated from particle density function and experimental data.

## VI. PRESSURE DROP AND GAS FLOW IN A PARTIALLY DEFLUIDIZED BED

### 6.1 Introduction

In order to study the gas flow behavior in both the slumped and fluidized sections of the bed, pressure drop across the bed at various locations of both regions were measured. The pressure drop data were plotted to obtain pressure loss profiles across both the active and the slumped sections of the bed. The resulting pressure loss profiles were then used to determine relative amounts of gas by pass through the slumped section as a percentage of the total gas flow.

### 6.2 Pressure Loss Profiles

The pressure probes and pressure transducers as described in section 3.2 were used to measure the pressure drop across the bed. As both sides of the bed was fluidized, the pressure reading was taken 20 times per second (once every 50 milliseconds) at various locations along the bed ( $x=0.05, 0.35, 0.48$  and  $0.76$  m) and at different superficial velocities ( $u=0.46, 0.61$  and  $0.76$  m/s). The pressure drop used in the study was obtained by finding the mean value from the measured data. It was found that there were pressure variations of  $\pm 0.5$  kPa between mean pressure drop and equivalent pressure drop ( $\Delta P=W/A$ ) at various locations along the bed (Figure 6.1).

As half of the bed was defluidized, the pressure readings at the previous locations were taken at various times after defluidization. It was found that there was no significant change in pressure

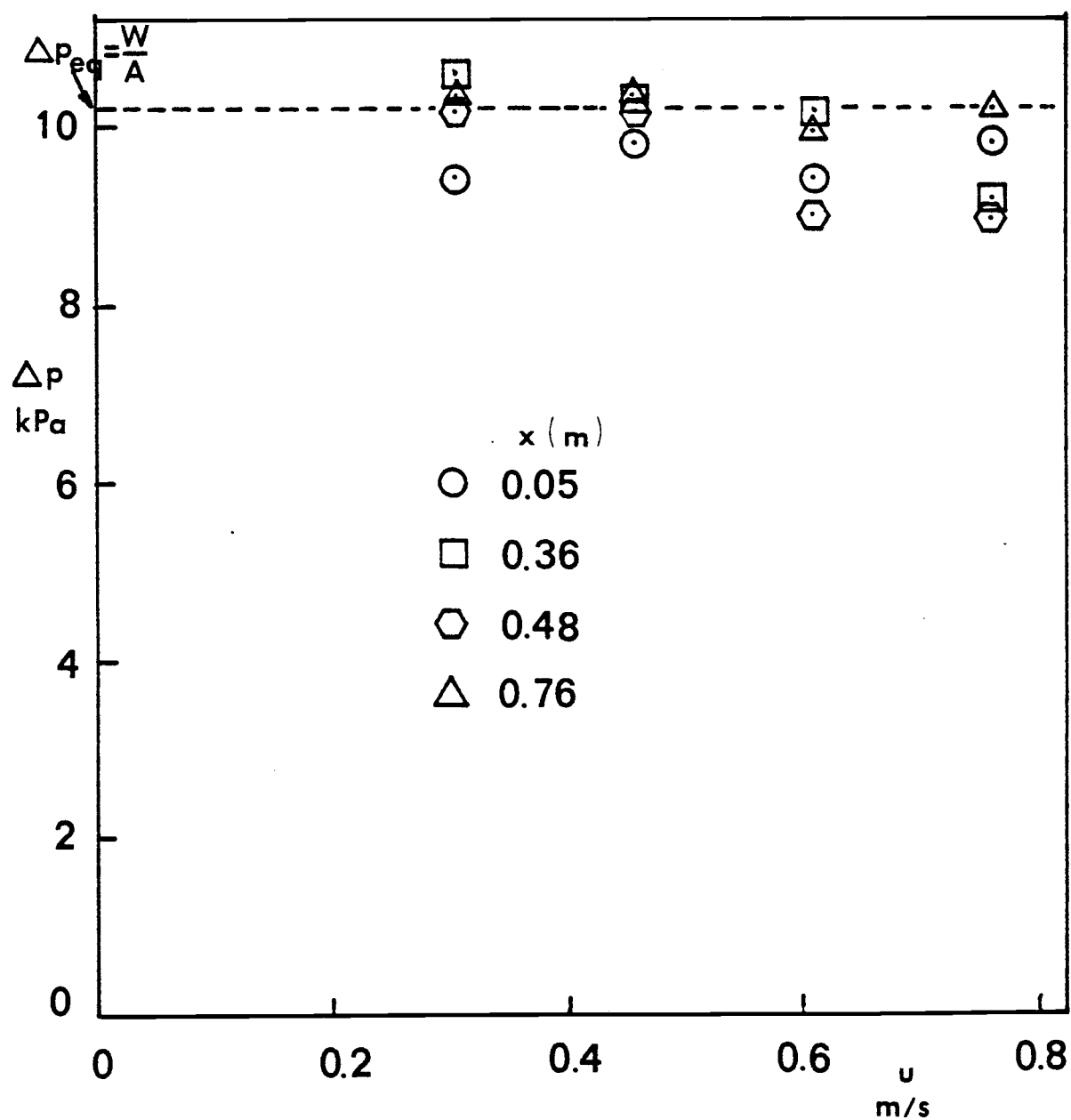


Figure 6.1 Pressure drop at various location along the bed and at different superficial velocity.

drop across the bed in both sections as the time after defluidization increased. The recorded pressures at various superficial velocities were then plotted against their locations in the bed to obtain the pressure drop profiles. The plots are shown in Figure 6.2.

### 6.3 Gas Flow in the Slumped Bed

Data obtained from measuring the pressure drop profiles in both the slumped and fluidized sections (Figure 6.2) was used to study the gas flow behavior in the slumped portion of the bed.

To compare the amount of flow in both sections of the bed, the gas flow rate must be determined by using the pressure drop relation given by Ergun (16).

$$\frac{\Delta P}{L} g_c = 150 (1-\epsilon_m)^2 \mu u / \epsilon_m^3 (\phi_s d_p)^2 + 1.75(1-\epsilon_m) g u^2 / \epsilon_m^3 \phi_s d_p \quad (6.1)$$

The pressure drop correlation in equation (6.1) indicates that the pressure drop across the bed is due to the viscous loss (first term) and the kinetic energy loss (second term). The kinetic energy loss could be neglected since the bed was tested at low velocity ( $Re_p < 20$ ). Thus, equation (6.1) can be simplified as,

$$\frac{\Delta P}{L} g_c = 150 (1-\epsilon_m)^2 \mu u / \epsilon_m^3 (\phi_s d_p)^2 \quad (6.2)$$

Since the void fraction in the packed bed ( $\epsilon_m$ ), size of particle ( $d_p$ ) and sphericity of a particle ( $\phi_s$ ) are constant during the test, equation (6.2) can be modified as,

$$\Delta p = K_1 u \quad (6.3)$$



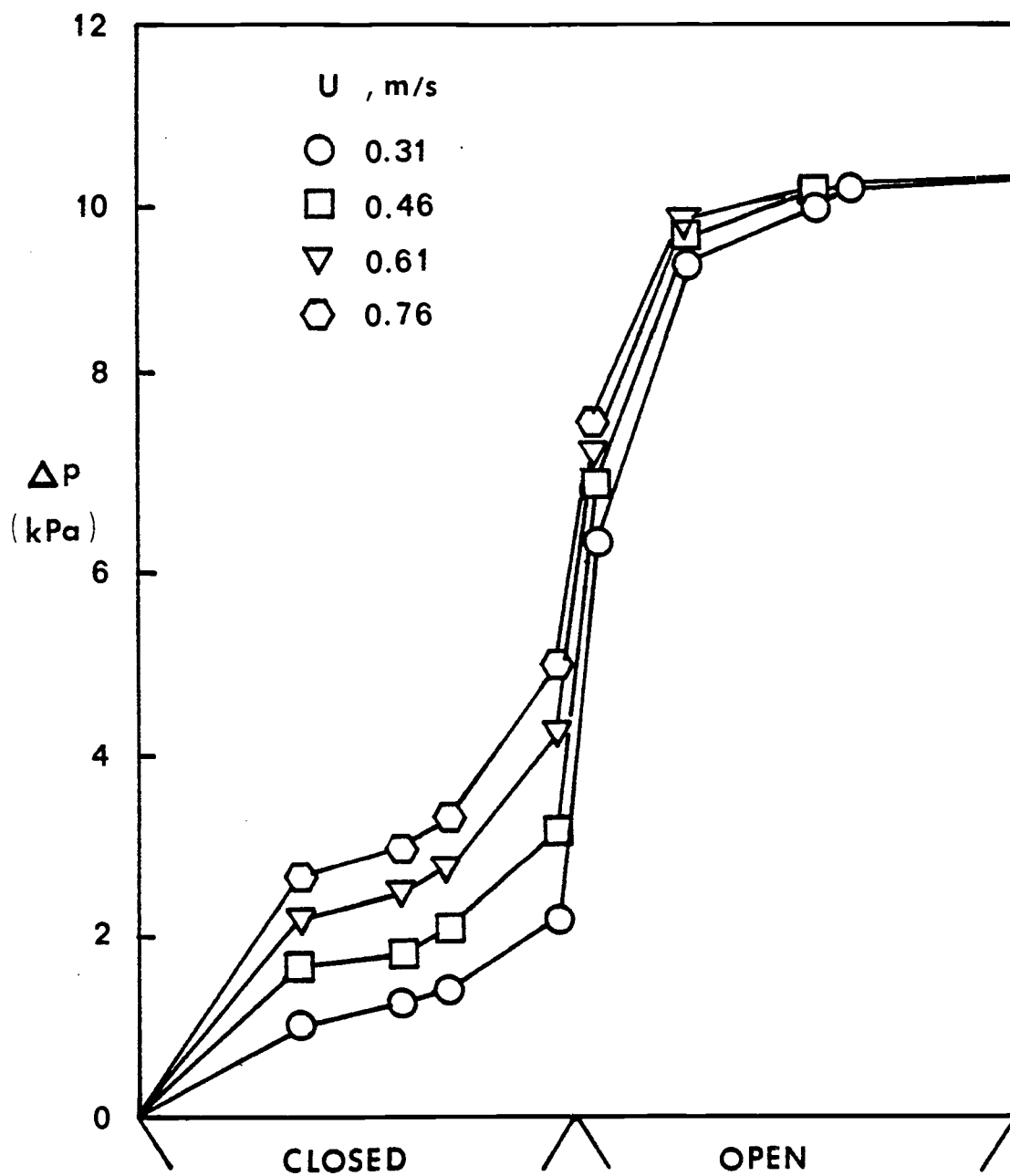


Figure 6.2 Pressure drop profiles in both slumped and active bed at various superficial velocity.

where

$$K_1 = \frac{150 (1 - \epsilon_m)^2 \mu L}{g_c \epsilon_m^3 (\phi_s d_p)^2} \quad (6.4)$$

Thus, 
$$u = \frac{\Delta p}{K_1} \quad (6.5)$$

which can be used to calculate the velocity if the pressure drop profile across the slumped bed is known. Data from Figure 6.2, which shows the pressure drop through the slumped bed for different superficial velocities are used. Using the Ergun equation, the continuity equation and the pressure loss profiles, the gas flow rate in the defluidized section can be determined from,

$$\dot{m}_d = \rho_f u_s A = \rho_f \frac{\Delta p_d A}{K_1} = K_2 \Delta p_d A \quad (6.6)$$

where 
$$K_2 = \rho_f / K_1 \quad (6.7)$$

At the minimum fluidizing condition, the gas flow rate is given by,

$$\dot{m}_{mf} = \rho_f u_{mf} A = \rho_f \frac{\Delta p_{mf} A}{K_1} = K_2 \Delta p_{mf} A \quad (6.8)$$

At the conditions above  $u_{mf}$ , the gas flow rate in the active section is given by,

$$\begin{aligned}
 \dot{m}_d &= \rho_f u_a A \\
 &= \rho_f u_{mf} A \frac{u_a}{u_{mf}} \\
 &= \dot{m}_{mf} \frac{u_a}{u_{mf}} \\
 &= K_2 \Delta p_{mf} A \frac{u_a}{u_{mf}} \quad (6.9)
 \end{aligned}$$

From the above equation, the gas flow in the defluidized section ( $\dot{m}_d$ ) can be obtained from equation (6.6) and the gas flow in the active section ( $\dot{m}_a$ ) from equation (6.9). To find the percentage of gas flow through the defluidized region, equation (6.6) is divided by equation (6.9).

$$\begin{aligned}
 \text{percent of gas by pass} &= \frac{K_2 \Delta p_d A}{K_2 \Delta p_{mf} A \frac{u_a}{u_{mf}}} \times 100 \\
 &= \frac{\Delta p_d A u_{mf}}{\Delta p_{mf} A u_a} \times 100 \quad (6.10)
 \end{aligned}$$

In the numerator,  $(\Delta p_d)A$  can be obtained from integrating the area under the curve of the closed section in Figure 6.2 ( $\Delta p$  v.s.  $x$ ). In the denominator,  $(\Delta p_{mf})A$  can be obtained directly since  $\Delta p_{mf}$  is constant across the active side of the bed.

The resulting calculations gave the following percentage of gas flow through the slumped bed.

<u>u(m/s)</u>	<u>% of gas bypass through slumped region</u>
0.30	6.6
0.46	6.6
0.61	6.6
0.76	6.3

The results indicate that the percentage of gas bypass through the slumped section does not depend on the superficial velocity.

#### 6.4 Discussion

The pressure drop profiles shown in Figure 6.2 indicated that there were significant changes in pressure drop across the slumped bed at different superficial velocities. The pressure drop will increase as the superficial velocity in the active bed increases. This implies that as the superficial velocity in the active bed increases, more fluidizing gas leaks from the fluidized bed into the slumped bed. The gas bypass from the fluidized bed through the slumped section of the bed results from the pressure gradient in the slumped section between the distributor plate and the bed surface being different from the gradient in the fluidized section.

The percent of gas bypass from the active bed through the slumped bed was found to be independent of the superficial velocity. However, this may cause the reduction of the air-fuel ratio required for the combustion of coal in the active bed. The feeding of coal to the active bed must be reduced so that there will be sufficient air to maintain a complete combustion.

Furthermore, gas bypass may result in a continued combustion of char particles in the slumped section of the bed. This tends to reduce the temperature gradients along the interface region between both sides of the fluidized bed.

## VII. REFLUIDIZATION OF A SLUMPED SECTION

As half of the fluidized bed was defluidized or slumped, bed material was transferred from the active side to the slumped side of the bed due to the effect of erupting bubbles in the fluidized section. The details were already discussed in Chapter 5. In order to bring the bed up to full capacity which is meant to refluidize the slumped portion of the bed, the air supply was returned to the stagnant half of the bed. It was found that refluidization of the slumped section could not be obtained easily. If the wind box is not compartmented or if the compartments are too large, then the air flow may bypass that portion and exit the bed through the shallow fluidized portion, thereby preventing it from fluidizing. In this study it was found that refluidization of the slumped bed in some cases could not be achieved in spite of the fact that the compartmented wind box was available. To study the refluidization of the slumped portion, the necessary conditions needed to obtain a complete refluidization must be determined by using both qualitative and quantitative results.

### 7.1 Qualitative Studies

To study the refluidization of the slumped compartment of the bed after a long time slumped condition, results from slumped bed surface profiles (section 4.3) was used. An expected slumped bed surface profile was built in the slumped section. The refluidization was obtained by opening the air valve to that slumped compartment and closing the air bypass valve simultaneously, leaving the air velocity

in the active side of the bed unchanged. A movie camera was used to film both the front view and side view of the slumped compartment during the refluidization. Pressure variation in the slumped compartment was also measured by using the pressure transducers and amplifier as described in section 3.2. Pressure signals were taken and recorded at every 50 milliseconds at various locations in the slumped section. Pressure readings were used as an indicator, along with visual observations, as to when the bed was refluidized. The velocities used in the study of the refluidization of the slumped bed were varied from  $1.5 u_{mf}$  to  $5.0 u_{mf}$ .

## 7.2 Results and Discussion

From the studies of pressure-time recordings and observations from the film taken, it was indicated that the complete refluidization of the slumped compartment started when the first bubble was detected at the middle of the ridge. Thus, pressure-time traces obtained from the pressure taps installed at the middle of the ridge were used to monitor the time required for a complete refluidization. The time required to completely refluidize the slumped portion of the bed is the time between the instant the inlet valve is opened and the time that the first bubble is detected in the pressure-time trace obtained from the pressure tap at the middle of the ridge. When a bubble passes a pressure tap, a large fluctuation in pressure is obtained in the pressure-time trace. A sample of the pressure-time traces are shown in Figure 7.1 and 7.2.

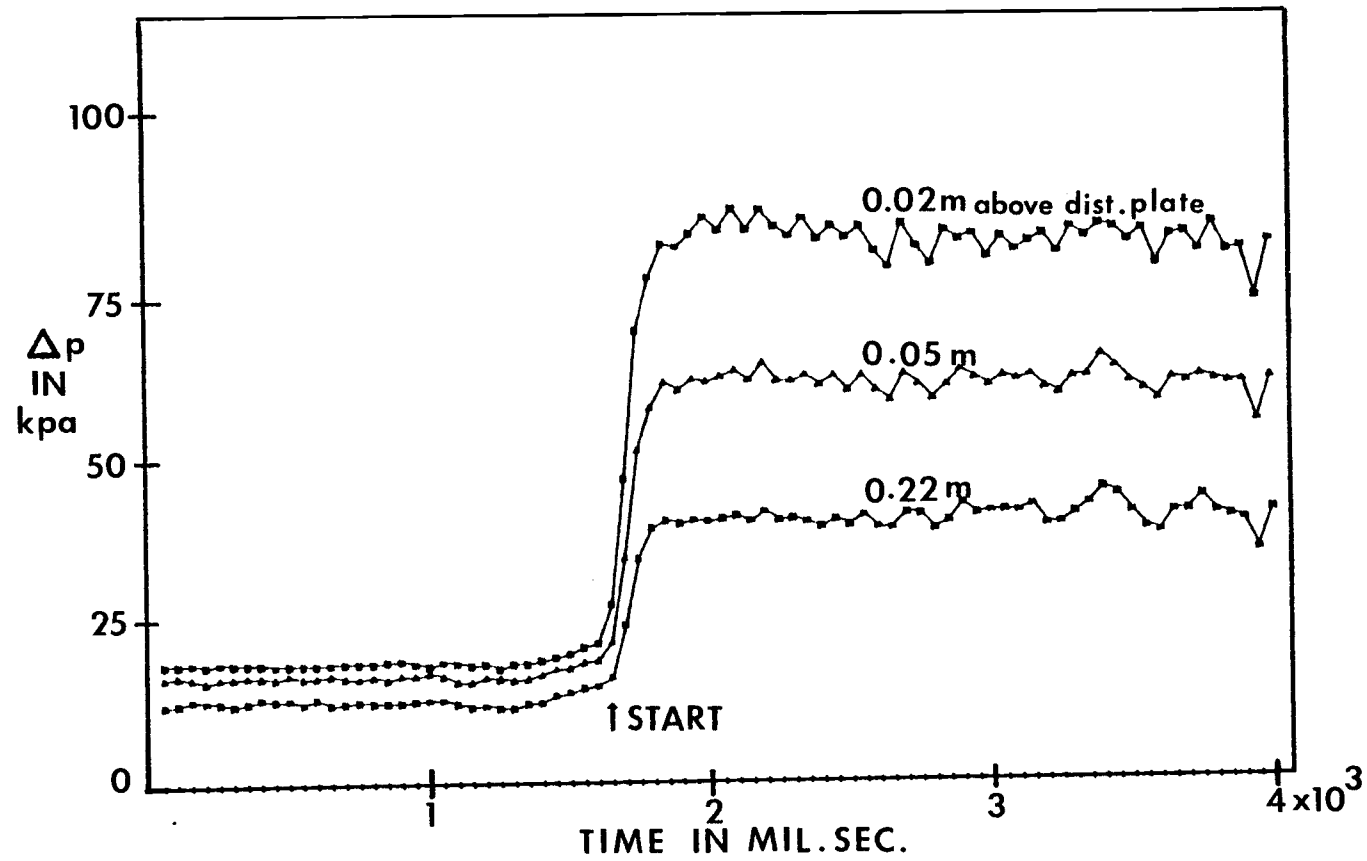


Figure 7.1 Pressure time trace during refluidization at  $x = 0.48$  m and  $u = 0.22$  m/s.



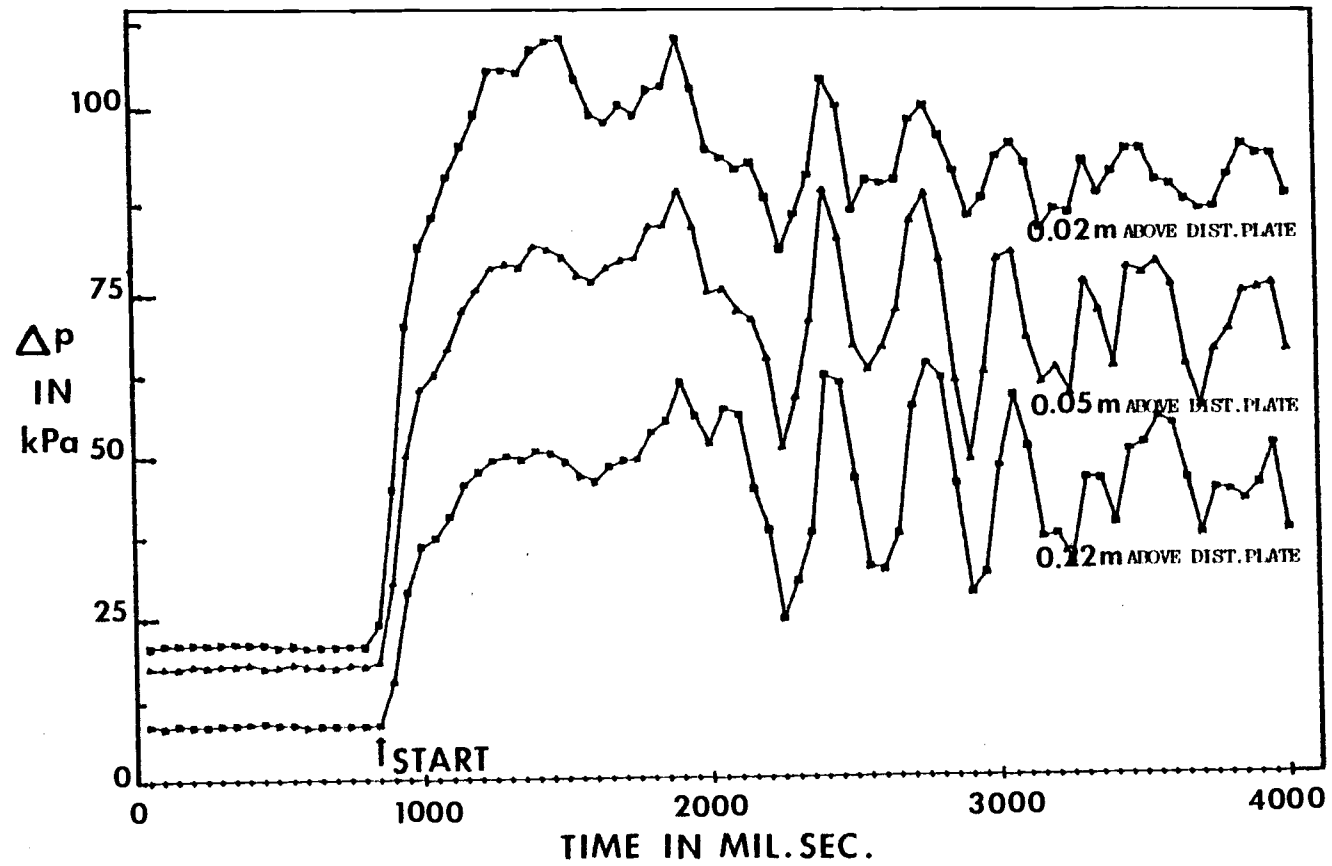


Figure 7.2 Pressure time trace during refluidization at  $x = 0.48$  m and  $u = 0.46$  m/s.

In Figure 7.1, a low velocity (0.22 m/s) was used to refluidize the slumped compartment. It was observed that no bubble was detected in the pressure-time trace, therefore, complete refluidization could not be achieved. Observation from the film also confirmed this result. In Figure 7.2, a high refluidizing velocity (0.46 m/s) was used. A bubble was observed in the pressure-time trace at about 1.5 seconds after supplying air to the slumped compartment, and the slumped bed was completely refluidized. This was also confirmed by the motion picture observation.

The time to refluidize the slumped portion of the bed which was measured from pressure-time traces was observed to depend on the fluidizing velocity. Figure 7.3 shows the required time for complete refluidization at different superficial fluidizing velocities. Both qualitative studies as reviewed on motion pictures and pressure-time trace indicate that complete refluidization of the slumped compartment can not be accomplished at superficial velocity which is less than  $2u_{mf}$  and that velocity is termed a critical velocity.

At the velocities that are less than the critical velocity, the ridge shape changed from a sharp peak to a lower bellshaped curve but complete refluidization would not occur. At superficial velocities above the critical velocity, the entire slumped portion refluidized rapidly as indicated from measurements plotted in Figure 7.3.

To further investigate the refluidization of the slumped compartment, pressure loss across the slumped bed, especially at the middle of the ridge, were measured and plotted as a function of the refluidizing

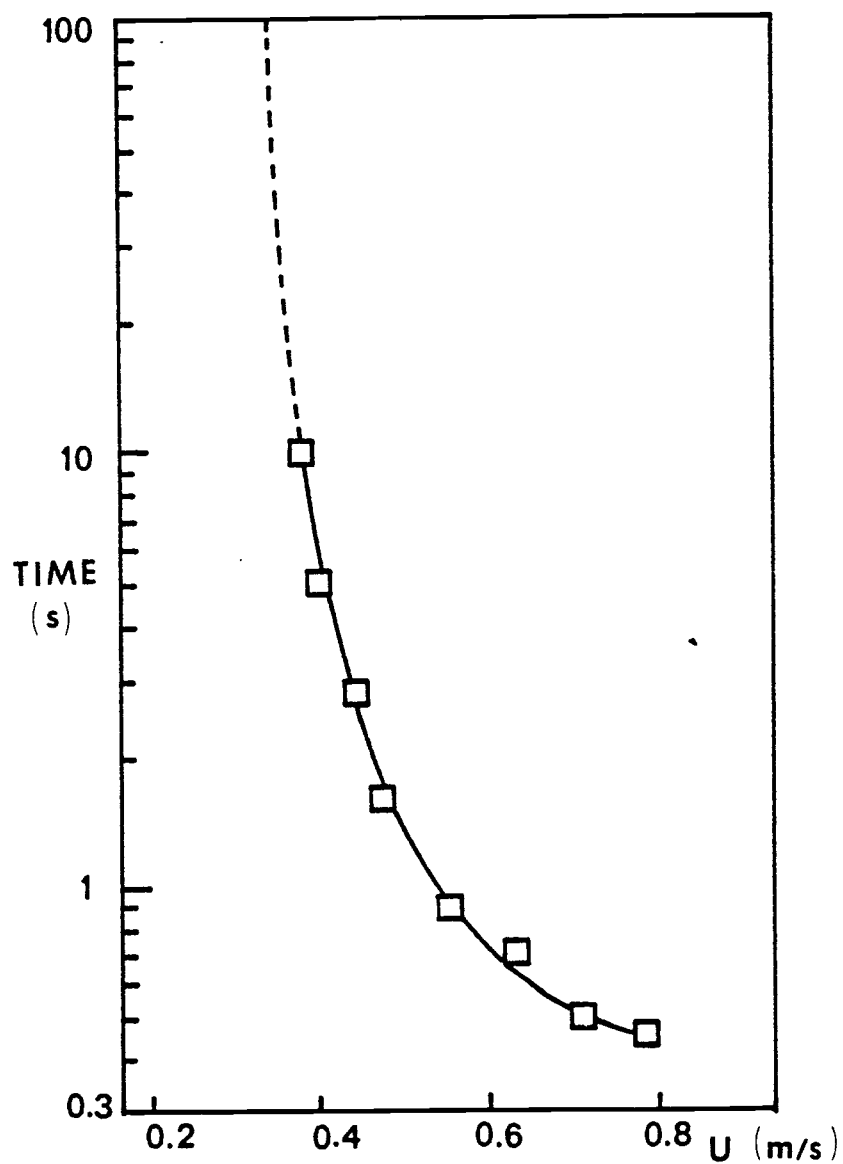


Figure 7.3 Time required to refluidize the slumped part of the bed as a function of superficial velocity.

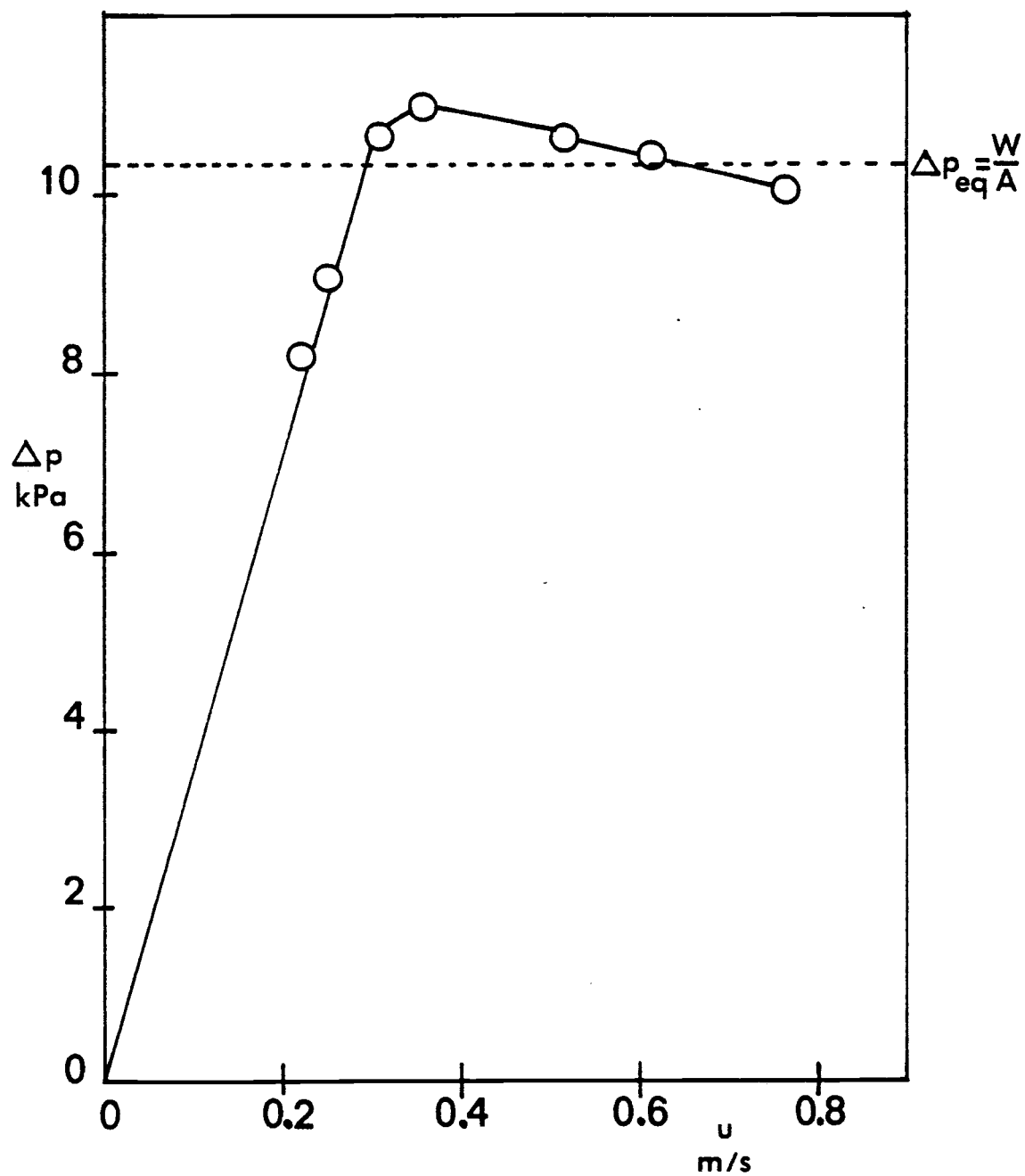


Figure 7.4 Pressure drop across the slumped bed at the middle of the ridge.

velocity. The plot is shown in Figure 7.4. It can be seen that from Figure 7.4 that the complete refluidization or the sudden disappearance of the ridge shape will occur at the superficial velocity 0.3 m/s which is about  $2u_{mf}$ . At that velocity, the pressure drop of the slumped bed at the middle of the ridge exceeds the equivalent pressure drop ( $\Delta p = W/A$ ).

It is interesting to study the effects that prohibit refluidization when the velocity is less than  $2u_{mf}$ . Usually, a fluidized bed can be obtained by increasing the velocity of flow through a packed bed or fixed bed. Thus, at the minimum fluidizing velocity, it is expected that there will be a sharp transition between a fixed bed and a fluidized bed. However, this happens in an idealized system only. In practice, there will be a large transition region and the fixed bed will not become a fluidized bed at the minimum fluidizing velocity. Richardson (45) indicated that the whole of the bed is not fluidized until all the particles are fully supported in the fluid and the pressure drop becomes exactly equal to the buoyant weight per unit area ( $\Delta p_{eq} = W/A$ ). He also defined that velocity as the "full supporting velocity" ( $u_{fs}$ ) which is about 50% greater than  $u_{mf}$ .

In the slumped compartment, the effect of material transfer creates the slumped bed surface profiles (section 4.3). The profile contains the peak and slopes to both the interface front and the bottom of the ridge in the slumped section. The equivalent pressure drop which is defined as the buoyant weight of particles per unit area of bed in each section of the bed will not be equal. It can be seen that  $\Delta p_{eq}$  at a location far from the interface region (the profile is a horizontal line) will be

less than  $\Delta p_{eq}$  at the middle of the ridge. Thus, at the full supporting velocity ( $u_{fs}$ ) which is about  $1.5 u_{mf}$  (45), part of the slumped bed away from the interface front will refluidize first. The total refluidizing air will then bypass through that shallow section of the slumped bed, and the complete refluidization will not occur. However, at a critical velocity ( $2 u_{mf}$ ), the pressure drop across the middle of the ridge exceed  $\Delta p_{eq}$  and the slumped bed is completely refluidized.

## VIII. SOLIDS MIXING STUDIES IN A PARTIALLY DEFLUIDIZED BED

### 8.1 Introduction

To turn down a fluidized bed combustor, a section of the fluidized bed needs to be defluidized by cutting off the air supply and the flow of coal to that region. With the air and coal supplies, cut off, the temperature of the slumped section will decrease since the combustion stops in that part of the bed. To bring the bed up to full capacity, the air supply is returned to that stagnant part of the bed. The minimum velocity required to refluidize the slumped section has to exceed the critical velocity which has already been discussed in the previous section of this thesis. When the refluidization of the slumped portion begins, solids in the slumped part will transfer to the adjacent active section causing the rapid mixing of the solids in the fluidized section. If the mixing of solids is too rapid, the temperature of the fluidized section will drop below the operating temperature (1050 K), and sulfur will no longer be effectively removed from the stack gases. Thus, it should be useful to find the rate of mixing of bed material between the slumped section with the active section after refluidization.

Several methods have been proposed for the study of the solid movement and solids mixing in a fluidized bed. The first method considered was to dump tagged particles in the slumped section of the bed, then refluidize the slumped bed, dropping the entire bed and then finding the tagged particles in both sections of the bed. This method was dismissed because it would be time consuming and very difficult to

locate tagged particles by this manner. Another method considered was to collect simultaneous samples from various locations along the bed after refluidization. This method which was used by Highly and Merrick (28) was rejected because of the complication of getting simultaneous samplers at many points in the bed. The last method was to monitor solid tracer concentrations at various location within the bed. Many kinds of tracer have been considered in the study. Radioactive tracers were rejected because of their inherent danger and complication as well as low performance. The technique finally selected used a ferro magnetic tracer with soft-magnetic properties. This technique was conceived and developed by Fitzgerald (17), and was successfully to study solids movement in a fluidized bed by Deaton (14).

The appearance of ferrite particles in any region of the bed could be detected by means of induction coils located within dummy heat exchange tubes. When a ferrite particle moves into the vicinity of an inductor, the inductance of that inductor will increase instantly. Deaton (14) found that the inductance of the coil increases linearly with respect to the volume fraction occupied by ferrite particles. In this experiment, the calibration test was conducted with the percent of ferrite changed from one percent to twenty percent. It was found that the inductance increased linearly with the percent of the ferrite.

The using of ferrite tracers and inductors was first developed to study the movement of solids in fluidized combustors. In these studies the ferrite modelled the movement of coal particles. This technique could also be applied to the study of the solids mixing after



refluidization. An amount of ferrite particles was dumped at a particular location in a slumped section of the bed. After the slumped bed is refluidized, the ferrite particles will mix with the bed media in that particular location instantly. The time required for the ferrite tracer to mix with the bed particles was found to be under 10 seconds. The concentration of ferrite tracers at that moment will represent the concentration of the bed particles in that particular location. The ferrite tracer will then spread throughout the entire fluidized bed. Ferrite tracer and bed material are assumed to spread out or diffuse at the same rate since they become homogenous after mixing. The concentration of ferrite tracer at any location in the bed will then represent the amount of bed materials that spread out from the initial location or the location that ferrite particles are introduced into the bed. It can be concluded that the amount of bed material from the slumped side that cross the interface region to the active side after refluidization can be represented by the amount of ferrite particles detected in the active section of the bed.

## 8.2 Procedure

To study the mixing of solids between both sections of the bed after refluidization, ferrite tracer particles were introduced in a slumped part of the bed. The tracer particles were buried evenly, 0.076 m, under the fixed bed level at a particular location in the slumped bed. An expected slumped condition was built in the slumped section by cutting off the air supply to that portion of the bed and by letting the slumped bed build up until the steady state slumped

bed surface profile was obtained. The inductance probes already described in section 3.4 were used to monitor the concentration along the bed. The inductance probe signals were sampled once every 50 milliseconds and then digitized. Data was collected on all six channels for approximately 10 seconds before refluidizing the slumped section of the bed in order to determine accurately the background or zero level for each of the inductors. Then, the slumped section of the bed was refluidized. Data was collected on all six channels for 304 seconds.

After a refluidization was made and data collected, the ferrite tracer had to be separated from the bed media before another set of experiments could be made. This was accomplished by draining the mixture of bed media and ferrite particles, at a constant rate, onto a ferrite removal system which was described in section 3.4.

The velocity used to refluidize the slumped part of the bed was varied from 0.60 m/s to 0.90 m/s. Three locations were chosen to introduce the ferrite tracer to the slumped bed. Table 8.1 shows the experimental conditions of each particular run.

### 8.3 Experimental Results

The concentration of ferrite particles from the experiments were plotted for each of the six data channels as a function of time. A sample of the plots of the concentration versus time are shown in Figure 8.1. From the plot for each run, three plots on the left hand side represent the concentration from each inductor coil in the slumped side where the location of coils in the bed ( $z$ ) are 0.1143, 0.5461 and

Table 8.1 Summary of experiments.

Bed height	0.30 m. (1 ft.)
Sand size	Zirconia ( $d_p = 305$ microns), 680 kg ( 1500 lbs)
Tracer size	Ferrite ( $d_p = 1500$ microns ), 6.8 kg ( 15 lbs)

Run number	Initial location of ferrite in the slumped side of the bed <sup>*</sup>	Superficial gas velocity ( m/s.)
1	1 <sup>**</sup>	0.90
2	1	0.76
3	1	0.60
4	2	0.90
5	2	0.76
6	2	0.60
7	3	0.90
8	3	0.76
9	3	0.60

\* Ferrite particles are buried evenly in the slumped section of the bed at 0.225 m. above distributor plate.

\*\* Code, 1 - from interface region ( $x=0$ ) to  $x=0.30$  m.

2 - from  $x=0.30$  m. to  $x=0.60$  m.

3 - from  $x=0.60$  m. to  $x=0.90$  m.

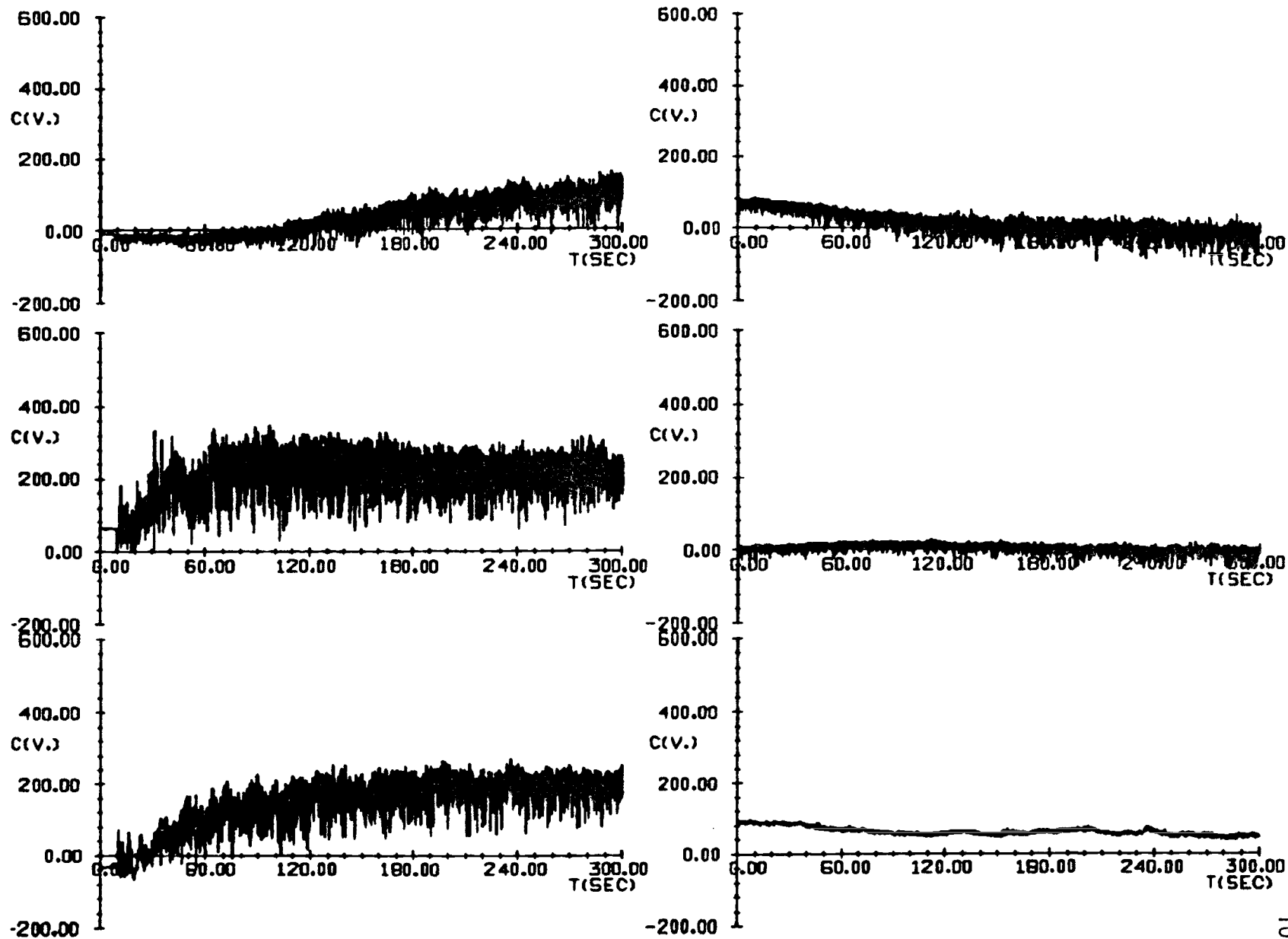


Figure 8.1 Data of the ferrite concentration readings of all six probes from run number 6.

0.9780 m. The other three plots on the right hand side represent the concentration from each coil in the active side where the location of coils in the bed (z) are 1.4097, 1.8415 and 2.2733 m. The concentration scale on the plot is measured in volts. One volt is equal to 0.427 kilograms of ferrite in each cubic meters. It is important to remember that one percent of ferrite by weight in a vicinity of a probe is approximately  $32.036 \text{ kg/m}^3$ .

#### 8.4 Discussion

The collected data as shown in Figure 8.1 had to be smoothed to attenuate the effect of bubbles passing the probes. When a bubble comes close to a probe, the ferrite tracer will be separated from the probe, causing a decrease in the apparent concentration of ferrite. When the bubble moves away from that probe, the ferrite particles come back within the vicinity of the inductance probe and the concentration reading goes up again. In order to get rid of the effect of bubbles, a computer program was used. First, the program was developed to find the average values of the first 100 data points (5 seconds) from all six channels and the resulting average value from each channel was used as a background data or zero concentration. Next, the program will choose the maximum data from each of the ten consecutive raw data. Since the consecutive raw data points correspond to a half second of data sampling, the effect of bubble reducing concentration signal in a period of a half second can be eliminated. The difference between the maximum data chosen in a period of a half second and the back ground data was used as the reduced concentration data. The sample of the reduced concentration data

is shown in Figure 8.2. This method was used successfully to eliminate the effect of bubbles passing through the probe by Deaton (14).

However, it can be seen from the reduced concentration data plot in Figure 8.2 that this proposed method to eliminate the effect of bubbles passing the probes can not be applied to this set of experimental data. The output signals from all channels tend to drift from the expected trends. The effect of signals drifting may come from the change of temperature in the bed and in the main console. The change in temperature causes about a 10 percent change in the resistance in the inductor coils. Therefore, the output signals which are quite sensitive to the change in the resistance of the coils may drift from the original trends as the bed temperature changes slightly.

A new method to eliminate the effects of drifting and the bubbles passing the probes was proposed. It is first assumed that when a bubble passes a probe or is in a vicinity of a probe, ferrite particles are separated from the probe, causing a drop in an output signal. The concentration output signal at that moment is assumed to be zero concentration. However, not all of the bubbles that pass a probe are in full contact with the probe, or in other words, some bubbles partially pass the probe and causing a partial drop in concentration signal outputs which are not sufficient to be assumed as zero concentration. It is further assumed that in a period of one second, there is at least one bubble that fully passes a probe, causing a large drop in a signal output which is sufficient to be assumed as a zero concentration.

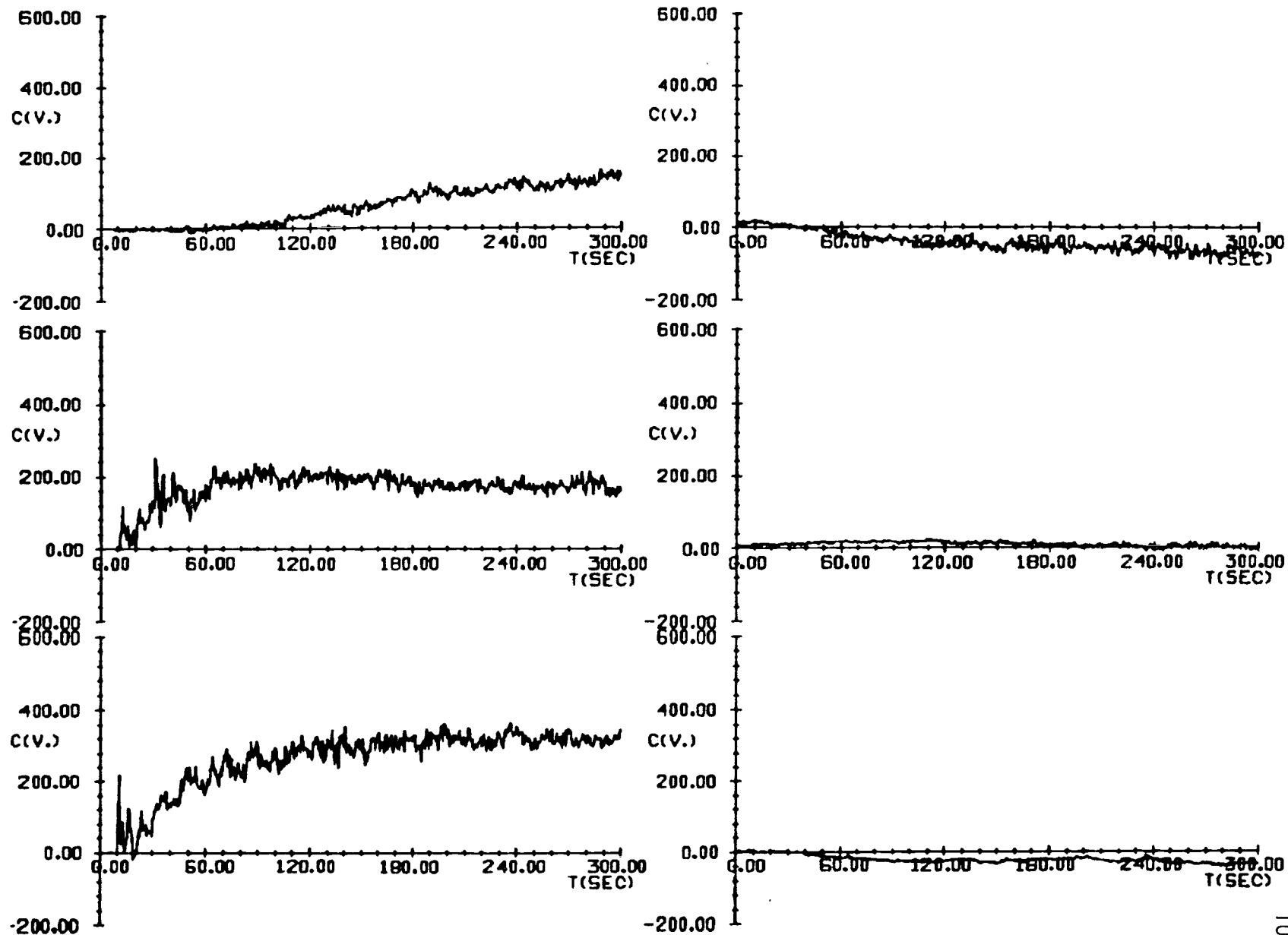


Figure 8.2 Reduced data from run number 6 by using the method proposed by Deaton (14).

A computer program was developed to use this method. The minimum and the maximum points of each 40 consecutive raw data points which correspond to a one second duration were chosen. Each of the minimum data points which were chosen would represent the zero concentration in each one second period, and each of the maximum data points which were chosen would represent the highest concentration of ferrite appearing in the same period of time. The difference between a chosen maximum data point and a chosen minimum data point was defined as the reduced concentration data as shown in Figure 8.3. In Figure 8.3, however, there are still some concentration fluctuations. In order to obtain usable concentration values at any particular time, a smooth line which represented a mean concentration value of the fluctuations was drawn. It was doubtful that the mean concentration obtained by drawing a smooth line passing through the fluctuations would represent the true value of concentration. Hence a second test was conducted by taking another set of data after the bed was refluidized for one hour. It was expected that the material on both sides of the bed would be completely mixed and the ferrite material would spread through out the bed. After the data sampling was completed, the raw data was reduced by the new proposed method. The smooth line was finally drawn to obtain the mean concentration from the resulting reduced concentration data. The result indicated that all of the smooth line drawn for every channels were straight lines and represented the equilibrium concentration ( $c^*$ ) which was about one percent of the bed media by weight ( $32.036 \text{ kg/m}^3$ ).



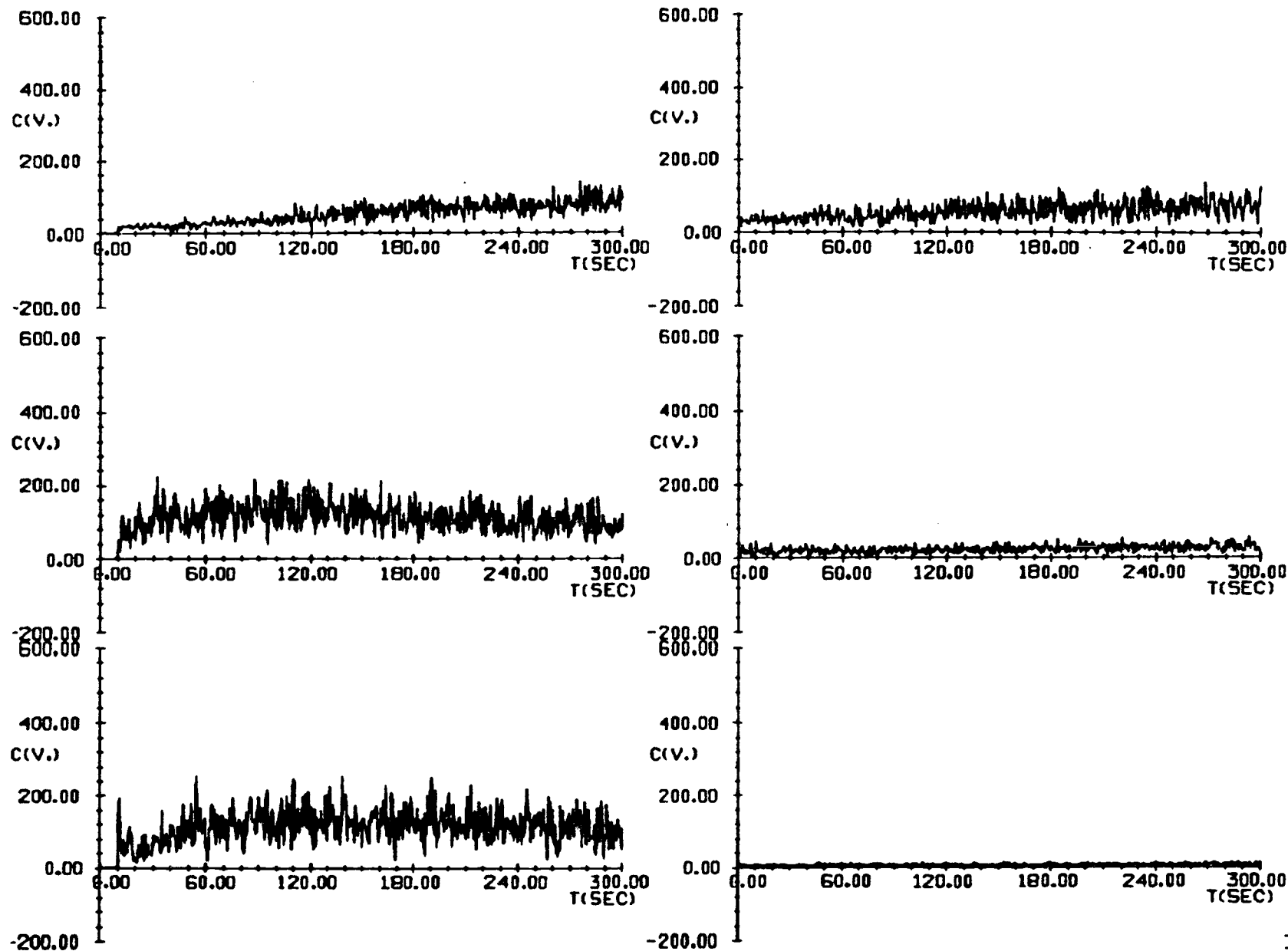


Figure 8.3 Reduced data from run number 6 by the method proposed in this study.

The resulting mean concentration versus time plots from all six channels can be used to obtain the ferrite concentration profile which is the distribution of the ferrite tracer as a function of the location in the bed. The concentration profile will change as time increases. The series of time from the start ( $t=0$ ) to the end ( $t=290$ ) were chosen so that the concentration profile would change dramatically and successively. A modified Fibonacci sequence of time ( $t=10, 20, 30, 50, 80, 130, \dots$ ), where each number is the sum of the previous two was used. This series was chosen because it represented natural decaying functions or exponential functions in a characteristic manner and the changes in ferrite concentration in this study were expected to be rapid in the first sixty seconds then slower as time progressed. The set of concentration profiles at different times ( $t=10, 20, 30, 50, 80, 130, 210$  and  $290$  s) from one run is shown in Figure 8.4. It is important to remember that at time  $t=0$  the slumped bed starts to refluidize while the first concentration versus time plot (Figure 8.1, 8.2 and 8.3).

### 8.5 Model of the Solids Mixing in a Partially Defluidized Bed

Since the concentration profile of the ferrite tracer in the bed at a series of time is known, it will be useful if a model that describes the spreading rate of the ferrite tracer or the rate that ferrite tracer disperses in a fluidized bed is developed.

#### Mechanism of solids mixing

The solids mixing in a fluidized bed results from the upward movement of the gas bubbles in the bed. Rowe and Partridge (49) found that

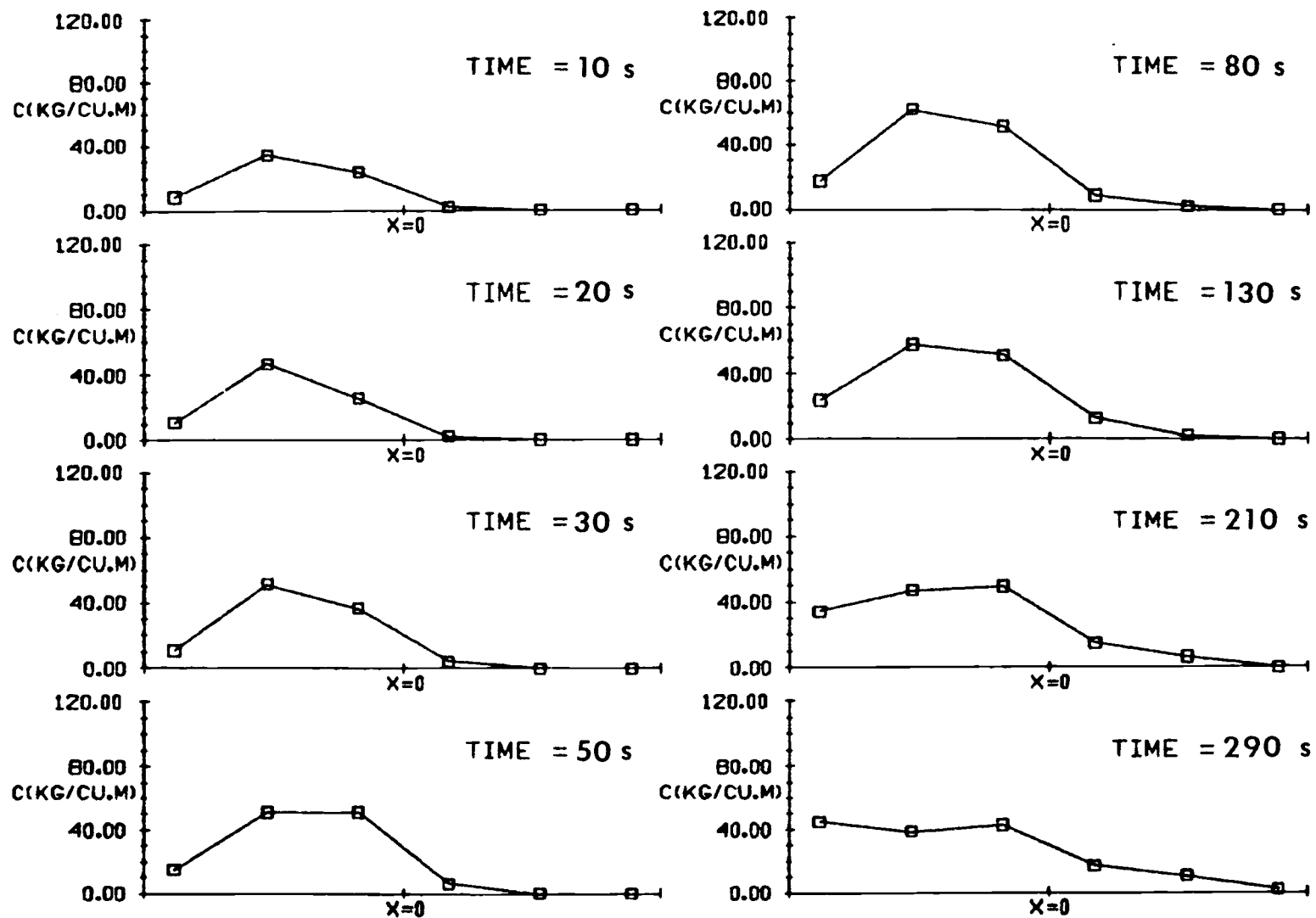


Figure 8.4 Concentration profiles of ferrite tracer from run number 6.

when gas bubbles rise in a fluidized bed, solids are entrained in the wake behind the bubble, resulting in an instability, partial collapse of the bubble, and the turbulent mixing behind it. The same authors also indicated that the wake is about 30 percent of the bubble volume and it is continually shed and replaced as the bubble rises causing the movement of solids in a vertical direction. Thus, movement and the resulting mixing of solids results from wake transport.

Sutherland (57) and Rowe and Sutherland (51) also found that the mixing of solids in a fluidized bed was generally caused by bubbles and the mixing increased as the gas velocity increased above  $u_{mf}$ . They observed that no bubbles and no mixing occurred at gas velocities close to  $u_{mf}$  and significant improvements in mixing at velocities only 1.2 times  $u_{mf}$ .

### Diffusion equation

When the composition of a mixture varies from one point to another, each component has a tendency to flow in the direction that will reduce the local differences in concentration (56). In this experiment, the concentration of ferrite particles in the bed was found to vary with location in the bed and time. The concentration of ferrite tracer in the bed satisfies the unsteady state diffusion equation.

$$\frac{\partial c}{\partial t} = D_w \frac{\partial^2 c}{\partial w^2} + D_y \frac{\partial^2 c}{\partial y^2} + D_z \frac{\partial^2 c}{\partial z^2} \quad (8.1)$$

However, since the width ( $w$ ) of the bed is small, the concentration gradient in the  $w$ -direction can be lumped. Thus,

$$\frac{\partial c}{\partial t} = D_y \frac{\partial^2 c}{\partial y^2} + D_z \frac{\partial^2 c}{\partial z^2} \quad (8.2)$$

Furthermore, as bubbles rise in a fluidized bed, solids are drawn into the bubble wake and completely mixed in the wake. Particle circulation within the wake causes lateral displacement of the solids shed through the bed and at the surface. A consideration of these mechanisms indicates that vertical mixing should be more rapid than lateral mixing (28). Thus, the concentration gradient in the vertical direction ( $y$ ) can be neglected in comparison with the lateral concentration gradient.

$$\frac{\partial c}{\partial t} = D_z \frac{\partial^2 c}{\partial z^2} \quad (8.3)$$

Equation (8.3) can be solved if two appropriate boundary conditions and one initial condition are known. In the experiment, one percent by weight of the ferrite tracer ( $32.036 \text{ kg/m}^3$ ) is dumped evenly in the slumped section of the bed at  $z=a$  to  $z=b$ . The concentration in that interval ( $a$  &  $b$ ) before the refluidization starts which is defined as  $c_i$  is calculated to be equal to  $c^* L / (b-a)$ . The schematic representation of the coordinate and location of  $a$  and  $b$  is shown in Figure 8.5. Thus,

$$\text{Initial condition : } t = 0, \quad c = c_i (U(z-a) - U(z-b)) \quad (8.4)$$

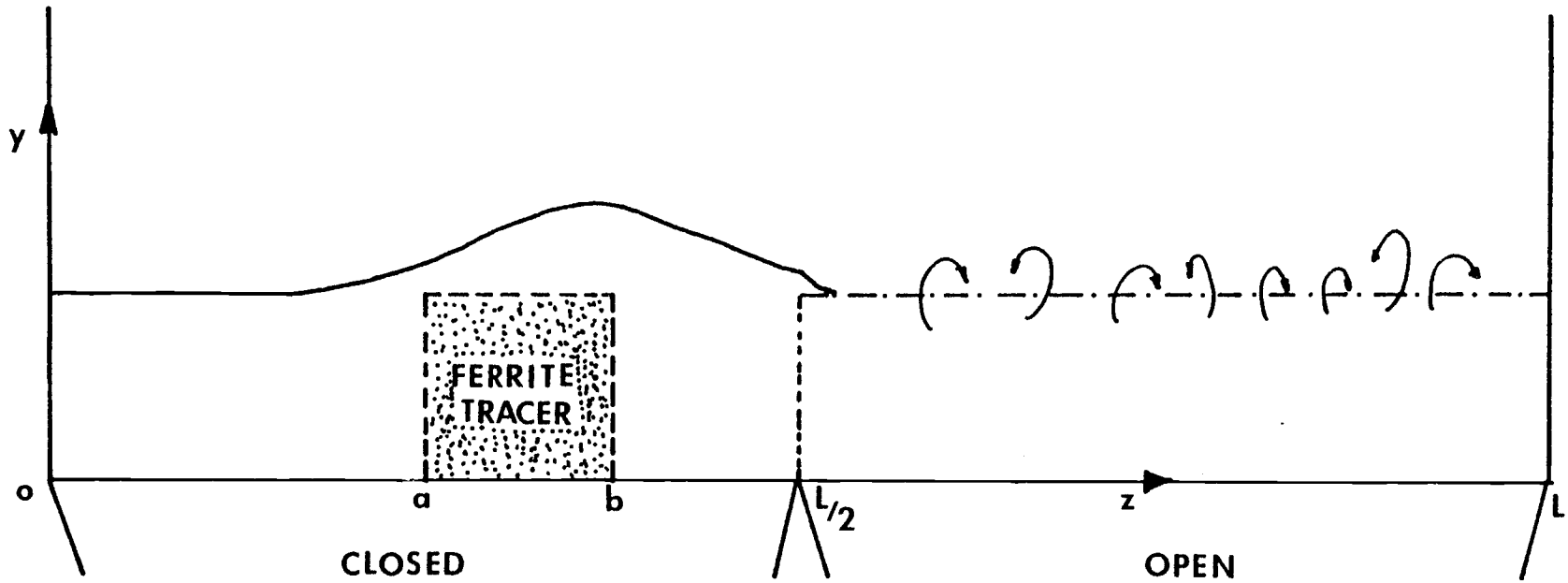


Figure 8.5 Schematic representation of the coordinate and the location of the ferrite tracer initially introduced to the slumped bed.

where  $U(z-a)$  and  $U(z-b)$  are unit step functions.

For the boundary conditions, it can be seen that there will be no concentration gradient at both ends of the bed. Thus,

$$\text{Boundary condition : } z = 0, \quad \frac{\partial C}{\partial z} = 0 \quad (8.5)$$

$$z = L, \quad \frac{\partial C}{\partial z} = 0 \quad (8.6)$$

The solution of equation (8.3) can be obtained by using both boundary conditions, equation (8.5) and (8.6) and the initial condition, equation (8.4), and can be expressed as,

$$c(z,t) = c^* + 2 \frac{c_i}{L} \sum_{n=1}^{\infty} \frac{(\sin \lambda_n b - \sin \lambda_n a)}{\lambda_n} \exp(-D_z \lambda_n^2 t) \cos \lambda_n z \quad (8.7)$$

$$\text{where } \lambda_n = n\pi/L \quad n=1,2,3,\dots$$

#### Lateral dispersion coefficient of solids

From equation (8.7), the concentration of ferrite tracer is expressed in terms of concentration of ferrite tracer at equilibrium or steady condition ( $c^*$ ), the location in the bed ( $z$ ), the time after refluidization ( $t$ ) and the initial location of ferrite tracer in the bed ( $a, b$ ). The lateral dispersion coefficient of solids ( $D_z$ ) can be solved since the concentration of tracer at a particular place and time ( $c(z,t)$ ) is known from the experiment and the other quantities i.e.,  $c^*$ ,  $c_i$ ,  $L$ ,  $t$  and  $z$  are known.

In order to determine  $D_z$ , numerical methods were used. Equation (8.7) can be rewritten in terms of the unknown  $D_z$  as,

$$f(D_z) = c(z,t) - \frac{2c_i}{L} \sum_{n=1}^{\infty} \left( \frac{\sin \lambda_n b - \sin \lambda_n a}{\lambda_n} \right) \exp(-D_z \lambda_n^2 t) \cos \lambda_n z \quad (8.8)$$

The technique called Newton's Root Finding Method (6) was used to find the zeros of  $f(D_z)$  in equation (8.8). For an iterative process,  $D_z$  can be determined from the expression,

$$D_{z_{k+1}} = D_{z_k} + \frac{f(D_{z_k})}{f'(D_{z_k})} \quad (8.9)$$

and the final  $D_z$  is obtained if the following expression holds,

$$\left| \frac{D_{z_{k+1}} - D_{z_k}}{D_{z_k}} \right| < 10^{-4} \quad (8.10)$$

The time ( $t$ ) in equation (8.8) is a fixed constant. The values of  $D_z$  obtained from all six different values of  $z$  (6 probes) were found to be slightly different. The value of  $D_z$  from the test at one particular time was obtained by finding the average of  $D_z$  from all six locations.

$$D_z(z, t_1) = \frac{1}{6} (D_z(z_1, t_1) + D_z(z_2, t_1) + \dots + D_z(z_6, t_1)) \quad (8.11)$$

Furthermore, the data of concentration profiles are provided at various time ( $t=10, 20, 30, \dots, 290$  s). The real value of  $D_z$  from each run can be finally obtained by the finding the average value of  $D_z$  from all different times.



$$D_z(z,t) = \frac{1}{8} (D_z(z,t_1) + D_z(z,t_2) + \dots + D_z(z,t_8)) \quad (8.12)$$

where  $t_1=10$ ,  $t_2=20$ ,  $t_3=30$ , ...,  $t_8=290$  seconds.

After the final value of  $D_z$  from all nine runs were obtained, it was found that  $D_z$  was mainly a function of the superficial velocity and the plot of  $D_z$  at various superficial velocity is shown in Figure 8.6.

After the values of  $D_z$  were obtained, the theoretical concentration profiles were plotted by using equation (8.7) and compared with the experimental concentration profiles. Samples of the plots at various superficial velocities are shown in Figures 8.7a, b, and c.

Several investigators have conducted experiments and developed models to determine the lateral dispersion coefficients of solids in fluidized beds (19, 42, 32, 28). The summary of the conditions of the experiments and the correlations of  $D_z$  obtained is shown in Table 8.2. In order to compare the values of  $D_z$  obtained from this experiment and from the other investigators, it is necessary to estimate values of the unknowns in the correlations listed in Table 8.2 from this experiment. For the correlation proposed by Mori and Nakamura, equation (8.14), the values of  $d_b$  at various superficial velocities can be obtained from equation (5.16). In equation (8.15), the fraction of bed occupied by bubbles ( $\delta$ ) can be estimated by measuring the height of the expanded bed and the fixed bed. The fraction of the bed occupied by bubbles ( $\delta$ ) can be approximated by the ratio of the difference between the height of the fixed bed and the expanded bed and the height of the fixed bed, and is found to vary from 0.125 at  $u = 0.60$  m/s to 0.20 at  $u = 0.90$  m/s. The voidage of the bed at the minimum fluidizing velocity is assumed

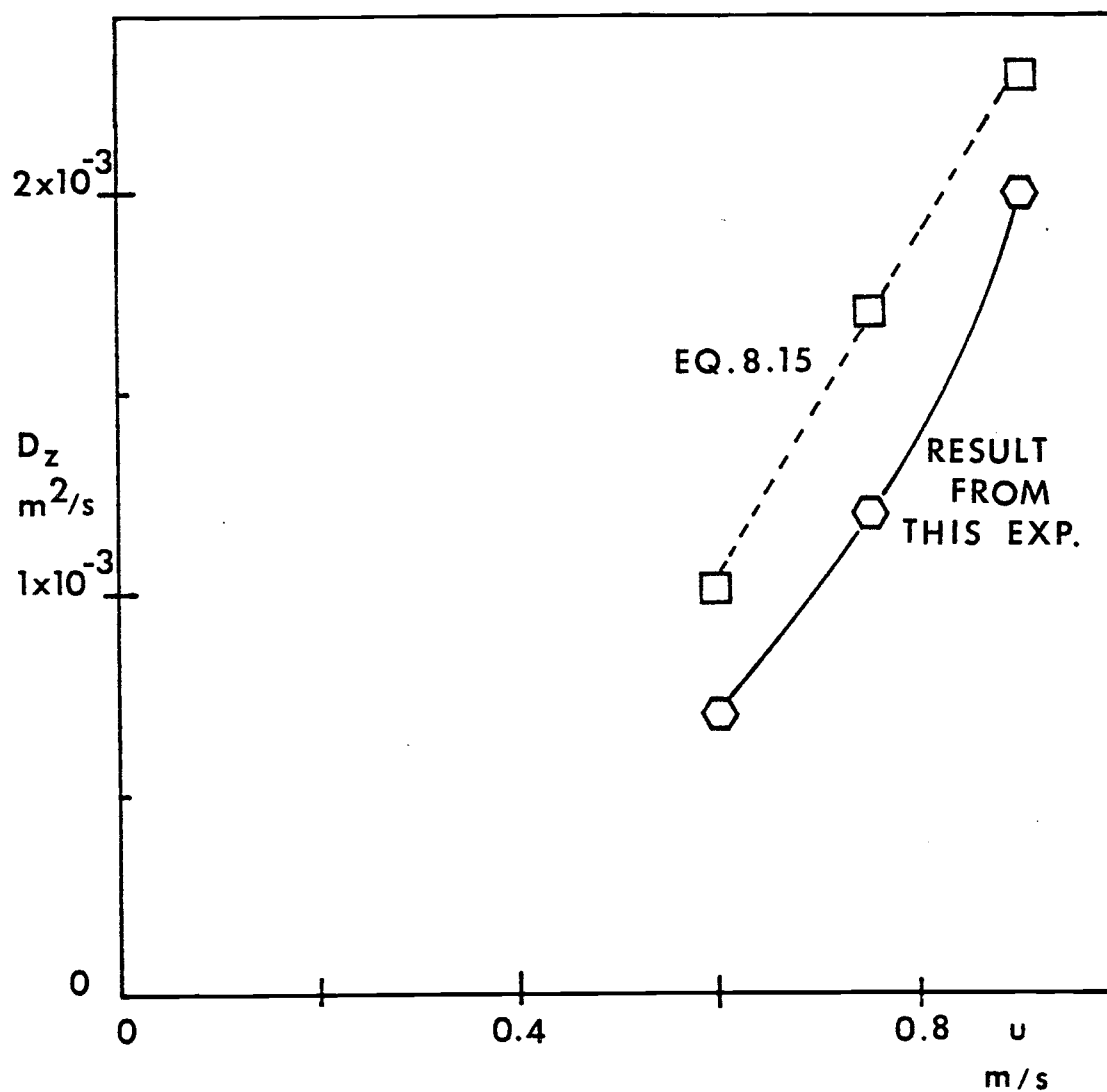


Figure 8.6 Plots of dispersion coefficient of solids obtained from the experiment as a function of superficial velocity.

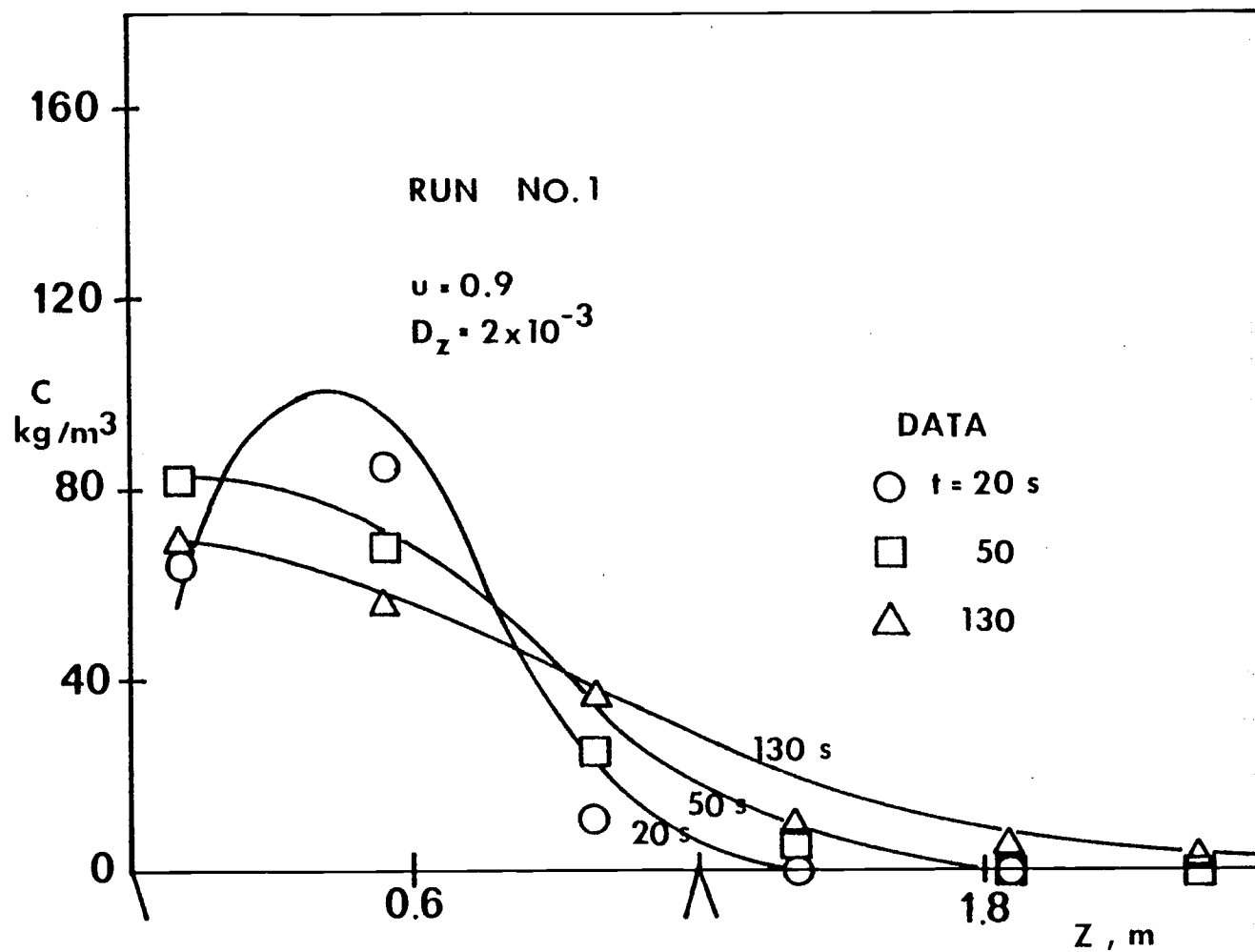


Figure 8.7a Concentration profiles from run number 1 by using equation (8.7) with  $D_z = 0.002 \text{ m}^2/\text{s}$ .

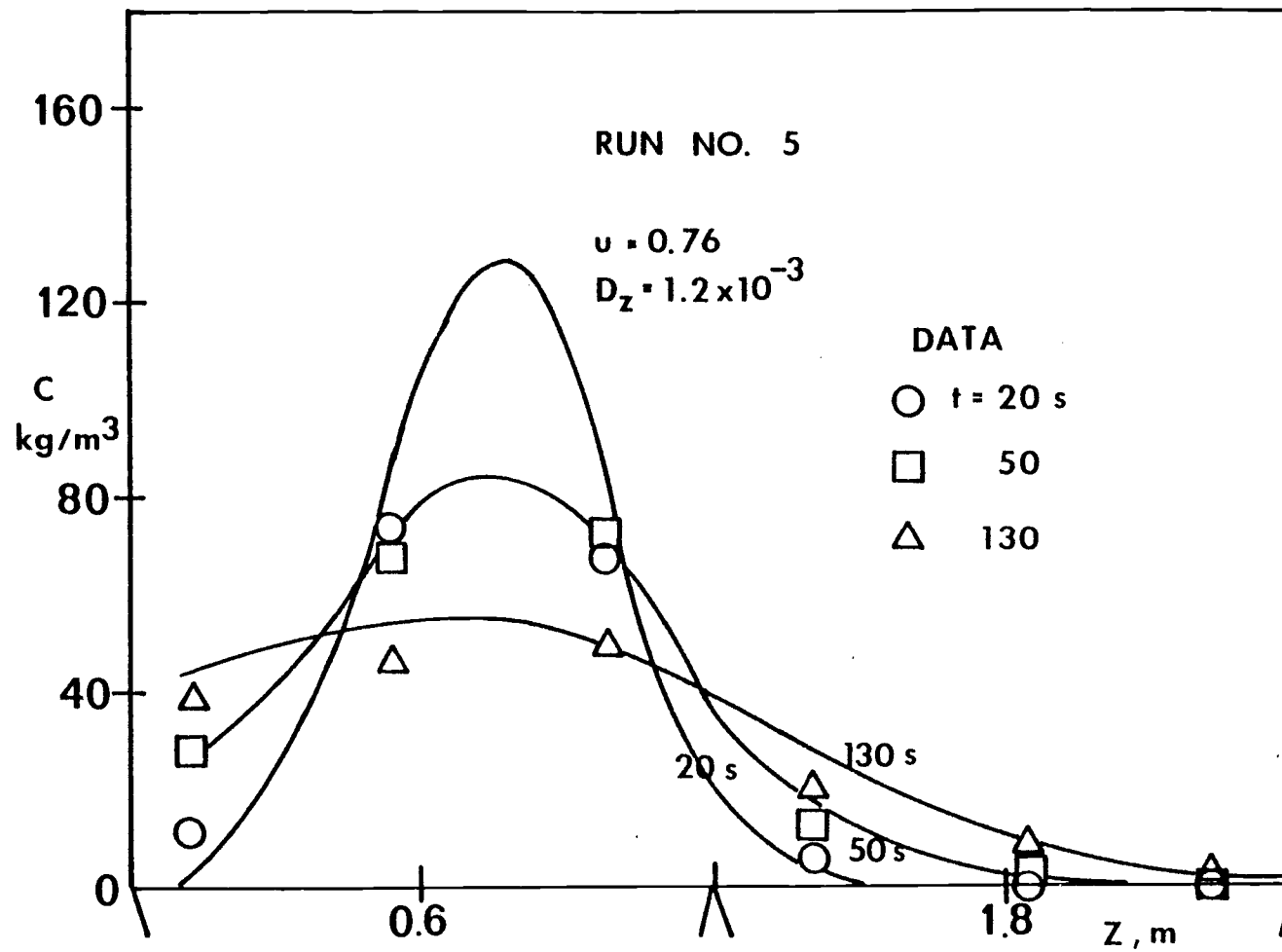


Figure 8.7b Concentration profiles from run number 5 by using equation (8.7) with  $D_z = 0.0012 \text{ m}^2/\text{s}$ .

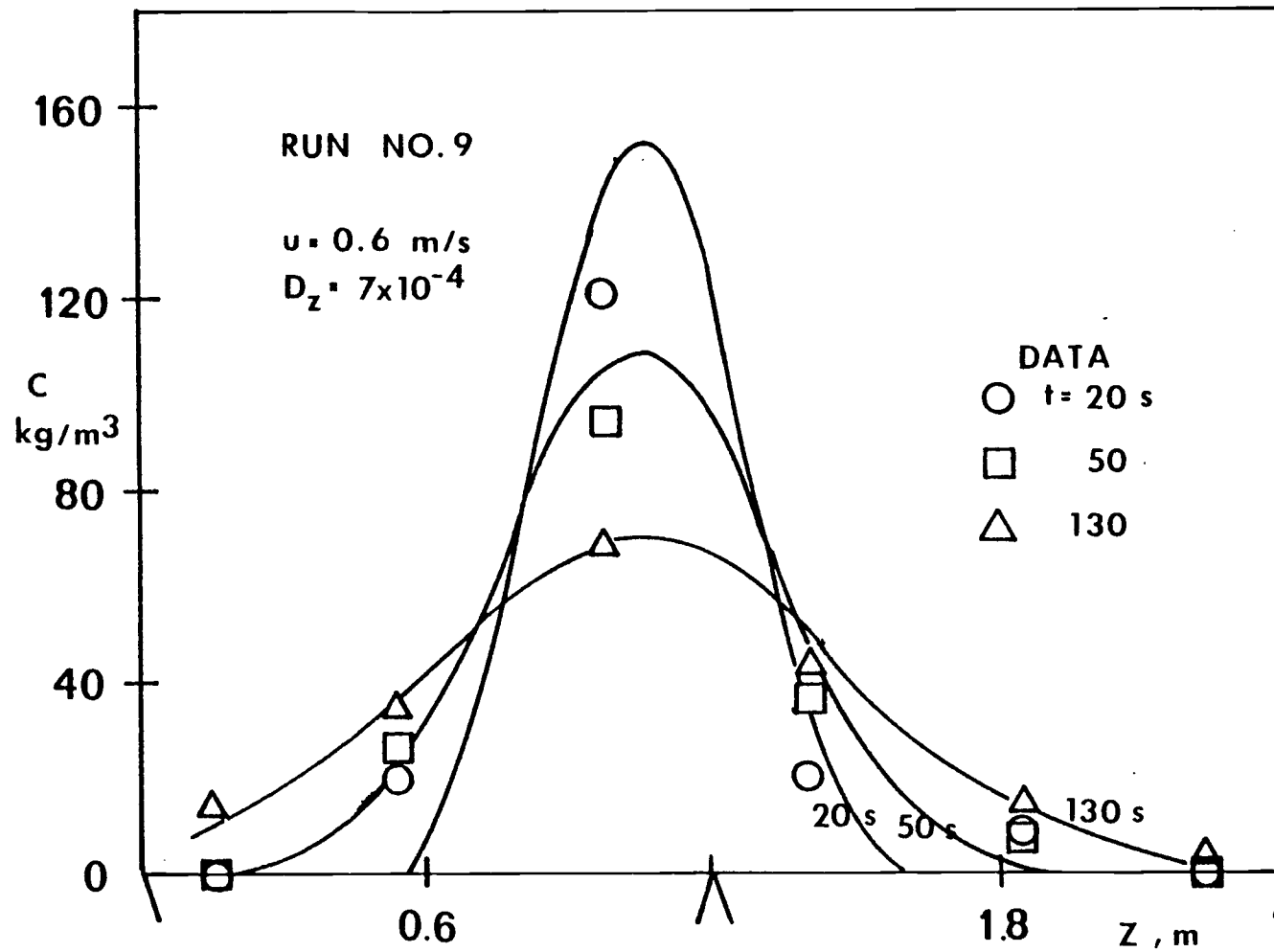


Figure 8.7c Concentration profiles from run number 9 by using equation (8.7) with  $D_z = 0.0007 \text{ m}^2/\text{s}$ .

Table 8.2 Summary of the experimental conditions and values of  $D_z$  obtained.

Investigator	Bed	Solids	$D_z (m^2/s)$
Gabor (19)	0.78m by 0.05m packed with steel spheres and brass cylinders	copper and nickel shot 88-330 $\mu$	$D_z = L((u - u_{mf})/d_p \epsilon_{mf})^{1.15} \chi$ $3.72 \times 10^{-7}$ (8.13)
Mori and Naka- mura (42)	0.9 m by 0.3 m	polyvinyl chloride 595 $\mu$	$D_z = 2.7 d_b^{2.0}$ (8.14)
Kunii and Levenspiel (32)			$D_z = \frac{3}{16}(\delta/1-\delta)u_{mf}d_b/\epsilon_{mf}$ (8.15)
Highly and Merrick (28)	1.5 m diameter	coal and char	$D_z = 7.43 \times 10^{-3} - 1.48 \times 10^{-2}$ (no tube array) $D_z = 3.90 \times 10^{-3} - 7.9 \times 10^{-3}$ (with tube array)

to be 0.5. The predicted values of  $D_z$  from various investigations are calculated and are shown in Table 8.3. It can be seen that by using the reasonable values of  $\delta$  and  $\epsilon_{mf}$ , the predicted dispersion coefficients are in good agreement with the experimental values.

#### The mixing rate of solids between the refluidized section and the fluidized section

In order to determine the mixing rate of solids between both sections of the bed after the refluidization, the rate and the total amount of solids from the refluidized portion of the bed that transfer across the interface region to the fluidized portion must be determined. Equation (8.7) which expresses the concentration distribution of ferrite tracer after refluidization in terms of location and time ( $c(z,t)$ ) was used.

However, some modifications on equation (8.7) had to be made first. Equation (8.7) was primarily developed to use in the case where ferrite tracer was partially introduced to the slumped section (between location  $a$  and  $b$ ). In reality, to determine the rate of solids mixing between both sections of the bed, ferrite tracer must be introduced on the entire slumped section of the bed. Thus, the distance  $b$  was equal to the half of the bed length,  $b=L/2$ , and the distance  $a$  can be dropped out,  $a=0$ . Equation (8.7) was then modified as,

$$c(z,t) = c^* + \frac{2c_i}{L} \sum_{n=1}^{\infty} \sin \lambda_n \frac{L}{2} \frac{1}{\lambda_n} \exp(-D_z \lambda_n^2 t) \cos \lambda_n z \quad (8.16)$$

Table 8.3 Comparison of  $D_z$  from various investigators.

superficial velocity (m/s)	$D_z$ (m <sup>2</sup> /s)		
	equation (8.14)	equation (8.15)	this experiment
0.60	0.038	0.0010	0.0007
0.76	0.053	0.0017	0.0012
0.90	0.063	0.023	0.0020



where  $\lambda_n = \frac{n\pi}{L}$

$$c(z,t) = c^* + \frac{2c_i}{L} \sum_{n=1}^{\infty} \sin \frac{n\pi}{2} \frac{1}{\lambda_n} \exp(-D_z \lambda_n^2 t) \cos \lambda_n z \quad (8.17)$$

To determine the total amount of solids from the refluidized bed that transferred across the interface front to the fluidized bed at time  $t=t_1$  after refluidization, the concentration profile at time  $t=t_1$  was first determined by evaluating equation (8.17) at time  $t=t_1$ .

$$c(z,t_1) = c^* + \frac{2c_i}{L} \sum_{n=1}^{\infty} \frac{1}{\lambda_n} \sin \frac{n\pi}{2} \exp(-D_z \lambda_n^2 t_1) \cos \lambda_n z \quad (8.18)$$

The total amount of the transferred solids found in the active bed was equal to the summation of the predicted concentration in the active bed times the volume of the active bed. Thus,

$$m_c = \int_{\frac{L}{2}}^L c(z,t_1) A(z) dz \quad (8.19)$$

The cross-sectional area of the active bed can be taken out of the integration sign since it is constant.

$$\begin{aligned} m_c &= A \int_{\frac{L}{2}}^L c(z,t) dz \\ &= A \int_{\frac{L}{2}}^L \left[ c^* + \frac{2c_i}{L} \sum_{n=1}^{\infty} \frac{1}{\lambda_n} \sin \frac{n\pi}{2} \exp(-D_z \lambda_n^2 t) \cos \lambda_n z \right] dz \\ &= A \left[ c^* \frac{L}{2} - \frac{c_i}{L} \sum_{n=1}^{\infty} \frac{1}{\lambda_n^2} [1 - (-1)^n] \exp(-D_z \lambda_n^2 t) \right] \end{aligned} \quad (8.20)$$

If  $m^*$  is the total amount of solids from the original slumped section that diffused to the originally active sections at the steady state condition. Thus,

$$\begin{aligned}
 m^* &= A \int_{\frac{L}{2}}^L c^*(z,t) dz \\
 &= A \int_{\frac{L}{2}}^L c^*(t) dz \\
 &= A c^* \frac{L}{2}
 \end{aligned} \tag{8.21}$$

Finally, the relative amount of solids transfer ( $M$ ) which was defined as the ratio of  $m_c$  and  $m^*$  can be obtained and expressed as,

$$M = \frac{m_c}{m^*} = 1 - \frac{2}{L^2} \frac{c_i}{c^*} \sum_{n=1}^{\infty} \frac{[1 - (-1)^n]}{\lambda_n^2} \exp(-D_z \lambda_n^2 t) \tag{8.22}$$

From equation (8.22), plots of  $M$  at various times and superficial velocities are shown in Figure 8.8. In Figure 8.8, plots are obtained from three different superficial velocities, 0.60, 0.76 and 0.90 m/s where the corresponding values of  $D_z$  are 0.002, 0.0012 and 0.0007 m<sup>2</sup>/s respectively.

## 8.6 Conclusions

From the studies of solids mixing in a partially defluidized bed, it can be concluded that the technique of using ferrite tracer with inductance probes to represent the bed material transfer is successful.

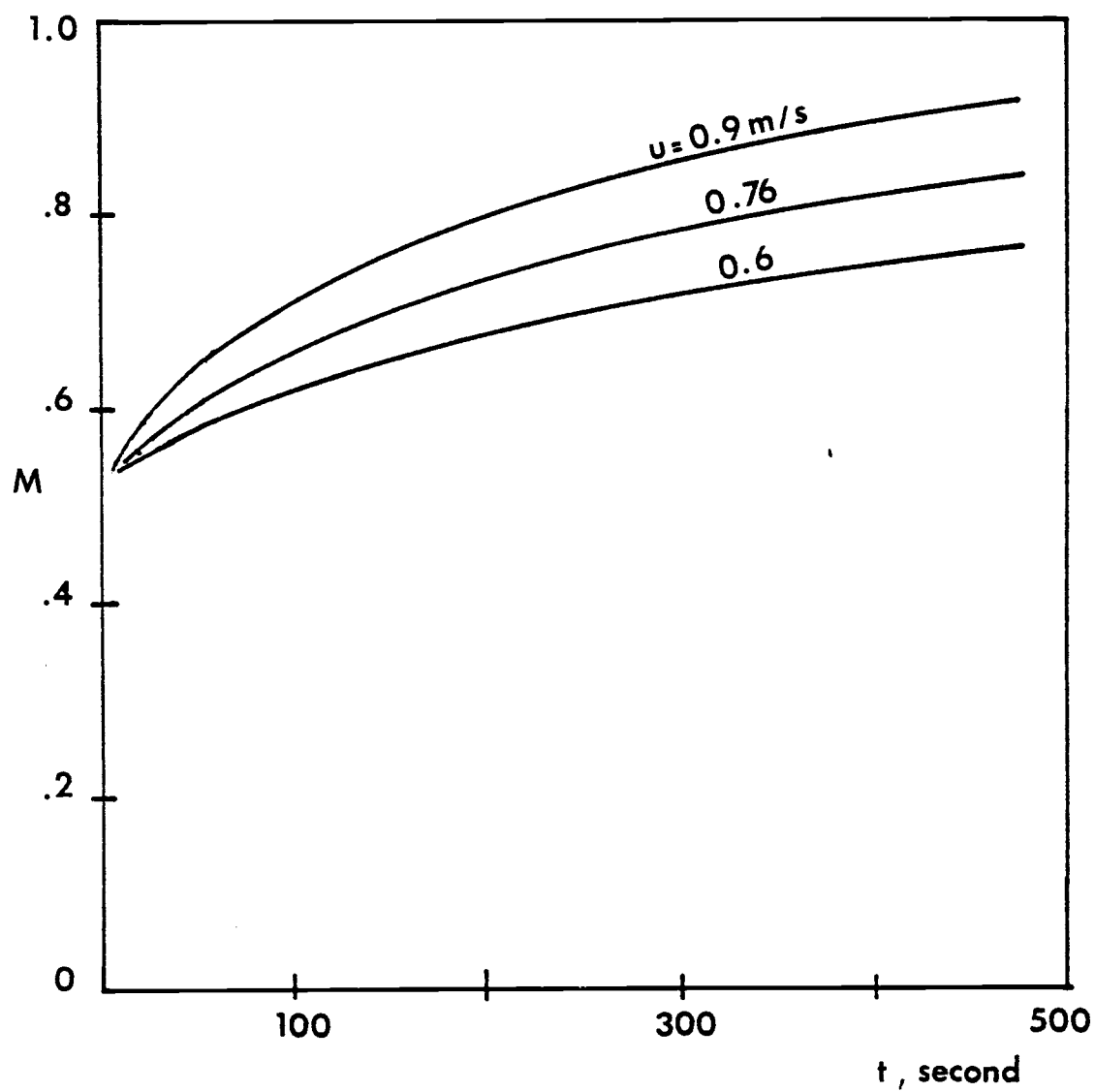


Figure 8.8 The relative amount of solids transfer ( $M$ ) as a function of time after refluidization.

The data obtained from sampling ferrite concentration was first obscure and ambiguous because of the effect of drifting and the effects of bubbles passing through probes. However, after the sampled data was reduced by appropriate techniques, reasonable reduced data was obtained.

The diffusion equation model can be used successfully to represent the rate of mixing of solids from both sections of the bed. The dispersion coefficient of tracer was obtained and was found to be a function of superficial velocity. Comparison between the dispersion coefficient obtained from the experiment and that by applying Einstein's random walk equation (equation (8.15)) which was proposed by Kunii and Levenspiel (32) indicated that there were good agreement between these two numbers.

Finally, the rate of solids mixing which was the rate that solids from the refluidized bed diffused across the interface region to the active bed was obtained. The value of  $M$  which was defined as the relative amount of transferred bed material detected in the active bed and was plotted in Figure 8.8 indicated that the mixing of solids from both sections would be reduced if the refluidizing velocity was decreased. However, the low refluidizing velocity should always exceed the critical refluidizing velocity.

## IX. THE CONVERSIONS OF RESULTS FOR FLUIDIZED BED COMBUSTORS

The data from the cold phase partially defluidized bed which consists of the slumped bed surface profiles, bed material transfer and solids mixing has been collected. In order to obtain useful information for the high temperature fluidized bed combustors, conversions using the scaling factors from the similarity analysis were applied.

The experimental cold phase fluidized bed used in this study resembles a 1.22 m wide by 9.65 m long high temperature fluidized bed combustor with the static bed height of 1.20 m. After half of a fluidized bed combustor is turned down, a slumped bed surface profile which is similar to the one in the cold phase bed but 3.76 times larger in size is expected to appear in the slumped section of the fluidized bed combustor.

The amount of bed material transfer in the fluidized bed combustor could also be obtained by using the results of bed material transfer in the cold phase bed. In the cold phase bed, if  $m_C$  represents the amount of bed material transferred at a particular time, then, the amount of bed material transferred in the fluidized bed combustor,  $m_H$ , at that particular moment will be calculated as follows,

$$\text{volume of material transfer in a cold phase bed } (V_C) = \frac{m_C}{\rho_{sc}} \quad (9.1)$$

volume of material transfer in a fluidized bed combustor

$$(V_H) = K^3 V_C \quad (9.2)$$

$$\begin{aligned}
 \text{then, } m_H &= \rho'_{sH} V_H \\
 &= \rho'_{sH} K^3 V_C \\
 &= K^3 m_C (\rho'_{sH} / \rho'_{sC}) \quad (9.3)
 \end{aligned}$$

In this experiment, the bulk density of zirconia sand was found to be  $3000 \text{ kg/m}^3$ , and the bulk density of the bed material in the fluidized bed combustor (99% limestone, 1% coal) was estimated to be  $1750 \text{ kg/m}^3$ . Thus,

$$m_H = 31.0 m_C \quad (9.4)$$

The total amount of bed material transferred in the fluidized bed combustor can be estimated to be 31 times the total amount of bed material transferred in the scaled bed.

In the qualitative study of the refluidization of a slumped section, since the ratio of gas velocity in the fluidized bed combustor to that in the cold phase bed was found to be 1.94, the speed of movies taken in the cold phase bed was 1.94 times faster than that in the fluidized bed combustor. In real time the fluidized bed combustor system was 1.94 times slower than the cold phase fluidized bed system. Thus, in order to simulate the real situation in the combustor, the speed of the movie projector used must be reduced to about half of the speed of the movies taken. Therefore, the time to refluidized the slumped section of the fluidized bed combustor was determined to be double of that in the cold phase scale bed.

In the studies of solids mixing in a cold phase slumped bed, it was found that the gas velocity and, thus, the number and size of bubbles have a very pronounced and direct effect on the solids mixing. Now, the question rises whether the size of bubbles in the fluidized bed combustor can be related to that in the cold phase scale bed by using the scaling factor. Fitzgerald and Crane (18) observed the bubble sizes and bubble growth rate in two hydrodynamics similar fluidized beds (sand/Freon system and cork/air system). They asserted that there were similarities in bubble growth and solids flow patterns between two beds at  $u_{mf}$  and various multiples of  $u_{mf}$ . However, this result could not yet be applied to the cold phase bed/high temperature bed system because the flow of gas bubbles in the cold phase scale bed and that in the high temperature bed are in different regimes (7). In the cold phase scaled bed, the bubble is rising in the small particle bed and is characterized as a "fast bubble" where gas enters the lower part of the bubble, leaves at the top, swept around and then returns forming a captive cloud around the bubble. On the contrary, a "slow bubble" phenomena where gas uses the bubble as a convenient shortcut on its way through the bed occurs in the large particle fluidized bed.

Bubble size in a room temperature fluidized bed can be presented in terms of superficial velocity and the height above the distributor plate, i.e., equation (5.11). However, no correlation of bubble size in a large particle bed at high temperature has been previously developed. An experiment at high temperature was conducted in a 0.30 m by 0.60 m high temperature bed using large particles, one grain with  $d_p = 3200$  microns and density  $2600 \text{ kg/m}^3$ . Data concerning the bubble

size in large particle high temperature bed were collected in term of bubble eruption diameter which can be related to the bubble diameter at the surface of the bed by the relationship  $d_{bm} = 0.858 d_o$  (61). It is interesting to point out that the relationship between the bubble eruption diameter and the mean bubble diameter in a bed with small particles is significantly different from that in a bed with large particles. The bubble eruption diameter in a large particle high temperature fluidized bed is plotted as a function of excess gas velocity and is shown in Figure 9.1. The details of the study can be obtained from (55). By using the similarity analysis, the operating condition for the scaled bed (i.e., particle size, bed height, bed area, and gas velocity) can be established. The scaling factor which was equal to 3.76 was obtained, thus, the particle size in the scaled bed was 3.76 times smaller and the gas velocity in the scale bed was about half of the gas velocity in the high temperature bed.

Using equations (5.9) to (5.11), the bubble diameter at the surface of the bed in an open bed (no internal tube) can be expressed as,

$$d_{bmC} = 0.594 (u - u_{mf})^{0.4} (h_{max} + 4\sqrt{A_0})^{0.8} / g^{0.2} \quad (9.5)$$

The resulting bubble diameter are plotted as a function of excess gas velocity and are shown in Figure 9.1. Finally, by using the scaling factor of 3.76, the bubble diameter at the surface in large particles high temperature bed ( $d_{bmH}$ ) was obtained as,

$$d_{bmH} = 3.76 d_{bmC} \quad (9.6)$$



The resulting bubble in a high temperature bed by using the scaling factor are also plotted in Figure 9.1. It can be seen that there are good agreement between experimental data and equation (9.6). However, at higher excess gas velocities the bubble size in the bed will actually increase very rapidly (7,30) (curve of  $d_{bm}$  has a positive curvature) and the equation (9.6) which has a negative curvature will be no longer applicable.

Since there is a similarity in bubble growth between the high temperature bed and the scale bed at low excess gas velocity, it is expected that the solids mixing study by using the diffusion equation model in the scaled bed can also be valid for the high temperature case. In the diffusion equation, it was found that there was good agreement of the dispersion coefficient of solids between the experimental data and that presented by Kunii and Levenspiel by using Einstein random walk equation.

$$D_z = \frac{3}{16} (\delta/1-\delta) u_{mf} d_b / \epsilon_{mf} \quad (8.15)$$

In equation (8.15), the magnitude of the term  $(\delta/1-\delta)/\epsilon_{mf}$  between the two beds are in the same order. Thus, the dispersion coefficient of solids in the high temperature bed will be in the order of  $K^{1.5}$  greater than that in the scaled bed, and the mixing of the solids in the high temperature bed will be more rapidly.

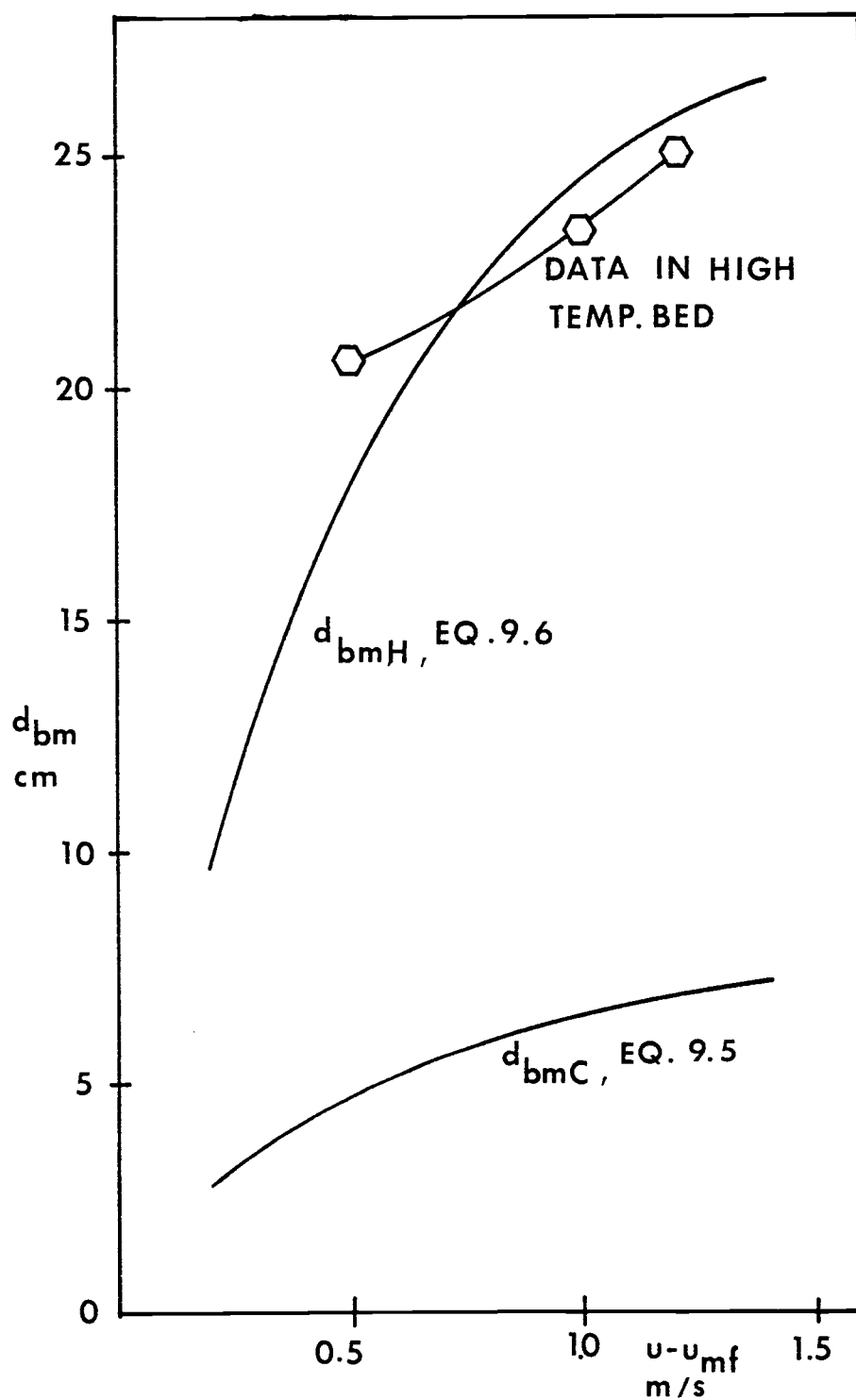


Figure 9.1 The comparison of  $d_{bm}$  in high temperature bed between experimental data and equation (9.6).

## X. SUMMARY AND RECOMMENDATION

In order to operate a fluidized bed combustor that can successfully follow the electrical load pattern, a section of the fluidized bed combustor is defluidized, that is, cutting off the flow of air and coal to that region. As the section of the fluidized bed combustor is defluidized, solids or bed materials are entrained from the remaining active section and fall onto the slumped region causing substantial depletion of the bed material in the active portion.

The transferred bed material instantly create a ridge on the slumped section where the surface profile of the ridge changes with time. It is observed that the slumped bed surface profiles can be divided into three separate regions and each region can be presented in terms of excess gas velocity and time after defluidization. Equation (4.1) to (4.6) which generate the surface profiles are obtained by using the regression method to best fit the experimental data.

In the study of the solids entrainment from the active bed, it is found that the cause of entrainment is from the effect of bubble erupting at the bed surface. As the bubble erupts, the bed particles are ejected from the bursting bubble. The initial velocities of those ejected particles are developed by using the potential flow theory and can be expressed as,

$$u_i = 2.0(u - u_{mf} + 22.26d_{bm}^{0.5}) \cos \theta \quad (5.8)$$

The correlation of the bubble diameter at the bed surface for a fluidized bed with immersed heat exchange tube array is developed and compared to other investigators' results. It is found that the correlation which can be expressed as,

$$d_{bm} = 0.594 (u - u_{mf})^{0.4} (h_1 + 4\sqrt{A_0})^{0.8} / g^{0.2} + (-0.036 + 0.004(u - u_{mf}))(h_{max} - h_1) \quad (5.16)$$

gives good agreement with other experimental works.

To determine the rate of bed material transfer from the active bed, equations of motion for the ejected particles are developed by using the knowledge of equations (5.8) and (5.16) to determine the trajectories of all ejected particles. The amount of each ejected particle is calculated by determining the thickness of the bubble bulge at the bed surface. The products of the trajectories and the amounts of each trajectory represent the distribution of the transferred material in the slumped bed. The frequency of the bubble eruption at the surface of the active bed is measured. The distribution of the transferred material associated with the frequency of the eruption represents the rate of the bed material transferred from the active bed to the adjacent slumped bed. Comparison between experimental data and the proposed model indicates good agreement. However, since this model required the exact location where the bubble erupts at the bed surface, the assumption about the location where the bubble erupts in this study, which has limited accuracy, may cause an error in the result. Future work about the location and the distribution of the bubble eruption at the fluidized bed surface is recommended.

To obtain exact and usable information, the data about the bed material transfer is collected in a form of the particle density function where the correlation about the particle density function is established and is presented as,

$$\phi_d = \exp((2.60-11.15y)-(11.30-10.50y)x+(9.50-8.53y)(u-u_{mf})) \quad (5.32)$$

using the proposed correlation which fits very well to the experimental data, the total amount of bed material transfer during the defluidization is obtained by integrating the particle density function over the entire slumped bed section and over the duration of defluidization. The results indicate good agreement with the experimental data.

In the study of the pressure drop in the slumped bed, it is found that the pressure drop in the slumped bed varies with its location in the slumped bed and the superficial gas velocity in the active bed. By using the Ergun equation, the amount of gas flow in the slumped bed can be obtained from the knowledge of the pressure drop profiles. The percentage of gas flow through the slumped bed are found to be independent of the superficial gas velocity and are found to be approximately 6-7 percent of the total flow.

In the study of the refluidization of the slumped section, both the qualitative and quantitative studies indicate that the complete refluidization of the slumped section will not occur if the refluidizing velocity is less than  $2u_{mf}$  which is termed a critical velocity. At low refluidizing velocity, the ridge shape changes from a sharp peak to a lower bell shaped curve. At high refluidizing velocities (above the entire  $2u_{mf}$ ) slumped portion refluidizes rapidly.

In the study of the solids mixing between both sections of the bed after the refluidization, it can be observed that the mechanism of solids mixing, or the dispersion of the solids from the refluidized section to the active section can be represented by the diffusion model. The unsteady diffusion equation is solved by using appropriate boundary conditions and initial conditions and the solution can be presented as,

$$c = c^* + \frac{2c_i}{L} \sum_{n=1}^{\infty} \frac{1}{\lambda_n} \sin \lambda_n L/2 \exp(-D_z \lambda_n^2 t) \cos \lambda_n z \quad (8.16)$$

The dispersion coefficient of solids is determined by fitting the set of experimental data to the diffusion solution. It is found that the dispersion coefficient of solids increases significantly with the superficial gas velocity.

The relative amount of bed material that transfer or diffuse from the refluidized section across the interface region to the active bed after the refluidization is finally obtained and is expressed as,

$$M = 1 - \frac{2}{L^2} \frac{c_i}{c^*} \sum_{n=1}^{\infty} \frac{(1-(-1)^n)}{\lambda_n^2} \exp(-D_z \lambda_n^2 t) \quad (8.22)$$

The resulting values of M indicate that the total amount of material diffused from the refluidized side to the active side increases with the refluidizing velocity.

All of the data and information that was gathered from the cold phase scaled bed can be related to the required information for the high temperature fluidized bed combustor by using the scaling factor from the similarity analysis study.

Since the experiment was conducted in only one configuration, the height of the fixed bed, the location and the type of the tube array in the bed were held unchanged during the entire experiment. Thus, some correlation proposed in this study will lack all of the information that was previously mentioned. Future work that involves these parameters, for example, varying the fixed bed height, the location and the type of the tube array in the bed, is highly recommended.

## BIBLIOGRAPHY

1. Andrews, J.M., " Kinetic Study of Fluidized Solids Entrainment," Ind. Eng. Chem. ,52, 1, 85 (1960)
2. Arguriou, D.T., List, H.L., and Shinnar, R., " Bubble Growth by Coalescence in Gas Fluidized Beds," AIChE J., 17, 1, 122 (1971)
3. Bauver II, W.P., Bianca, J.D., Jones, B.C., and Matthews, F.T., " Evaluation of Slumped Testing for Industrial Application of Fluidized Bed Combustion," U.S. DOE, EX-76-C-01-2473 (1977)
4. Botterill, J.S.M., George, J.S. and Besford, H., " Bubble Chains in Gas Fluidized Beds," Chem. Eng. Prog. Symp. Ser., 62, 62, 7 (1966)
5. Bushnell, D.J., and Sitthiphong, N., " Experimental Modeling of a High Temperature Partially Defluidized Bed," The Proce. of the Sixth Int. Conf. on Fluidized Bed Combustion,2, 632 (1980)
6. Carnahan, B., Luther, H.A., and Wilkes, J.O., " Applied Numerical Methods, John Wiley, N.Y. (1969)
7. Catapovic, N.H., Jovanovic, G.N., and Fitzgerald T.J., " Regimes of Fluidization for Large Particles," AIChE J., 24, 3, 543 (1978)
8. Chao, H.H., " An Investigation of Slumping Behavior in Cold-Phase Fluidized Bed," M.S. Thesis, Oregon State University, Corvallis, OR (1979)
9. Chen,T.P., and Saxena, S.C., " A Theory of Solids Projection from a Fluidized Bed Surface as a First Step in the Analysis of Entrainment Processes," Proc. of the Second Eng. Foundation Conf., Cambridge England (1978)
10. Clift,R., and Grace,J.R., " Bubble Interaction in Fluidized Beds," Chem. Eng. Prog. Symp. Ser.,66, 105, 14 (1970)



11. Clift, R., and Grace, J.R., " The Coalescence of Bubble Chains in Fluidized Beds," Tran.Inst. Chem. Eng., 50, 364 (1972)
12. Darton, R.C., LauNauze, R.D., Davidson, J.F., and Harrison, D., " Bubble Growth Due to Coalesence in Fluidized Bed," Tran. Inst. Chem. Eng., 55, 4, 274 (1977)
13. Davidson, J.F. and Harrison, D., Fluidized Particles, Cambridge University Press, N.Y. (1963)
14. Deaton, W.W., " Solids Movements in a Tube-Filled Fluidized Bed," Master Thesis, Oregon State University, Corvallis, OR (1980)
15. DO, H.T., Grace, J.R., and Clift, R., " Particle Ejection and Entrainment from Fluidized Beds," Powder Tech., 6, 1975 (1972)
16. Ergun, S., " Fluid Flow Through Packed Columns," Chem. Eng. Prog. 48, 89 (1952)
17. Fitzgerald, T.J., Catapovic, N.H. and Jovanovic, G.N., " Solid Tracer Studies in a Tube-Filled Fluidized Bed," Paper presented at the Fifth Int. Conf. on Fluidized Bed Combustion (1977)
18. Fitzgerald, T.J., and Crane, S. " Cold Fluidized Bed Modeling," Paper presented at the Sixth Int. Conf. on Fluidized Bed Combustion (1980)
19. Gabor, J.D. " Lateral Solids Mixing in Fluidized Packed Bed," AICHE J. 10,3, 345 (1964)
20. Geldart, D., " The Expansion of Bubbling Fluidized Beds," Powder Tech., 1, 355 (1972)
21. Geldart, D., " The Effect of Particle Size and Size Distribution on The Behavior of Gas Fluidized Beds," Powder Tech. 6, 201 (1972)
22. Geldart, D., and Kapoor, D.S. " Bubble Sizes in a Fluidized Bed at Elevated Temperatures," Chem. Eng. Sci., 31, 842 (1976)

23. Geldart, D., " The Size and Frequency of Bubbles in 2 and 3- D Gas Fluidized Beds," Powder Tech., 4, 41 (1970)
24. George, S.E., and Grace, J.R., " Entrainment of Particles from Aggregative Fluidized Bed," AIChE Sym. Ser., 76, 176, 67 (1978)
25. Grace, J.R., and Clift, R., " On the Two Phase Theory of Fluidization," Chem. Eng. Sci., 29, 335 (1974)
26. Grace, J.R., and Harrison, D., " The Behavior of Freely Bubbling Fluidized Beds, Chem. Eng. Sci., 24, 497 (1969)
27. Harrison, D. and Laung. L.S., " The Rate of Rise of Bubbles in Fluidized Beds," Tran. Inst. Chem. Eng., 40, 146 (1962)
28. Highly, J. and Merrick, D., " The Effect of the Spacing Between Solids Feed Points on the Performance of a Large Fluidized Bed Reaction," AIChE Sym. Ser., 67, 116, 219 (1971)
29. Jackson, R., " Fluid Mechanical Theory " in Fluidization, Davidson, J.F., and Harrison, D., ed., 65, Academic Press, N.Y. (1971)
30. Javanovic, G.N., " Gas Flow in Fluidized Beds of Large Particles, Experiment and Theory," Ph.D thesis, Oregon State University, Corvallis, OR (1979)
31. Kato, K., and Wen, C.Y., " Bubble Assemblage Model for Fluidized Bed Catalytic Reactors," Chem. Eng. Sci., 24, 351, (1969)
32. Kunii, D., and Levenspiel, O., " Lateral Dispersion of Solid in Fluidized Beds," J. of Chem. of Japan, 2, 2, 122 (1969)
33. Kunii, D., and Levenspiel, O., Fluidization Engineering, John Wiley, N.Y. (1969)
34. Lackey, M.E., and Withers, H.W., " Cold Slumping Characteristic of a Fluidized Bed," Paper presented at the Sixth Int. Conf. on Fluidized Bed Combustion (1980)

35. Lewis, W.K., Gilland, E.R., and Lang, P.M., " Entrainment from Fluidized Beds," Chem. Eng. Prog. Symp. Ser., 38, 58, 65 (1962)
36. Leung, L.S., " Design of Gas Distributors and Prediction of Bubble Size in Large Gas-Fluidized Beds," Powder Tech., 6, 189 (1972)
37. Lockwood, D.N., " An Investigation of the Effects of Immersed Heat Exchange Tube Spacing and Arrangement on the Quality of Fluidization in a Cold Phase Two-Dimensional Fluidized Bed," Master Thesis, Oregon State University, Corvallis, OR (1976)
38. Loew, O., Shmutter, B. and Resnick, W., " Particle and Bubble Behavior and Velocities in a Large-Particle Fluidized Bed with Immersed Obstacles," Powder Tech., 22, 45 (1979)
39. McGaw, D.R., " The Development of a Mechanism for Gas-Particle Heat Transfer in Shallow Fluidized Beds of Large Particles," Chem. Eng. Sci., 32, 11 (1977)
40. McKenzie, E.C., " Burning Coal in Fluidized Beds," Chem. Eng., 85, 18 (1978)
41. Mii, T., Yoshida, K., and Kunii, D., " Temperature- Effects on the Characteristics of Fluidized Beds," J. of Chem. of Japan, 61, 1, 10 (1973)
42. Mori, Y., and Nakamura, K., " Solid Mixing in a Fluidized Bed," Kagaku Kogaku, 4, 1, 154 (1966)
43. Mori, S., and Wen, C.Y., " Estimation of Bubble Diameter in Gaseous Fluidized Bed," AIChE J., 21, 1, 109 (1975)
44. Nguyen, H.V., Potter, O.E., and Whitehead, A.B., " Bubble Distribution and Eruption Diameter in a Fluidized with a Horizontal Tube Bundle," Chem. Eng. Sci., 34, 1163 (1979)

45. Richardson, J.F., " Incipient Fluidization and Particulate Systems," in Fluidization, Davidson, J.F. and Harrison, D., ed., 25, Academic Press, N.Y. (1971)
46. Rowe, P.N., " Prediction of Bubble Size in a Gas Fluidized Bed, Chem. Eng. Sci., 31, 285 (1976)
47. Rowe, P.N., " Experimental Properties of Bubbles," in Fluidization, Davidson, J.F., and Harrison, D., ed., 121, Academic Press, N.Y. (1971)
48. Rowe, P.N., and Everett, D.J., " Fluidized Bed Bubble Views by X-Rays, " Tran. Inst. Chem. Eng., 50, 42 (1972)
49. Rowe, P.N., and Partridge, B.A., " The Interaction Between Fluids and Particles," Inst. Chem. Eng. of London, 135 (1962)
50. Rowe, P.N., and Sutherland, K.S., " Solids Mixing Studies in Gas Fluidized Beds," Tran. Inst. Chem. Eng., 43, T157 (1963)
51. Rowe, P.N., and Sutherland, K.S., " Solids Mixing Studies in Gas Fluidized Beds," Tran. Inst. Chem. Eng., 42, T55 (1962)
52. Sabersky, R.N., Austa, A.J., and Hauptmann, E.G., Fluid Flow, Chapter 5, Macmillan, N.Y. (1971)
53. Scharff, M.F., Goldman, S.R., Flanigan, T.M., and Gregory, T.K., " Project to Provide an Experimental Plan for the Merc 6x6 Bed Cold Test Model," U.S. DOE, EY-76-C-21-8156 (1977)
54. Singh, B., Rigby, G.R., and Callcott, T.O. " Measurement of Minimum Fluidization Velocities at Elevated Temperatures," Tran. Inst. Chem. Eng., 51, 93 (1973)
55. Sitthiphong, N., George, A. and Bushnell, D.J., " Bubble Eruption Diameter in a Fluidized Bed of Large Particles at Elevated Temperatures," Paper submitted to Chem. Eng. Sci.

56. Skelland, A.H.P., Diffusional Mass Transfer, John Wiley, N.Y. (1974)
57. Sutherland, K.S., " Solid Mixing Studies in Gas Fluidized Beds,"  
Tran. Inst. Chem. Eng., 39, 128 (1961)
58. Wen, C.Y., and Hashinger, R.F., " Elutriation of Solid Particle  
from a Dense Phase Fluidized Bed," AICHE J., 6, 2, 220 (1960)
59. Wen, C.Y., and YU, Y.H., " A Generalized Method for Predicting  
the Minimum Fluidizing Velocity," AICHE J., 12, 610 (1960)
60. Werther, J., " Bubble in Gas Fluidized Beds," Tran. Inst. Chem. Eng.  
52 (1954)
61. Whitehead, A.B., " Some Problems in Large Scale Fluidized Beds,"  
in Fluidization, Davidson, J.F., and Harrison D., ed., 781,  
Academic Press, N.Y. (1971)
62. Whitehead, A.B., and Young, A.D., " Fluidization Performance in  
Large Scale Equipment," Proc. Int. Sym. on Fluidization, Eindhoven,  
Netherland (1967)
63. Zenz, F.A., and Weil, N.A., " A Theoretical-Empirical Approach to  
the Mechanism of Particle Entrainment from Fluidized Beds,"  
AICHE J., 4, 472 (1958)

## APPENDIX A

## Zirconia Sand Sieve Analysis

The mean surface diameter,  $d_p$ , of zirconia sand was found to be 305 microns. The calculations were based on the method presented in (33), by using the formular,

$$d_p = \frac{1}{\sum_{\text{all } i} (x/d_p)_i}$$

where  $d_p$  = mean surface particle size ( $\mu$ )

$x_i$  = fraction of material in size interval  $i$

$d_{pi}$  = average diameter of size interval  $i$  ( $\mu$ )

The results of the calculation is shown in Table A1.

TABLE A1

## Zirconia Sand Sieve Analysis

Cumulative Weight of a Representative 1372 gm Sample      With Diameter Smaller Than ( $\mu$ )

0	147
86	175
195	208
386	249
536	295
858	417
1085	495
1317	589
1372	833

Diameter Range ( $\mu$ )	$d_{pi}(\mu)$	$x_i$	$(x/d_p)_i$
147-175	161	0.063	$3.913 \times 10^{-4}$
175-208	192	0.080	$4.166 \times 10^{-4}$
208-249	229	0.140	$6.113 \times 10^{-4}$
249-295	319	0.111	$3.479 \times 10^{-4}$
295-417	356	0.236	$6.629 \times 10^{-4}$
417-495	456	0.166	$3.640 \times 10^{-4}$
495-589	542	0.170	$3.136 \times 10^{-4}$
589-833	711	0.040	$0.560 \times 10^{-4}$

$$(x/d_p)_i = 3.27 \times 10^{-3}$$

$$d_p = \frac{1}{\sum_{\text{all } i} (x/d_p)_i} = \frac{1}{3.27 \times 10^{-3}} = 305$$

## Computer Printout

```

PROGRAM PROFILE (INPUT,OUTPUT,TAPE5=INPUT,TAPE6=OUTPUT)
C
C THIS PROGRAM IS USED TO FIND THE AREA UNDER THE SURFACE PROFILE OF THE COLD
C SLUMPED FLUIDIZED BED
C
C X IS HORIZONTAL DISTANCE MEASURED FROM INTERFACE REGION (M.)
C Y IS VERTICAL DISTANCE MEASURED FROM FIXED LEVEL (M.)
C XP,YP IS LOCATION OF THE PEAK OF THE RIDGE IN X-Y DIRECTION (M.)
C XC IS THE LOCATION WHERE SLOPE CHANGES
C U IS SUPERFICIAL VELOCITY (M/SEC.)
C UMF IS MINIMUM SUPERFICIAL VELOCITY (M/SEC.)
C T IS TIME AFTER DEFLUIDIZED HALF OF THE BED (MIN.)
C DT IS THE TIME INTERVAL (MIN.)
C
C READ INPUT DATA
C
PRINT*, "ENTER U (M/SEC.), T (MIN.), DT (MIN.)"
READ(5,*) U, T, DT
UMF=0.1676
C
C CALCULATE CONSTANT
C
UD = U-UMF
C1 =0.1086*UD
C2 =0.3464*UD
C3 =3.1245-(1.64*UD)+(4.2222*(UD**2.0))
C4 =3.145E-3-(3.653E-2*UD)+(2.6666E-2*(UD**2.0))
C5 =-2.25+6.33*UD
C6 =1.13-1.17*UD
C7 =2.83+0.6324*UD
C8 =0.066+6.667E-2*UD
C
WRITE (6,100)
N =T/DT
T=0.0
DO 10 I=1,N
T =T+DT
C
C CALCULATE LOCATION OF PROFILES
C
XP =C2*T**0.1257
YP =0.03+C1*T**0.1333
XC =XP+0.01*EXP(C3+C4*T)
XL =XC+0.01*EXP(C5)*T**C6
YC =YP*(1.0-((XC-XP)/((EXP(C7)*T**C8)*0.01)))
C
C CALCULATE AREA UNDER PROFILES
C
A1 =0.5*(XL-XC)*YC
A2 =0.5*(XC-XP)*(YC+YP)

```



```

      A3 =SIMP(XP,UD)
      AT =A1+A2+A3
      VOLUME =AT*0.3048
      RMASS =VOLUME*3000.0
      WRITE (6,101) T,XP,YP,A1,A2,A3,XC,XL,YC,AT,RMASS
10    CONTINUE
100   FORMAT (1H1,"TIME",4X,"XP",4X,"YP",4X,"A1",4X,"A2",4X,"A3",4X,
1      "XC",4X,"XL",4X,"YC",4X,"AT",4X,"MASS")
101   FORMAT (1H ,F5.0,9F6.4,F10.3)
      RETURN
      END
      FUNCTION SIMP(A,UD)
      TWOH =A/10.0
      H =TWOH/2.0
      SUMEND =0.0
      SUMMID =0.0
      C9 =0.33426/UD**0.06046
      DO 1 K=1,10
      X =FLOAT(K-1)*TWOH
      SUMEND =SUMEND+0.03+C9*X**1.06146
1      SUMMID =SUMMID+0.03+C9*(X+H)**1.06046
      SIMP =(2.0*SUMEND+4.0*SUMMID+C9*A**1.06046)*H/3.0
      RETURN
      END

```

```

PROGRAM DISTRIB (INPUT,OUTPUT,TAPE5=INPUT,TAPE6=OUTPUT)
C
C THIS PROGRAM IS USED TO SOLVE THE ORDINARY DIFF. EQUATION
C BY USING THE FOURTH ORDER RUNGE-KUTTA METHOD TO FIND THE
C VELOCITY,TRAJECTORY AND DESTINATION OF EJECTED PARTICLES
C WHICH CAUSED BY BUBBLES ERUPTION IN A SLUMPED BED.
C
C U IS A SUPERFICIAL VELOCITY (CM/SEC)
C UMF IS MINIMUM FLUIDIZING VELOCITY (CM/SEC)
C URX IS VELOCITY OF EJECTED PARTICLES IN X DIRECTION (CM/SEC)
C URY IS VELOCITY OF EJECTED PARTICLES IN Y DIRECTION (CM/SEC)
C CD IS A DRAG COEFFICIENT
C ROF IS DENSITY OF FLUID (GM/C.C.)
C ROP IS DENSITY OF PARTICLES (GM/C.C.)
C T IS TIME (SEC)
C DT IS TIME INTERVAL (SEC)
C REX IS PARTICLE REYNOLD NUMBER IN X DIRECTION
C REY IS PARTICLE REYNOLD NUMBER IN Y DIRECTION
C DP IS PARTICLE DIAMETER (CM)
C DB IS BUBBLE DIAMETER (CM)
C VIS IS FLUID VISCOSITY COEF. (GM/CM-SEC)
C AAA IS THE DISTANCE FROM THE INTERFACE WHERE THE BUBBLE ERUPT
C
C DIMENSION XX(17),KOUNT(16)
C COMMON ROF,ROP,VIS,DP,U,DT
C PRINT*,"INPUT SUPER.VEL.,FIRST AND LAST ANGLE,STEP SIZE,HEIGHT,AA."
C READ*.U,M,N,ST,HEI,AAA
C WRITE (6,100)
C
C INPUT DATA
CC
C UMF =16.764
C ROF =1.16E-3
C ROP =5.60
C VIS =1.85E-4
C DP =3.05E-2
C XX(1) = 0.0
C AA = 3.75
C DO 10 I = 1,16
C KOUNT(I) = 0
C J = 1+1
C XX(J) = XX(I)+AA
10 CONTINUE
C
C CALCULATE CONSTANTS
C
C UD = U-UMF
C PPI = 22.0/7.0
C
C FIND DIAMETER OF BUBBLES

```

```

C
H = 30.0
A = 14.5162
G = 980.0
C1 = 0.593*(H+4.0*A**0.5)**0.8/G**0.2
DB = C1*(UD**0.4)

C
C FIND INITIAL CONDITION
C
DO 90 I = 1, N
DEG = FLOAT (I)
ZETA = (PPI/180.0)*DEG
UR = 2.0*(UD+22.26*(DB**0.5))*COS(ZETA)
URXI = UR*SIN(ZETA)
URYI = UR*COS(ZETA)
T = 0.0
X = 0.5*DB*SIN(ZETA)-AAA
Y = 0.5*DB*COS(ZETA)

C
C INPUT STEP SIZE
C
DT = ST
URX = URXI
URY = URYI

C
C USING RUNGE KUTTA METHODS
C
40 AK1 = F1(T,URX)
AK2 = F1 (T+DT/2.0,URX+AK1/2.0)
AK3 = F1 (T+DT/2.0,URX+AK2/2.0)
AK4 = F1 (T+DT,URX+AK3)
BK1 = F2(T,URY)
BK2 = F2(T+DT/2.0,URY+BK1/2.0)
BK3 = F2(T+DT/2.0,URY+BK2/2.0)
BK4 = F2(T+DT,URY+BK3)
URX = URX + (AK1+2.0*AK2+2.0*AK3+AK4)/6.0
URY = URY + (BK1+2.0*BK2+2.0*BK3+BK4)/6.0
DX = URX*DT
DY = URY*DT
T = T+DT
X = X+DX
OLDY = Y
Y = Y+DY
Y1 = Y
IF (Y1.GT.OLDY) GO TO 40
YMAX = OLDY
IF (YMAX.LT.HEI) GO TO 90
IF (Y.LE.0.0) GO TO 90
IF (Y.LT.HEI.AND.URY.GE.0.0) GO TO 40
IF (URY.GE.0.0) GO TO 40
IF (Y.GT.HEI) GO TO 40

```

```

      CALX = X
      DO 30 K = 1,16
      L = K+1
      IF (CALX.GE.XX(K).AND.CALX.LE.XX(L)) GO TO 50
30    CONTINUE
50    KOUNT(K) = KOUNT(K)+1
90    CONTINUE
C
C    OUTPUT
C
      DO 60 JJ=1,16
      WRITE (6,101) JJ,KOUNT(JJ)
60    CONTINUE
100   FORMAT (1H1,"DISTRIBUTION")
101   FORMAT (1H ".2I5")
      STOP
      END
      FUNCTION F1(T,URX)
      COMMON ROP,ROP,VIS,DP,U,DT
      REX = ROP*DP*URX/VIS
      A1 = (24.0/REX)*(1.0+0.15*REX**0.687)
      A2 = 0.42/(1.0+42500.0/REX**1.16)
      CDX = A1+A2
      A3 = -0.75*ROP/(ROP*DP)
      F1 = (A3*CDX*URX**2.0)*DT
      RETURN
      END
      FUNCTION F2(T,URY)
      COMMON ROP,ROP,VIS,DP,U,DT
      REY = ROP*DP*ABS(URY)/VIS
      B1 = (24.0/REY)*(1.0+0.15*REY**0.687)
      B2 = 0.42/(1.0+42500.0/REY**1.16)
      CDY = B1+B2
      B3 = -0.75*ROP/(ROP*DP)
      B4 = (ROP-ROP)*980.0/ROP
      F2 = (B3*CDY*(URY-U)**2.0-B4)*DT
      RETURN
      END

```